Dissertation

submitted to the Combined Faculty of
Natural Sciences and Mathematics
of the Ruperto Carola University Heidelberg, Germany
for the degree of
Doctor of Natural Sciences

Presented by
M. Sc. Saskia Höcker
born in Delft, The Netherlands
Oral examination: 20.09.21

The role of a satellite III RNA-associated nucleolar complex in Drosophila oogenesis

Referees:

Prof. Dr. Alexis Maizel

Prof. Dr. Sylvia Erhardt

Summary

Centromeric chromatin of metazoa is highly repetitive and cannot be classified as typically euchromatic or heterochromatic. Centromeric regions harbour few to no genes but they are transcribed into non-coding RNAs in many species studied to date. In *Drosophila melanogaster*, one of the transcribed (peri)centromeric sequences is the 359 bp satellite III (sat III) repeat. Sat III RNA transcripts localize to the (peri)centromere, where they stabilize the newly incorporated centromeric histone CENP-A (or CID in Drosophila). When sat III RNA levels are reduced, cells harbour mitotic defects, such as lagging chromosomes and micronuclei formation. Although sat III has an important role at the centromere, little is known about sat III RNA regulation and its interaction partners, as well as possible other functions.

In this thesis, I set out to identify new sat III RNA-associated proteins in a sat III RNA pulldown. Among the identified interacting proteins was a hitherto uncharacterized complex of four unknown proteins, which proved to be important for the Drosophila germline development. We, therefore, named it Centromeric Transcript-Associated Gonadal (Centagon) complex. I show that the Centagon complex proteins interact with each other as well as with sat III RNA. The sat III-interacting Centagon complex is expressed in the nucleoli of germ cells and somatic cells in the ovary and its knockdown results in severe germline defects.

Depletion of Centagon components by RNAi resulted in defects in the ovary germarium including a loss of germ cells resulting in rudimentary ovaries and agametic flies. Immunofluorescent stainings with a germ stem cell marker, suggest that the defect may be caused by a failure of the germ cells to properly differentiate. On the other hand, depletion in the ovary egg chambers resulted in a developmental arrest of the egg chambers and nurse cell chromatin aberrations. Importantly, sat III RNA levels were upregulated up to 50-fold in the Centagon depleted ovaries, indicating that the Centagon complex is involved in sat III RNA repression. Furthermore, my experiments show that the egg chamber developmental arrest and chromatin aberrations depend on high sat III transcript levels, since I could partially rescue the phenotype by reducing sat III RNA levels. Knockdown experiments in somatic ovary cells and the male germ line showed that the Centagon complex is also essential in other cell types and not ovary-specific.

In conclusion, I identified a new sat III RNA-associated protein complex that is involved in sat III RNA regulation and showed that sat III RNA has a negative effect on ovary development when upregulated.

Zusammenfassung

Das zentromerische Chromatin in Metazoen besteht aus hochrepetitiven Sequenzen und ist weder typisch euchromatisch noch typisch heterochromatisch. In den zentromerischen Regionen sind kaum bis keine Gene kodiert, aber diese Regionen werden in vielen Arten, die man bis heute schon untersucht hat, in nicht-kodierenden RNAs transkribiert. Eines dieser (peri)zentromerischen Transkripte in *Drosophila melanogaster* ist die Satellite III (Sat III) RNA mit einer 359 bp langen repetitiven Sequenz. Die Sat III RNAs häufen sich auf den (peri)zentromerischen Regionen des Chromosoms an, wo sie die zentromer-spezifischen Histone-Variante CENP-A, nach deren Einbau ins Chromatin, stabilisieren. Bei reduzierten Sat III RNA-Mengen zeigen Zellen mitotische Defekte wie auch unverteilte Chromosome während der Anaphase, das zur Entstehung von Mikro-Zellkernen führen kann. Obwohl Sat III RNA eine wichtige Funktion am Zentromer hat, ist größtenteils noch unbekannt wie Sat III-Transkripte reguliert werden, mit welchen Proteinen sie interagieren und ob Sat III RNA weitere Funktionen hat.

In dieser Doktorarbeit habe ich mit Hilfe eines Sat III RNA-Pulldowns neue Sat III-Interaktionspartner identifiziert. Unter den identifizierten interagierenden Proteinen war ein noch nicht beschriebener Komplex aus vier uncharakterisierten Proteinen, die wichtig für die Keimzellentwicklung in Drosophila sind. Diesen Komplex nannten wir „Centromeric Transcript-Associated Gonadal (Centagon)“ Komplex. Ich konnte zeigen, dass die Centagonproteine sich sowohl gegenseitig binden als auch mit Sat III RNA assoziieren. Der Centagonkomplex wird in den Nukleoli der Keimzellen und somatischen Zellen der Drosophila-Eierstöcke exprimiert und Depletion des Komplexes verursacht schwerwiegende Keimbahndefekte.

Depletion der Centagonproteine durch RNAi bewirkte ein Verlust der Keimzellen in den Germarien der Eierstöcke, das in rudimentäre Eierstöcke und unfruchtbare Fliege resultierte. Immunofluoreszente-Anfärbungen mit einem Stammzellmarker der Keimzellen zeigten, dass der Defekt auf Defekte während der Keimzelldifferenzierung basieren könnte. Depletion des Centagonkomplexes zu einem späteren Zeitpunkt, in den Eikammern der Eierstöcke, führt wiederum zu einer Hemmung der Eikammerentwicklung und Chromatinstörungen in den sogenannten „Nurse cells“. Dabei war eine wichtige Entdeckung, dass in Eierstöcken mit verringerten Mengen an Centagonkomplex, die Menge an Sat III RNAs bis zu 50-Fach hochregulierten. Das deutete darauf hin, dass der Zentagonkomplex an der Repression von Sat III RNA beteiligt ist. Außerdem zeigen meine Experimente eine Beteiligung der hohen Sat

III RNA-Werte bei der Hemmung der Eikammerentwicklung und den Chromatinstörungen, da diese Effekte in Fliegen mit reduzierten Sat III-Mengen weniger stark zum Ausdruck kamen. Weiterhin haben Experimente mit Centagonkomplex-Depletionen in somatische Zellen des Eierstocks und in männlichen Keimzellen gezeigt, dass der Komplex auch in anderen Zelltypen essenziell ist und nicht spezifisch für die Eierstöcke ist.

Zusammenfassend kann ich sagen, dass ich in dieser Doktorarbeit einen neuen Sat III RNA-assoziierten Proteinkomplex entdeckt habe, der an der Regulation von Sat III RNA beteiligt ist und dass erhöhte Sat III RNA Werte eine bisher unbekannte Auswirkung auf die Entwicklung der Drosophila Eierstöcke haben.

Contents

Abbreviations

CB	cystoblast
CPC	chromosomal passenger complex
DFC	dense fibrillar component
DSB	double strand break
EMSA	electrophoretic mobility shift assay
FC	fibrillar center
GC	granular component
GSC	germ stem cell
IF	immunofluorescence
KD	knockdown
LC-MS	liquid chromatography–mass spectrometry
LNA	locked nucleid acid
NAD	nucleolus-associated chromatin domain
NLS	nuclear localization sequence
PCR	polymerase chain reaction
qPCR	quantitative PCR
PGC	primordial germ cell
RISC	RNA-induced silencing complex
RNAi	RNA interference
RNase	ribonuclease
lncRNA	long non-coding RNA
piRNA	piwi-interacting RNA
rRNA	ribosomal RNA
siRNA	small interfering RNA
tRNA	transfer RNA
Sat III	satellite III
SC	synaptonemal complex
smFISH	single-molecule fluorescent in situ hybridization
TE	transposable element
WT	wildtype

1. INTRODUCTION

Cell division is one of the key determinants of life. Without it, there would be no reproduction, no growth and no tissue repair. In order to divide, a cell has to duplicate its genome and distribute both copies, together with other cell organelles, to the newly forming daughter cells. This procedure is highly coordinated with many checkpoints for quality control, as a small error during replication can have big consequences, ranging from cells with aneuploidy, having an abnormal chromosome number, to cancerous cells which divide uncontrolled, accumulating mutations and other genetic defects. The earlier during development a mitotic error occurs, the more impact it will have, if left unresolved. While a fully differentiated cell will not propagate any genetic defects, a stem cell will pass its genome on to all daughter cells and errors in the germline may affect the whole offspring.

The *Drosophila melaongaster* ovary is a well-studied model system for stem cell biology with many advantages. Not only are the gonads well characterized, during development as well as in the adult stage, also many molecular markers are available to mark stem cells and their differentiating daughter cells. This makes the germ stem cells easy to visualize. As all stages of germ cell differentiation are visible in the same ovary and rudimentary gonads due to stem cell loss are readily recognised, errors in stem cell maintenance and differentiation are straightforward to follow (DANSEREAU AND LASKO 2008).

1.1 THE DROSOPHILA GERM LINE

In an evolutionary sense, germ cells are the most important cells of an organism since they ensure the ability to have offspring and propagate an individual genetic make-up. It is therefore not surprising that the first set of differentiating cells during Drosophila embryogenesis are the future germ cells, the so called pole cells (SONNENBLICK 1941).

1.1.1 POLE CELLS AND MIGRATION

Pinched off at the posterior pole, approximately 10 cells are separated from the rest of the embryo before blastoderm formation (M. DEMEREC 1950). This action is determined by a specific group of ribonucleoproteins (RNPs), seen as polar granules under the microscope, which accumulate at the posterior end of the embryo in the germ plasm and are incorporated into the pole cells during cellularization (JAZDOWSKA-ZAGRODZIŃSKA 1966; ILLMENSEE AND MAHOWALD 1974; HUETTNER 1923). The formation of germ plasm presumably begins in the

unfertilized oocyte with the accumulation of oskar mRNA at the posterior pole, followed by its translation. The Oskar protein then recruits other proteins and RNAs to the posterior pole, such as the DEAD-box RNA helicase Vasa (often used as germ cell marker) and nanos, polar granule component, germ cell-less, cyclin B and more oskar mRNAs. Within this germ plasm, polar granules are formed consisting of RNPs with Oskar, Aubergine, Tudor and Vasa proteins as well as coding and noncoding RNAs (Bilinski et al. 2017). The components in the germ plasm can be divided into three overlapping groups: Some are important for assembly of the germ plasm and after that some will initiate germ cell formation while others are involved in abdominal development (Mahowald 2001). In the course of embryogenesis, the pole cells divide until they reach an average number of 55 cells (Rabinowitz 1941), which migrate through the organism until they reach their final destination in the mesoderm. There, they form contacts to their niche and coalesce into gonads. However, not all cells starting out as pole cells end up in the primordial gonads, most end up in the posterior yolk and may be involved in forming the primitive gut (Poulson 1947).

1.1.2 Gonad development

During the larval stages, the first differences between males and females become apparent. The ovaries of a newly hatched larva (24 h) are very small and consist out of only 8-12 primordial germ cells (PGCs) embedded in fat tissue. The testes are much larger at this stage with 36-38 PGCs and can be distinguished from the surrounding fat tissue when looking through the body wall of a living larva (M. Demerec 1950). While testis formation is largely completed during larval development, the morphogenesis of the ovaries occurs mostly after pupation (Villasante et al. 2009; Whitworth et al. 2012). During all larval stages, gonad development occurs independently from the development of the genital ducts and external genitalia. Their fusion only takes place during pupal stage (M. Demerec 1950).

Male larval gonads

In the male gonad, the PGCs form germ stem cells (GSCs) that connect to a specific cluster of somatic cells at the anterior side, the hub, which is important for stem cell maintenance (Fig. 1). Unpaired (upd), expressed by the hub cells, initiates the Jak/stat signalling pathway in GSCs, which is essential for maintaining their stem cell properties (Kiger et al. 2001). Next to each GSC are two somatic cyst progenitor cells also connected to the hub (Gönczy and DiNardo 1996). When the GSC divides asymmetrically to produce a gonialblast, this cell is accompanied by two cyst cells. While the gonialblast will divide and differentiate into 16 interconnected spermatogonia, the cyst cells do not divide, but envelop the germ cells to form a cyst (Yamashita et al. 2005). When the spermatogonia differentiate into spermatocytes,

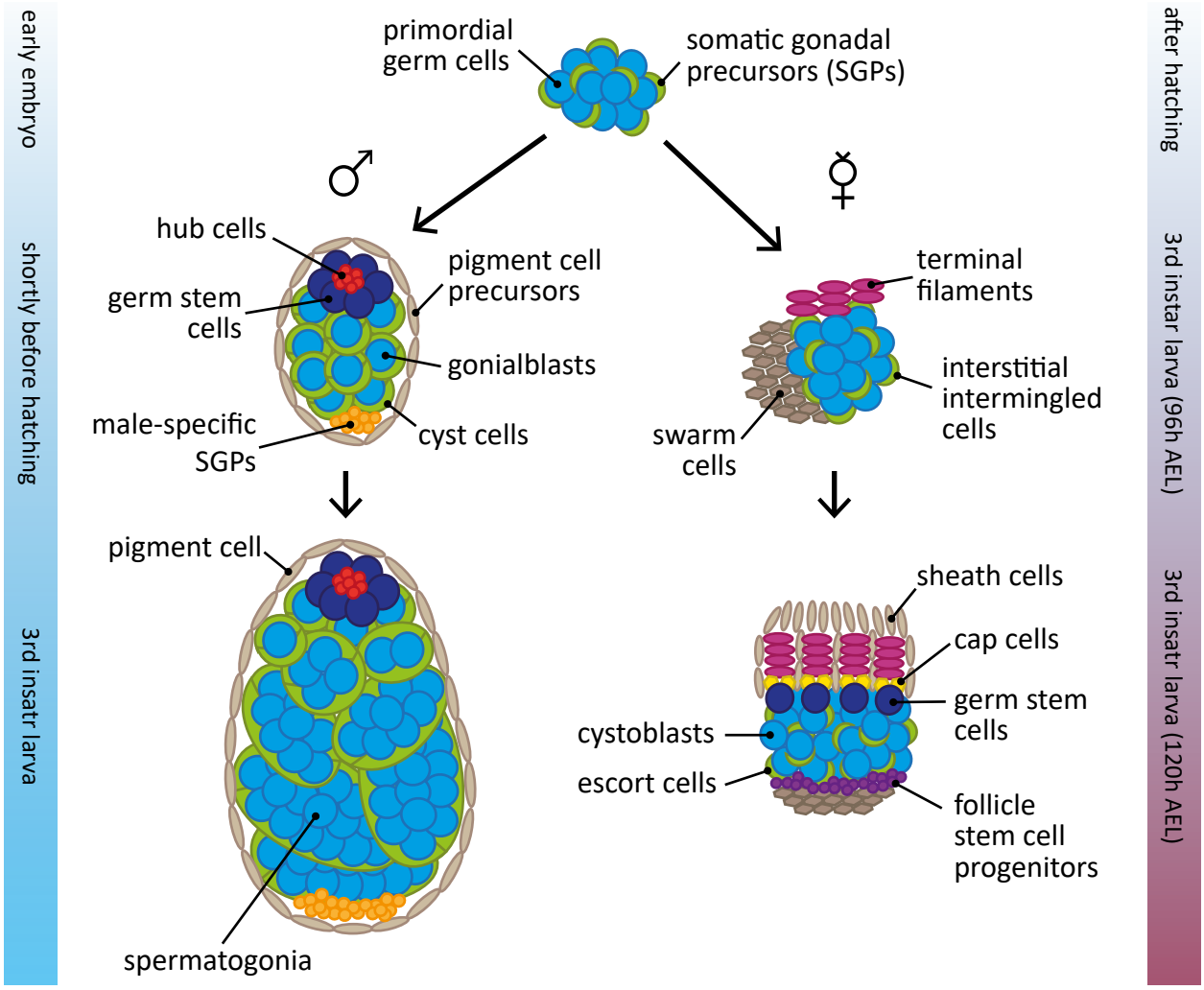

Figure 1: Gonad development in Drosophila

Differences between the male and female gonad development in Drosophila larvae. The male gonads start developing in the embryo and are bigger. The female gonads start differentiating in the the 3rd instar larva and consist of more cell types. The male stem cell niche consists of the hub and the female stem cell niche consists of the terminal filaments and cap cells. AEL = after egg laying. Modified from Whitworth et. al. 2012, Gilboa et. al. 2015 and Slaidina et. al. 2020.

they increase in size and fill up the whole posterior end of the larval testis (M. Demerec 1950). Additionally, the male gonads have male-specific somatic gonadal precursors and pigment cell precursors. The small male-specific somatic gonadal precursors are found at the posterior end of the gonad and will form the terminal epithelium (DeFalco et al. 2003), which is involved in the maturation of spermatids and may be important for the fusion with other parts of the male reproductive tract (Whitworth et al. 2012). The pigment cells form an outer sheath around the gonad (DeFalco et al. 2008).

Female larval gonads

In the early female gonads, cells mainly proliferate and only after 96 hours after egg laying, in the 3rd instar larvae, this shifts to mostly differentiation (Gilboa 2015) (Fig. 1). The ovary

of the 3rd instar larva consists of PGCs and 6 different types of somatic gonadal progenitor cells (Slaidina et al. 2020). Throughout ovary development, the PGCs are accompanied by interstitial intermingled cells (Li et al. 2003), which will mostly differentiate into escort cells in the adult ovary (Slaidina et al. 2020). The terminal filament cells are the first somatic niche cells to form. They start to differentiate in the 2nd instar larva and become 16-20 stacks of disc-shaped cells in the 3rd instar larva (Sahut-Barnola et al. 1996). The terminal filaments recruit interstitial cells which differentiate into cap cells, which in their turn recruit and connect to PGCs which become GSCs (Song et al. 2007; Song et al. 2002). Each terminal filament connects to 5-7 cap cells, which can sustain 2-3 GSCs. Furthermore, a group of apical cells, the sheath cells, will migrate in between the terminal filaments forming a basement membrane which separates the terminal filaments into the future ovarioles (King et al. 1968). Another group of somatic cells, the swarm cells, migrates to the posterior end of the larval gonad and contributes to the outer ovarian sheath in adults (Slaidina et al. 2020). Last but not least, the follicle stem cell progenitors, which probably give rise to both follicle stem cells and prefollicle cells, can be found between the interstitial cell and swarm cell population (Slaidina et al. 2020). All this time, the niche prevents the premature differentiation of PGCs by expressing the translational repressors Nanos and Pumillio, as well as through the Decapentaplegic (Dpp) signalling pathway, factors that are also important for GSC maintenance. In the pupa, this differentiation repression is limited to the GSCs attached to the cap cells and the first PGCs start to differentiate into cystoblasts (CBs) (Gilboa and Lehmann 2004).

1.1.3 Oogenesis

The germarium

In the adult ovary, each terminal filament with its recruited cap cells and GSCs has formed its own string of egg chambers or ovariole. The stem cell niche is found at the very tip, in the germarium which is divided into 4 regions (Fig. 2): region 1 harbours the stem cell niche and cystocyte divisions, in region 2a the oocyte is determined, in region 2b the follicle cells join the germ cell cyst and in region 3 the encapsulated cyst buds off (Riechmann and Ephrussi 2001). As mentioned before, the GSCs are connected to the cap cells by adherens junctions (Song et al. 2002) and this close proximity to cap cells and terminal filaments ensures they receive all signals necessary to maintain their stem cell properties, the most important signal being Dpp (Dansereau and Lasko 2008). Dpp is expressed by cap cells and terminal filaments and activates Mothers against dpp (Mad) phosphorylation in GSCs, leading to the nuclear translocation of the transcriptional activator Medea (Med) which among others,

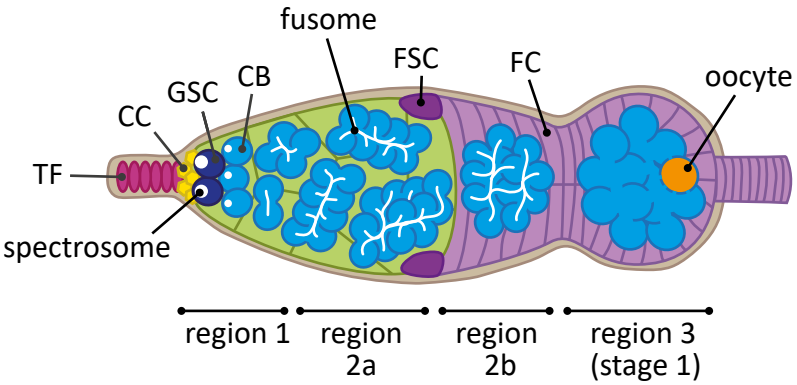

Figure 2: The morphology of the Drosophila germarium
The germ stem cells (GSC) are located in the stem cell niche consisting of terminal filaments (TF) and cap cells (CC). Their asymmetric division produces one GSC and one cystoblast (CB). These undergo several divisions without abscission to produce 16-cell germ cell cysts, which are enveloped by follicle cells (FC). One of the 16 cells becomes the oocyte. FSC = follicle stem cell

represses bag of marbles (bam) transcription (Song et al. 2004; Yamashita et al. 2005). Additionally, GSCs express the RNA-binding proteins Nanos and Pumillio which inhibit the translation of mRNAs involved in differentiation (Gilboa and Lehmann 2004). Without phosphorylated Mad (pMad) induced bam repression, the GSCs differentiate into CBs, as Bam downregulates Nanos, leading to the synthesis of proteins for differentiation (Li et al. 2009; Ohlstein and McKearin 1997). Because pMad levels are highest in GSCs (Song et al. 2004), it is often used as GSC marker. Another hallmark of the GSCs, is a cytoplasmic organelle called the spectrosome. It consists of membrane skeletal proteins such as α- and β-spectrin and Hu-li tai shao (Hts) (Lin et al. 1994), which are also used as markers. The spectrosome is located at the apical side of the GSC and anchors the mitotic spindle during division, orienting it perpendicular to the cap cells and forcing one of the daughter cells out of the stem cell niche. The spectrosome elongates during mitosis and is one of the factors that is asymmetrically inherited by the cystoblast (Deng and Lin 1997). From now on, the cystoblasts will undergo divisions without complete cytokinesis until they reach a 16 cell-cyst stage connected by cytoplasmic bridges called ring channels. During each mitosis the spectrosome elongates and is distributed among the new cells without abscission, forming a branched structure that connects the cystocytes, also called the fusome. The cystocyte divisions are precisely coordinated and always follow the same branching pattern, where one of the two cells with the most (4) ring channels becomes the designated oocyte and the rest of the cystocytes differentiate into nurse cells (Cuevas et al. 1997). For this differentiation to happen, the oocyte has to inherit specific mRNAs and proteins which are transported by a polarised microtubule network. Furthermore, meiosis is restricted to the oocyte and it inherits the centrioles (Riechmann and Ephrussi 2001). In region 1 of the germarium, cystoblast differentiation is supported by the escort cells which insulate the

germ cysts up to germarium region 2a/b, where the follicle cells take over and the escort cells undergo apoptosis (DECOTTO AND SPRADLING 2005). The follicle stem cells divide and produce approx. 30 follicle cells, which envelop the forming germ cell cyst (egg chamber) before budding of the germarium (NYSTUL AND SPRADLING 2010).

The egg chambers

Within one ovariole, several egg chambers of progressing stages (between 1-14) are found, with stage 14 being the developed egg, ready to be laid (JIA et al. 2016) (Fig. 3). During egg chamber stages 1-10, the polyploid nurse cells grow fast and synthesizes essential proteins and RNAs that are transported to the oocyte through the ring channels. The nurse cells then undergo apoptosis and only the oocyte remains. For the embryo to develop properly, the anterioposterior and dorsoventral axes have to be established. This happens through signalling with gurken (grk), bicoid (bcd) and oskar (osk) mRNA. grk mRNA is expressed by the oocyte nucleus and when translated, it signals to the overlaying follicle cells to adopt a dorsal fate and repolarize the microtubule network. This is necessary to transport the oocyte nucleus to anterodorsal corner of the oocyte during stage 7-8, which is accompanied by a relocalization of the grk mRNA and protein. Here, Grk signals to the follicle cells to adopt

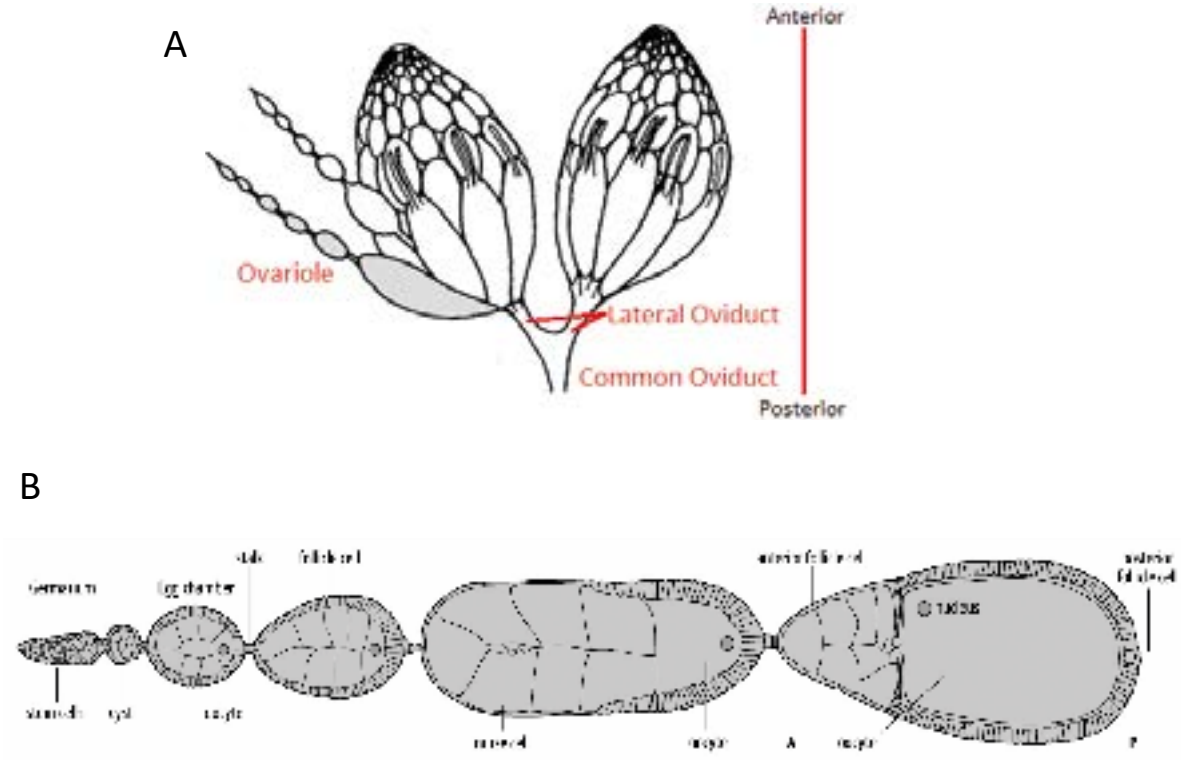

Figure 3: Morphology of the Drosophila ovary

A. The Drosophila ovaries consist of ovarioles containing the developing egg chambers.
B. The ovarioles each contain a germarium with stem cells, followed by egg chambers of progressing developmental stage. Each egg chamber contains 15 nurse cells and one oocyte.
From Mahowald AP, Kambysellis MP (1980) Oogenesis. In: Ashburner M, Wright TRF (eds)
The genetics and biology of Drosophila, vol 2c. Academic Press, London, UK, pp 141–224

a dorsal fate, creating the dorsoventral axis. The anterioposterior axis is determined by the localisation of bcd and osk mRNA. Both are produced by the nurse cells and transported to the oocyte, where the microtubule network transports bcd mRNA to the anterior pole and osk mRNA to the posterior pole of the oocyte during stages 8-10. Both mRNAs are locally translated, Bcd is important for the formation of anterior structures and Osk recruits the pole plasm components, which will be important for forming the polar cells in the next generation embryo, where the whole cycle of pole cell migration and gonad development starts anew (RIECHMANN AND EPHRUSSI 2001).

1.2 CHROMATIN ORGANIZATION DURING OOGENESIS

1.2.1 THE OOCYTE

GSCs are the only adult cells in Drosophila without chromosome pairing, instead they are found in the periphery of the nucleus next to the nuclear lamina. In differentiating CBs the chromosome localisation changes, they move away from the nuclear lamina (JOYCE et al. 2013), an environment which is associated with transcriptional repression (GUERREIRO AND KIND 2019). Additionally, a general transient transcriptional silencing takes place during the transition from GSC to CB, mediated by the transcriptional repressor polar granule component (pgc) which is necessary for CB differentiation. Possibly it helps clearing one expression program to make room for the next (FLORA et al. 2018). In order to form a haploid oocyte with a unique combination of genes, the oocyte has to undergo chromosome recombination and meiosis. In region 1 of the germarium, during the cystocyte divisions, the centromeres of homologous chromosomes start to pair up with the help of the synaptonemal complex (SC) which is completed by the time all 16 cells have been formed. In region 2a, the assembly of the SC continues along the chromosome arms in up to four of the cells, pairing the chromosomes for crossovers. While the cyst travels through region 2b, the SC will be broken down again in three of the cells as they back out of the meiotic program. Meanwhile, the leftover oocyte is subjected to crossovers of the chromosome arms. In region 2a, double strand breaks (DSBs) are formed shortly after the SC has assembled, which will subsequently be repaired as crossovers or non-crossovers. This results in approximately 1.2 crossovers per chromosome arm, but not at pericentric heterochromatic regions, which are recombinationally inert. By the time the germ cyst bud of the germarium, all DSBs will be repaired. Next, the oocyte genome is heavily compacted into the so called karyosome, where it resides away from the nuclear envelope. Apart from a short decondensation period around stage 9-10, the oocyte genome stays in the karyosome formation until meiosis (HUGHES et al. 2018).

1.2.2 NURSE CELLS

As soon as the oocyte has been determined in the 16-cell cyst, the oocyte and nurse cells go through drastically different cell cycle programs. While the oocyte is preparing for meiotic divisions, the 15 remaining nurse cells begin endocycling to form polytene chromosomes. Polytene chromosomes are very common in Drosophila: not only are the genomes of almost all larval tissues polytenized, of which the salivary gland has been especially well studied, also in adults endoreduplicating tissues can be found. Polytene chromosomes can form due to an altered cell cycle, the endocycle, with only an S phase and G phase, but no mitosis (SMITH AND ORR-WEAVER 1991). As a result, the genome is repeatedly reduplicated within the same cell, apart from some underreplicated regions. It has been suggested this may be more efficient for the cell, since the underreplicated regions consist of gene-poor and repetitive regions, which it does not really require (STORMO AND FOX 2017). Also satellite repeats are underreplicated, as has been shown in salivary glands (GALL et al. 1971). Polytene chromosomes have a distinct appearance: the homologous chromosomes are paired and the many copies of the chromosome arms are aligned, while all centromeres are clustered at the so called chromocenter (in salivary glands). This results in broad chromatin structures with

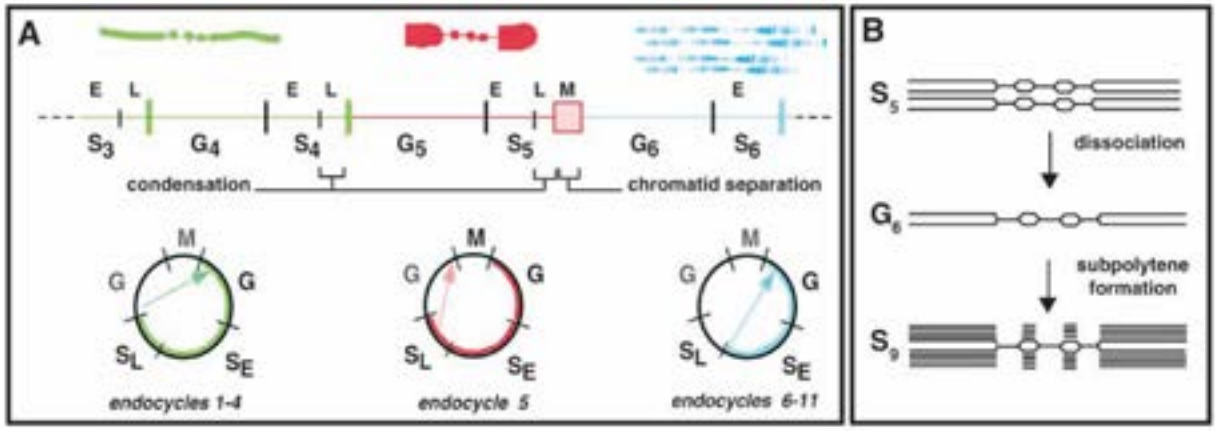

C

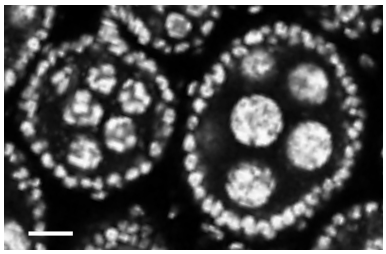

Figure 4: Nurse cell endocycles

A. Nurse cell endocycle changes during stage 4-6. Nurse cell polytene chromosomes first undergo compaction and then seperate into sister chromosome pairs between S5 and G6.

B. Schematic schowing the polytene chromosome changes during S5 - S9.

C. Example of an egg chamber during stage 5 (left) and after nurse cell chromatin dispersal (right).

A an B are from DEJ AND SPRADLING 1999

recognisable banding patterns that are caused by eu- and heterochromatic regions (Stormo and Fox 2017). Polyploidy has been suggested to have several advantages, ranging from increased cell size (eg. at the blood-brain-barrier) to facilitating increased protein synthesis (eg. in the ovary follicle cells which produce chorion for the eggshell and the nurse cells producing proteins for the oocyte) (Orr-Weaver 2015).

Interestingly, nurse cells undergo three different phases of endocycling (Fig. 4). During the first four endocycles, the genome is completely reduplicated including the satellite DNA. In contrast to the salivary gland, these polytene chromosomes have no chromocenter and all four chromosomes are separated, as well as more condensed. The second phase is seen during endocycle 5. Here the chromosomes condense even more and are clearly seen as 5 DAPI-rich regions in the nurse cell nucleus, also called the five-blob stage. Each 'blob' consists of a major chromosome arm (Dej and Spradling 1999). Then, exactly between S5 phases and G6 phase, the chromosomes disperse, which initiates the 3rd phase. The 64 chromosomes are divided into 32 polytene sister chromosome pairs, which is unique for polyploid cells. Probably, this is caused by a shortened S5 phase where the chromosomes are not fully replicated yet and cannot separate. Subsequently, the chromosomes continue endocycling similar to the salivary gland polytene chromosomes. The satellite repeats are omitted and they take on a similar banding pattern. In the cell, the chromosomes cannot be distinguished anymore, but DNA FISH experiments have shown, that each homologue chromosome pair including its copies still occupies a separate region of the nurse cell nucleus (Dej and Spradling 1999).

1.3 GSC maintenance

Asymmetric stem cell division, where one daughter cell differentiates into a progenitor cell and the other remains a stem cell, is essential for stem cell maintenance. Without it, the stem cell population in any tissue would soon be depleted or overcrowded. Generally, the factors influencing stem cell division can be categorised into intrinsic and extrinsic factors. In both cases the mitotic spindle is key for transporting fate-determining factors to the stem-cell or differentiating cell (Inaba and Yamashita 2012). As mentioned before, Drosophila GSCs are strongly influenced by extrinsic signals from the germline stem cell niche. In the ovaries, the stem cell niche is comprised of cap cells, terminal filament cells and inner sheath cells. Especially the cap cells seem to be important for GSC regulation with the production of signalling molecules and cell-cell adhesions. During the division of GSCs, one cell always stays in contact with the cap cells, receiving all the GSC-determining signals. The other daughter cell is further removed from the niche and differentiates into a CB (Lin 2002).

1.3.1 ASYMMETRIC DIVISION

The intrinsic factors influencing GSC division consist of proteins distributed asymmetrically during mitosis, of which there are many examples. As mentioned before, the spectrosome anchors the mitotic spindle at the side of the stem cell niche and is mainly retained in the GSC (DENG AND LIN 1997), but also proteins involved in mitosis like the centrosomes and midbody ring are asymmetrically inherited (SALZMANN et al. 2014). This is also the case for epigenetic information, as histones are asymmetrically divided. Studies in the Drosophila testis have shown that during GSC division, chromosomes with pre-existing H3 and H4 are selectively segregated into the new GSC, while CBs carry more newly synthesized H3 and H4. This asymmetry is already formed during replication, when pre-existing H3 is predominantly incorporated in the leading strand and newly synthesized H3 in the lagging strand. In contrast, no asymmetric divisions have been observed for the histones H1, H2A and H2B (TRAN et al. 2012; WOOTEN et al. 2019). Also the centromeric histone CENP-A (CID in flies) shows asymmetrical distribution during GSC divisions, but instead of old vs. new histones, the asymmetry of CID consists of histone quantity. CID incorporation is replication-independent and has been shown to be asymmetrically incorporated in the duplicated

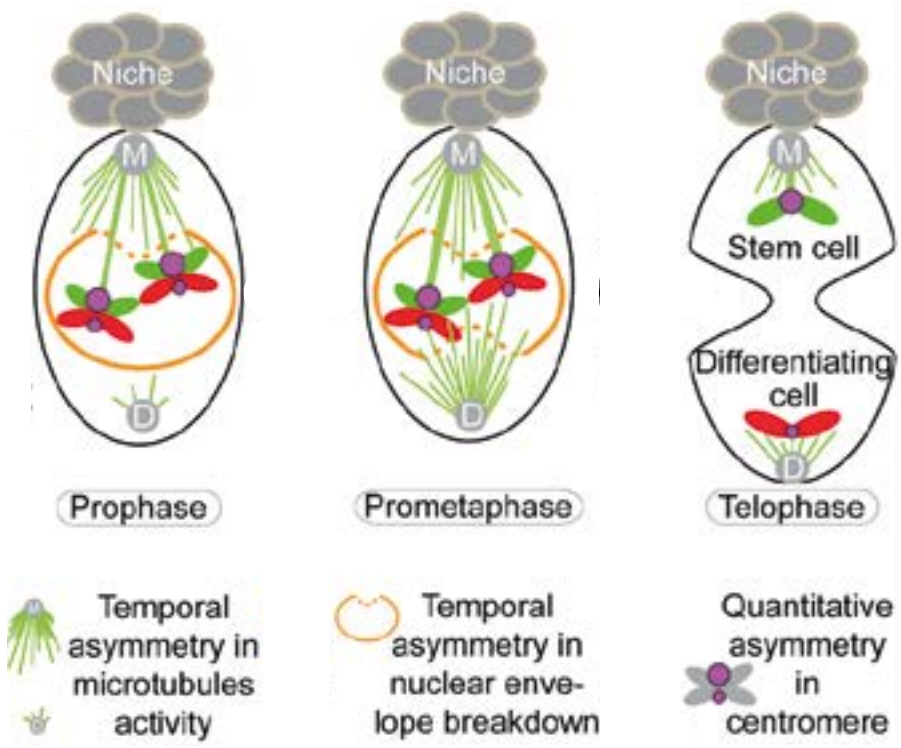

Figure 5: Asymmetric division of GSCs

Asymmetric division of GSCs occurs on many levels. Microtubules from the GSC side grow earlier, the nuclear envelope breaks down earlier at the GSC side and histones are incorporated in an asymmetric manner in the sister chromatids. M = Mother centrosome, D = Daughter centrosome RANJAN et. al. 2019

centromeres somewhere between mid/late G2 and early mitosis. Both in Drosophila testis and ovary, GSCs inherited more CID than the CBs. Consequently, also more kinetochore proteins are found at the GSC side, which catch more microtubules and both spindle formation and nuclear envelope breakdown are earlier at the GSC side, all contributing to an asymmetric division of chromosomes (Ranjan et al. 2019; Dattoli et al. 2020) (Fig. 5). This clearly demonstrates the importance of centromeres for the asymmetrical distribution of chromosomes during GSC divisions. However, asymmetrical inheritance in GSCs is not limited to histones or mitotic factors. Fichelson et. al. showed that also the nucleolar protein Wicked, a component of the U3 snoRNP required for 18S rRNA biogenesis, is inherited more by female GSCs and neuronal stem cells and is important for stem cell renewal (Fichelson et al. 2009).

1.3.2 Ribosome biogenesis and nucleolus

Stem cell maintenance seems to be tightly intertwined with ribosome biogenesis and nucleolus size. Ribosome biogenesis is essential for cell growth, since ribosome levels determine the protein synthesis rate (Rudra and Warner 2004; Frescas et al. 2007). As GSCs tend to double their size between every division, which is once a day (Neumüller et al. 2008), it is no surprise that perturbing ribosome biogenesis is detrimental for GSCs. GSCs have large nucleoli, which reflects their high rate of rDNA transcription, while in the differentiating CBs, both nucleolar size and rRNA levels decrease (Sanchez et al. 2016; Neumüller et al. 2008). In contrast, protein synthesis rates increase upon GSC differentiation and decrease again when the 16-cell cyst stage has been reached in the germarium (Sanchez et al. 2016). Accordingly, several proteins affecting the nucleolus/rRNA synthesis have been shown to affect GSC maintenance. Mei-P26, for example, seems to be involved in the RNA-induced silencing complex (RISC) pathway together with Ago1 and is highly expressed in CBs, but not in GSCs. In mei-P26 mutant ovaries, cell size and nucleolus size increase and the germaria are filled with spectrosome-containing cells. Conversely, mei-P26 overexpression results in GSC loss (Neumüller et al. 2008). The opposite effect is seen with Under developed (Udd), which is part of the RNA polymerase I regulatory complex and enriched in GSC nucleoli. Zhang et. al. showed that udd mutants have lower rDNA transcription levels and lose their GSCs in ovaries and testes. However, in bam mutant ovaries with impaired GSC differentiation, Udd and rRNA levels remained high in the germ cells. This suggests that the rate of rRNA transcription and GSC differentiation are connected (Zhang et al. 2014), although reduction of rRNA production is not sufficient to induce differentiation (Sanchez et al. 2016). Also the aforementioned protein U3 snoRNP Wicked is involved in rRNA biogenesis, namely 18S rRNA-maturation, and localizes to the nucleolus. Accordingly, ovaries of wcd mutants lose

their GSCs and also in neuronal stem cells wcd is necessary for proliferation and growth (Fichelson et al. 2009). These findings are reflected in an RNAi screen by Yan et. al. identifying genes affecting female GSC maintenance and differentiation, which showed a big overlap between genes involved in ribosome biogenesis and genes involved in neuronal stem cell maintenance (Yan et al. 2014). A second RNAi screen in Drosophila GSCs identified even more proteins involved in/part of ribosomes, the eIF3 translation initiation complex, RNA splicing, RNA polymerase I, II and III, and RNA and tRNA processing, that were important for GSC survival (Sanchez et al. 2016). Interestingly, ribosome subunits and factors involved in rRNA transcription were found more often in the GSC loss group, while ribosome assembly factors were enriched in the phenotype group with differentiation defects.

1.4 Nucleolus

The nucleolus is a large nonmembrane-bound organelle in the nucleus formed through phase separation, whose primary function is the synthesis and processing of rRNA, as well as ribosome assembly. It is organized around the rDNA genes, which are arranged in head-to-tail tandem repeat arrays, called nucleolar organizer regions (NORs) (Hernandez-Verdun et al. 2010). The nucleolus is comprised of three different subregions: the granular component (GC), the dense fibrillar component (DFC) and the fibrillar centre (FC). rDNA transcription takes place at the border between FC and DFC, while processing of the pre-rRNA transcripts occurs in the DFC and ribosome subunit assembly in the GC. (Boisvert 2007). Per cell, only a fraction of rDNA is transcriptionally active and the inactive rDNA loci are found in the nucleolus periphery, perinucleolar heterochromatin (Iarovaia et al. 2019). In *Drosophila melanogaster* the rDNA repeats are located on the X and Y chromosome, close to the pericentromeric heterochromatin (Lu et al. 2018). Apart from ribosome biogenesis, the nucleolus is also involved in many other nuclear processes, such as, but not limited to, 3D organization of the genome, stress response, DNA damage repair, cell cycle and proliferation control, transcription regulation and telomere maintenance. Centromeres are, for example, often found in close proximity to the nucleolus, because the nucleolus is important for centromeric heterochromatin formation and inhibition of RNA polymerase II transcription (Iarovaia et al. 2019; Hernandez-Verdun et al. 2010). The close proximity of the rDNA genes and the pericentromere may aid the nucleolar localization of the X and Y centromeres.

1.5 THE CENTROMERE

1.5.1 THE CENTROMERE IDENTIFIER CID

One of the components needed for cell division is the centromeric chromatin, which together with the kinetochore proteins forms the attachment between chromosomes and the mitotic spindle. It is essential for proper chromosome segregation that each chromosome exactly forms one functional centromere, since aberrant numbers result in chromosome loss and breakage (HEUN et al. 2006). However, the centromere location is not genetically defined (except for budding yeast) as centromeric DNA is not conserved between species and even differs between chromosomes of the same organism. Instead, epigenetic mechanisms are thought to define the centromere (CARROLL AND STRAIGHT 2006). The most important epigenetic centromere mark is the incorporation of the centromere-specific histone 3 variant, CENP-A, which is conserved from yeast and the holocentric *C. elegans* to monocentric animals (ALLSHIRE AND KARPEN 2008). It is sufficient to recruit inner kinetochore proteins and form functional kinetochores (HEUN et al. 2006; GUSE et al. 2011). Unlike canonical histones, CENP-A, is loaded in a replication-independent manner. In flies, CENP-A is called CID and is incorporated during mitosis by the chaperone Cal1 (ERHARDT et al. 2008; MELLONE et al. 2011; SCHUH et al. 2007), where it forms the inner kinetochore together with CENP-C. CID, Cal1 and CENP-C are interdependent and required for centromere formation (ERHARDT et al. 2008). Both depletion and overexpression of CENP-A perturb chromosome segregation, indicating that CENP-A levels are tightly regulated in vivo. Interestingly, both CENP-A depletion and overexpression lead to reduced assembly of kinetochore components. In the first case because CENP-A is missing and in the second case because the kinetochore proteins are recruited away to the ectopic CENP-A loci. In both cases reduced kinetochore protein levels impair the attachment of microtubules and lead to segregation defects (SHRESTHA et al. 2021; RÉGNIER et al. 2005; BLOWER AND KARPEN 2001; HEUN et al. 2006, RUNGE et al. 1991).

1.5.2 CENTROMERIC DNA

Although the underlying DNA sequence may not define the centromere and the deposition of CENP-A, its constitution is not entirely random. Centromeric chromatin has a unique post-translational modification pattern, which resembles neither eu- nor heterochromatic chromatin and it is often highly repetitive (SULLIVAN AND KARPEN 2004). Ectopic CENP-A is incorporated in a non-random fashion (SCOTT AND SULLIVAN 2014), indicating that even if not the exact sequence, other centromeric DNA properties like formation of heterochromatin, specific histone modifications or secondary DNA structure influence centromere localisation.

In this line, recent research has proposed that non-B form DNA structures and binding sites for specific DNA-binding factors may determine the localisation of (neo-)centromeres (Kasinathan and Henikoff 2018). The Drosophila dodeca sequence, for example, can form a dimeric i-motif, where two parallel duplexes form a four-strand intercalated structure (Garavís et al. 2015b) and the same has been shown for human alpha satellites and murine γ-satellites (Garavís et al. 2015a). Additionally, some primate centromeres harbour CENP-B boxes binding CENP-B, which directly interacts with CENP-A and CENP -C (Fachinetti et al. 2015; Haaf et al. 1995; Masumoto et al. 1989). CENP-B boxes and CENP-B are not present in *Drosophila melanogaster*. Recently, the Drosophila centromeric regions have been sequenced and were found to contain islands of complex DNA enriched in retroelements, flanked by blocks of simple satellite repeats. Non-LTR long interspersed nuclear element (LINE)-like elements called G2/Jockey-3 were especially abundant and the only element present at all centromeres. Although no centromere harboured unique elements, each centromere had a unique composition of repeats. It also should be notified, that none of the centromeric sequences identified are exclusively found at centromeres, but are also present in other heterochromatic and euchromatic regions. Surrounding these retrotransposons, several short satellite repeats are located, such as dodeca, AATAT, AAGAG, AATAG, AAGAT and the 10-bp satellite prodsat (Chang et al. 2019).

1.5.3 Pericentric DNA

The chromatin flanking the centromeric region is called the pericentric heterochromatin. Although the boundaries between centromeric and pericentric heterochromatin are not known yet, we do know that pericentric heterochromatin is also highly repetitive and consists of satellite sequences in many species. Mouse pericentromeres are constituted of major satellite repeats (minor satellite repeats are found predominantly at the centromere), humans have α-, β- and γ-satellites, as well as satellite I, II and III (Fioriniello et al. 2020), and Drosophilas harbour more than 17 different satellite repeats (Shatskikh et al. 2020). Some Drosophila satellite repeats are also found at the centromere, such as simple satellite repeats, dodeca and the intergenic spacer of ribosomal genes (IGS, 240 bp) (Chang et al. 2019). Others like the 1.688 family (260 – 372 bp) and Rsp repeats (120 bp) are located at the pericentromere, among other places (Shatskikh et al. 2020). In contrast to the centromere, the pericentromere possesses classic heterochromatic histone modifications such as H3K9me2, H3K9me3, and H3K27me3 and H4K20me3 and is bound by the heterochromatin protein HP1 (Nishibuchi and Déjardin 2017). Pericentric heterochromatin has been shown to have multiple roles: it maintains the boundary between the centromere and euchromatic chromatin, is important for proper sister chromatid cohesion and

chromosome segregation, represses meiotic recombination of centromeres and silences the transcription of transposable elements (Fioriniello et al. 2020). In mice and Drosophila, pericentric satellites are bound by HMGA1/D1, bundling the pericentric heterochromatin in chromocenters to facilitate nuclear assembly after cell division and preventing micronuclei formation (Jagannathan et al. 2018). Furthermore, it has been shown in multiple species that pericentric heterochromatin creates a repressive environment which also affects proximal loci. This is actively used by cells, which relocate genes to and from the pericentric heterochromatin in order to change their transcriptional status (Fioriniello et al. 2020).

1.5.4 (Peri-)centromeric transcription

Since the centromere is embedded in the pericentric heterochromatin, both were long believed to be transcriptionally silent. However, increasing numbers of RNA polymerase sightings have been reported at the centromere, and (peri)centromeric satellite transcripts have been documented in numerous species. This ranges from fission yeast (Volpe et al. 2002; Kato et al. 2005; Choi et al. 2011), Arabidopsis (May et al. 2005), maize (Du et al. 2010), Drosophila (Usakin et al. 2007; Salvany et al. 2009; Rošić et al. 2014), beetles (Pezer and Ugarković 2009), Xenopus (Blower 2016; Grenfell et al. 2016) to humans (Wong et al. 2007; Valgardsdottir et al. 2008; Ting et al. 2011), mice (Gaubatz and Cutler 1990; Rudert et al. 1995; Bouzinba-Segard et al. 2006) and horses (Cerutti et al. 2016). While satellite RNAs are often found in mitotic as well as interphase cells, centromeric RNA synthesis levels have been reported to be cell cycle-dependent, mostly occurring during mitosis. In murine cells, minor satellite repeats are transcribed at low levels during S phase into short transcripts and at high levels during G2/M phase with a large variety of transcript lengths (Ferri et al. 2009; Lu and Gilbert 2007). In Drosophila S2 cells RNA polymerase II was only detected at the centromere during M/G1 phase and not during S/G2 (Bobkov et al. 2018). On the other hand, the FACT complex, which allows the progression of the transcriptional machinery through chromatin, was localizing to the Drosophila centromere both in mitosis and interphase (the latter at lower levels) (Chen et al. 2015). Also in HELA cells, RNA polymerase II has been found at the centromere during mitosis. There, alpha satellite transcript levels reduced drastically when the RNA polymerase II was specifically inhibited during mitosis (Chan et al. 2012). In most systems, centromeric transcripts seem to be synthesized by RNA polymerase II (Talbert and Henikoff 2018) and a subset of them were found to be polyadenylated (Topp et al. 2004; Choi et al. 2011; Wei et al. 2020).

(Peri)centromeric transcripts and heterochromatin formation

Depending on the organism, (peri)centromeric transcripts may be further processed by the RNAi machinery. This is well established in fission yeast, where dsRNA is cleaved by Dicer to form small interfering RNAs (siRNAs) of 22-24 nucleotides which are loaded by Ago1 and together with other factors form the RNA-induced initiation of transcriptional gene silencing (RITS) complex which initiates heterochromatin formation. The siRNAs target the complex to specific chromatin regions probably by base pairing with DNA or nascent RNA (Biscotti et al. 2015). When the RNAi pathway is disturbed, the centromeric chromatin is derepressed and centromeric transcripts accumulate (Volpe et al. 2002). This means, that centromeric RNAs can repress their own transcription by inducing heterochromatin formation. Similarly, it has been suggested that murine satellite RNA is bound by Dicer (Gutbrod et al. 2021) and in chicken–human hybrid DT40 cells, Dicer loss-of-function resulted in α-satellite transcript accumulation and HP1 mislocalization to chromosome arms, also pointing towards a heterochromatin maintenance role for Dicer-processed centromeric transcripts.

In Drosophila, a similar pathway seems to be involved, namely the piRNA pathway which is responsible for the silencing of transposable elements (TE) throughout the whole genome in the germline. In short, the highly abundant and repetitive TEs can replicate and insert themselves in new genomic locations, which can lead to DNA damage, which is especially detrimental in the germ line, where it can cause sterility. To protect germ cells from transposition, the piRNA-induced silencing complex (pi-RISC), consisting of a protein from the PIWI subfamily of the Argonaute nucleases and a piRNA, silences TE expression. piRNAs are generated from active TE copies or from transcripts from piRNA clusters, which contain inactivate TE remnants. The piRNA is then bound by the PIWI protein and guides it to complementary TE transcripts in the cytoplasm for cleaving. Furthermore, in the nucleus, the piRNA pathway also recruits repressive chromatin modifications to the genomic loci of TEs to inhibit transcription. Many additional proteins have been identified to play a role in the piRNA pathway, be it for transcribing piRNA clusters, processing piRNAs, piRNA loading or creating more piRNAs from cleaved TE transcripts (the ping-pong cycle) (Tóth et al. 2016).

Coming back to the role of the piRNA pathway in regulating satellite repeats in Drosophila, it has been reported that the piRNA pathway proteins Aub, Piwi and Spn-E derepress pericentric heterochromatin when mutated (Pal-Bhadra 2013) and depletion of Spn-E increases satellite transcripts in ovaries (Usakin et al. 2007). Additionally, complex satellite transcripts seem to be bound by the Piwi, Aub and Ago3 proteins of the piRNA pathway in

the Drosophila ovary. Last, the genomic loci of satellite repeats have been shown to interact with the non-canonical Rhino-Deadlock-Cutoff pathway which licenses transcription from dual-strand piRNA clusters in Drosophila ovaries. However, depletion of Rhino did not lead to an accumulation of satellite transcripts, so these results are still inconclusive (Wei et al. 2020). Another example in flies, are the AAGAG repeats. In Drosophila embryos, AAGAG repeat transcripts associate with early forms of heterochromatin and are essential for larval survival. The AAGAG RNA is also visible in spermatocytes and at chromocenters in polytene salivary glands. When depleted in testes, the AAGAG transcripts impair histone-protamine exchange and cause nuclear organization defects, leading to sterility (Pathak et al. 2013; Mills et al. 2019).

(Peri)centromeric transcripts and centromere function

Interestingly, the (peri)centromeric transcripts also seem to be important for centromere and kinetochore function, either directly or through the formation of pericentric heterochromatin, as mentioned before. In mice, for example, CENP-A, Aurora B and Survivin (both belonging to the chromosomal passenger complex (CPC) involved in correct spindle attachment) have been detected in a minor satellite RNA-pulldown and both Aurora B kinase activity as well as its binding to CENP-A were shown to be RNA dependent (Ferri et al. 2009). Also in Xenopus egg extracts centromeric lncRNAs were detected at mitotic chromosomes and the spindle. They were shown to interact with Aurora B and to be important for its proper localization, while knockdown (KD) of the centromeric RNAs resulted in aberrant kinetochore-microtubule attachments (Blower 2016). A similar mechanism has been found in humans, where satellite I transcripts localize to the centromere in interphase and bind Aurora B and INCENP (another CPC protein) during mitosis. Also here, KD of satellite I leads to mislocalization of the CPC and impaired microtubule connection to chromosomes (Ideue et al. 2014). Additionally, α satellite transcripts bind to CENP-C and there are indication that also CENP-A and CENP-B may be bound (Wong et al. 2007; McNulty et al. 2017). It is still debated whether human α satellite transcripts stay attached at the transcription location. While co-localisation of α satellite transcripts with their genomic locus during mitosis, as well as with CENP-C during interphase in the nucleolus, has been shown (Wong et al. 2007; McNulty et al. 2017), this could not be verified by Bury et. al. where α satellite RNA barely co-localized with centromeric regions during the cell cycle (Bury et al. 2020). Nonetheless, KD of α satellites reduced CENP-A and CENP-C levels at the centromere and led to lagging chromosomes during mitosis (Chan et al. 2012; McNulty et al. 2017). Also in Drosophila, centromeric transcripts have been detected at the centromere and KD of the 359 bp satellite III (sat III) repeat leads to chromosome missegregations in S2 cells as well as embryos. The

observed lagging chromosomes harbored less CID and CENP-C than the correctly separating chromosomes and it was shown that Satellite III RNA is important for stabilizing new CID at the centromere (Rošić et al. 2014; Bobkov et al. 2018).
It should be noted, that not only the centromeric transcripts themselves, but also the act of transcription is important for the centromere. Specifically, it has been shown that the progression of the transcription machinery through centromeric DNA is necessary for new CID deposition (Chen et al. 2015; Molina et al. 2016; Bobkov et al. 2018).

Misregulation of satellite repeat expression

Although the presence of satellite transcripts are important for mitosis and heterochromatin formation, RNA levels need to be tightly regulated as overexpression of satellite transcripts in both mouse and human cells has been shown to induce mitotic defects (Bouzinba-Segard et al. 2006; Chan et al. 2017). The expression of high levels of centromeric transcripts seems to occur when the cell is stressed (Jolly et al. 2004; Valgardsdottir et al. 2005; Valgardsdottir et al. 2008; Hédouin et al. 2017), upon aging (Swanson et al. 2013; Cecco et al. 2013), in cancers (Ting et al. 2011) and has been connected to drug resistance (Kanne et al. 2021). Whether a causative or only as a secondary effect, high satellite RNA expression only may be an indication for cells experiencing a form of deregulation. Furthermore, disruption of the nucleolus increases satellite RNA levels. In humans, it has been shown that localization of centromeres to the nucleolus in interphase helps to repress α satellite transcription, while localisation of centromeres to the nucleolus has been suggested to be dependent on α satellite RNA. Disruption of the nucleolus by inhibiting RNA polymerase I, resulted in higher α satellite levels, as well as α satellite mislocalisation away from the nucleolus (Bury et al. 2020; Wong et al. 2007). In Drosophila, in contrast, KD of (peri) centromeric AAGAG repeats resulted in nucleolus fragmentation, showing that a reciprocal dependency may exist (Pathak et al. 2013).

The Drosophila 359 bp repeat Satellite III

Since our lab has shown that depletion of sat III transcripts reduces CENP-A and CENP-C levels at the centromere during mitosis and leads to mitotic defects in S2 cells and Drosophila embryos (Rošić et al. 2014), we set out to investigate the role of sat III RNA in more detail.
Sat III belongs to the 1.688 satellite family, which includes repeats of similar length and sequence, which are expressed as ncRNAs in many tissues including the gonads. E.g. 1.688 RNA FISH showed foci in primary spermatocytes and in ovary nurse cells (Wei et al. 2020). The 359-bp repeat sat III is found along an estimated 11 Mb stretch on the X-chromosome, next to the rDNA locus, covering its pericentric region (Blattes et al. 2006). The other

repeats belonging to the 1.688 family are found at the chromosome arms 2L and 3L (Usakin et al. 2007). Sat III is transcribed by RNA polymerase II in both sense and antisense direction forming transcripts of several repeat lengths. The longest transcript obtained by cloning was 4 repeats long and polyadenylated (Rošić et al. 2014). However, most likely a large subset of sat III transcripts are non-polyadenylated (Wei et al. 2020). As to the localization of sat III transcripts, different observations have been made. The transcripts were both shown to only localise to the (peri)centric region of the X-chromosome and in *trans* to other centromeres (Bobkov et al. 2018; Rošić et al. 2014) and it is not yet clear which applies. While overexpression did not show any defects in S2 cells, LNA depletion of sat III severely affected mitosis, as mentioned before (Rošić et al. 2014). It has been shown that sat III RNA is already expressed in the pre-blastodermal embryo, where the involvement of the transcription factor homothorax (hth) has been suggested, since hth mutants have lower sat III levels including mitotic defects (Salvany et al. 2009). Furthermore, sat III RNA is one of the satellite repeats that was bound by the piRNA pathway proteins Piwi, Aub and Ago3 (Wei et al. 2020). Interestingly, there is a fly line, zhr^1, which lacks (most of) the sat III locus on chromosome X due to a translocation with the Y-chromosome (Sawamura et al. 1993; Ferree and Barbash 2009) (Fig. 6). While these flies are viable, their embryos show increased mitotic defects when stressed and will subsequently die (Rošić et al. 2014), which resembles the phenotype seen in S2 cells and embryos with sat III depletion. Therefore, zhr^1 flies are a very useful control when investigating the role of sat III RNA.

Until now, it remains unknown whether sat III RNA is modified (apart from polyadenylation) and how the non-coding transcripts are regulated, as well as which proteins are involved in these processes.

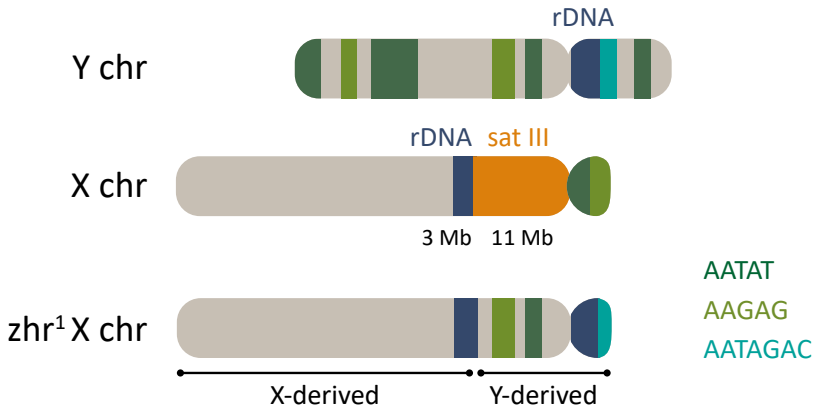

Figure 6: Drosophila X and Y chromosome

Sat III repeats are located at the pericentromere of the X chromosome, next to the rDNA locus. The zhr^1 X-chromosome has lost (the majority of) the sat III locus due to a translocation with the Y-chromosome. Other satellite repeats present on the X and Y chromosome are indicated.
Modified from Lu et. al. 2018

1.6 Aim

(Peri)centromeric RNAs have turned out to be vital for heterochromatin formation and proper chromosome segregation. In *Drosophila melanogaster* sat III RNA localises to the centromere and is important for stabilization of new CENP-A/CID. However, it is not clear how sat III transcripts carry out their centromeric function and how they are regulated. Furthermore, sat III RNA may have more functions in combination with other proteins. It has been shown for example, that sat III is expressed in the germline at a stage where no further divisions take place, which makes a role at the centromere less likely. To address this question, I performed a sat III RNA-pulldown to identify new sat III RNA binding candidates and characterized these proteins and sat III RNA in the context of the Drosophila female germline.

2. Results

2.1 Identification of novel sat III RNA binding partners

Sat III RNA transcripts are important for proper chromosome segregation in S2 cells, but its mechanism of action remains elusive. We set out to identify interactors of sat III RNA to shine more light on the pathways it might be involved in.

2.1.1 Sat III RNA pulldown

In order to identify binding partners of sat III RNA, I performed RNA-pulldowns (Fig. 7A). Sat III sense and antisense RNAs containing streptavidin-binding S1m loops (Leppek and Stoecklin 2014) were synthesized by in vitro transcription and incubated with Drosophila S2 cell lysate. Streptavidin beads were added and after a few washing steps proteins bound to sat III RNA were eluted by adding RNase A and subsequently analysed by LC-MS (at the Mass Spectrometry facility of the ZMBH). Because we were not sure whether the cell lysis conditions allowed the extraction of proteins tightly incorporated into the chromatin, in a second pulldown, I repeated the experiment with a higher lysis buffer salt concentration (500 mM instead of 150 mM NaCl) that may allow the extraction of more tightly bound chromatin factors to be eluded. On the downside, this may have caused the disruption of proteins bound more loosely to the RNA. Therefore, the two repeats of the RNA-pulldown are not completely identical but complement each other. As controls for the pulldowns, I used

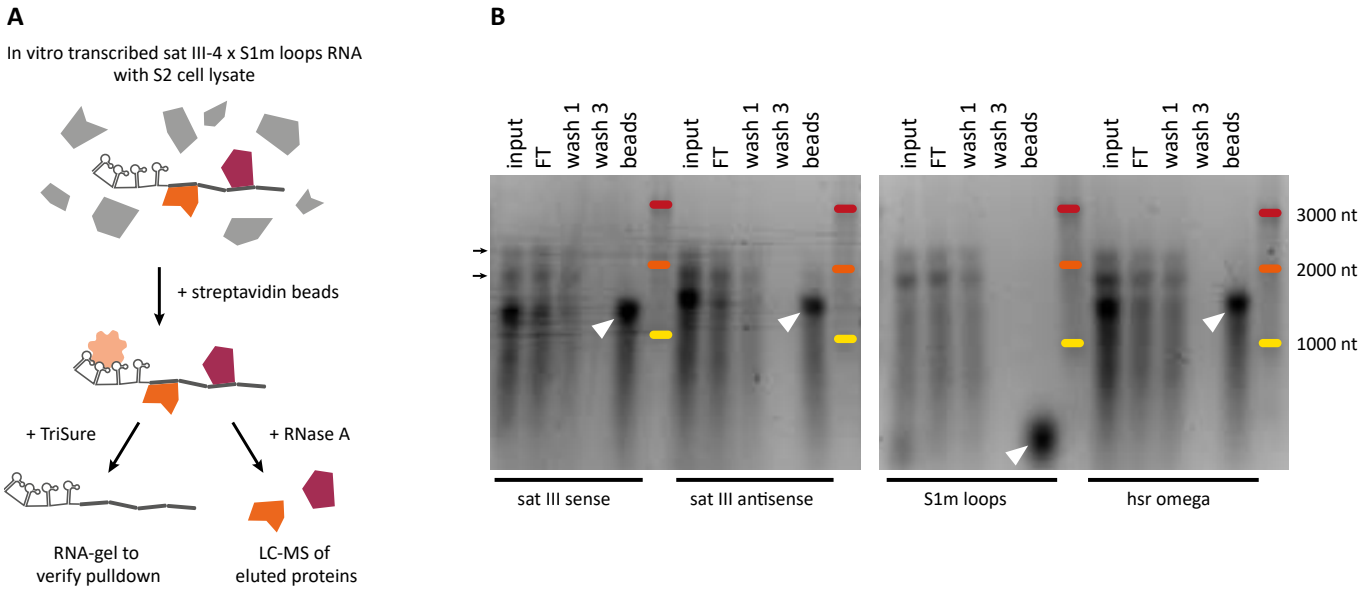

Figure 7: sat III RNA pulldown

A. Overview of the sat III RNA pulldown experiment.

B. Denaturing RNA gel of different steps of the RNA pulldown experiment. The RNA ladder is indicated by coloured bands. White triangles point to the RNA pulled down. Black arrows indicate the rRNA bands.

the S1m loop sequence on its own and hsr omega RNA with S1m loops (the latter only in the second repeat). Hsr omega is a lncRNA, which is increasingly expressed after heat shock and whose different isoforms are found in the nucleus or the cytoplasm (PRASANTH et al. 2000; MCKECHNIE et al. 1998). I used the sequence that was closest in length to the full length sat III sense and antisense sequence, which is the cytoplasmic hsr omega-c transcript.

To monitor the quality of the RNA pulldown, I extracted RNA from samples taken during the different pulldown steps and ran them on a denaturing RNA gel (Fig. 7B). In the input lanes a clear band of the in vitro transcribed RNAs is visible, together with rRNA bands originating from the S2 cell lysate (black arrows). Because the in vitro transcribed RNAs bind to the beads, only little is detectable in the flowthrough. The last lane shows the RNA bound to the beads before the elution step with RNase A. A band of the corresponding RNA transcript size is clearly visible for each pulldown (white triangle). A smear below the actual RNA band suggests that there was some RNA degradation.

2.1.2 OVERVIEW OF THE PUTATIVE SAT III RNA-BINDING PROTEINS

After filtering out the proteins that were human contaminants, I selected the proteins that had an enriched peptide count in the sat III sense pulldown compared to the S1m loop control. This resulted in 254 hits for the first and 149 for the second pulldown with an overlap of 72 proteins (Fig. 8A, B, Suppl. table 1, 2). The lower number of enriched proteins in the second repeat is likely the result of the more stringent cell lysing conditions which may disrupt more interactions. Notably, in the first repeat, peptide counts from the sat III antisense pulldown were predominantly lower than from the sat III sense RNA pulldown and partially also lower than the S1m loop control (Fig. 8C). Therefore, I focused on the proteins enriched in the sat III sense pulldown. In the second pulldown, I included the lncRNA hsr omega and as it turned out, many proteins that were pulled down with sat III sense and antisense transcripts were also found in the hsr omega sample. The list of proteins that were enriched in the sat III pulldowns but not in the hsr omega or only S1m-loops sample, consisted mostly of ribosomal proteins. Therefore, I did not exclude proteins that also bound to hsr omega, but did take the peptide counts into account while choosing my candidates. In contrast to the first repeat, the second sat III antisense pulldown had many hits, some even specifically enriched in the antisense sample (Fig. 8C). Especially tRNA synthetases and ribosomal proteins had high peptide counts in the sat III antisense sample. The tRNA synthetases were only identified in the second pulldown and are, therefore, not found in the diagram. Among the proteins that were enriched in both the sat III RNA pulldowns, 50% were ribosomal proteins, 21% were RNA-processing proteins and 8% were uncharacterised proteins (Fig. 8D). Furthermore, also

histones, translation initiation factors and proteins involved in cytoskeleton organization were found. We were surprised to find many uncharacterised proteins among the hits with the highest enriched peptide counts. Among them where CG13096 and CG12128 (Fig. 8E), which had been linked to the centromere before, and are detailed below. Additionally, I chose three additional uncharacterised proteins, which were only found in the first sat III pulldown, but seemed to interact with CG13096 and CG12128 according to some STRING

A

	1st pulldown	2nd pulldown
Number of identified proteins	402	195
- w/o human proteins and streptavidin	393	171
- with at least 1 peptide in sat III S or AS pulldown	359	162
- with more peptides in sat III S pulldown compared to loops only	254	149

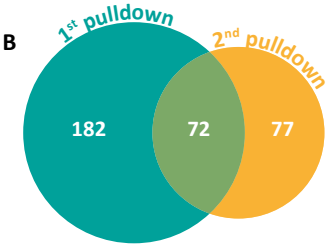

C

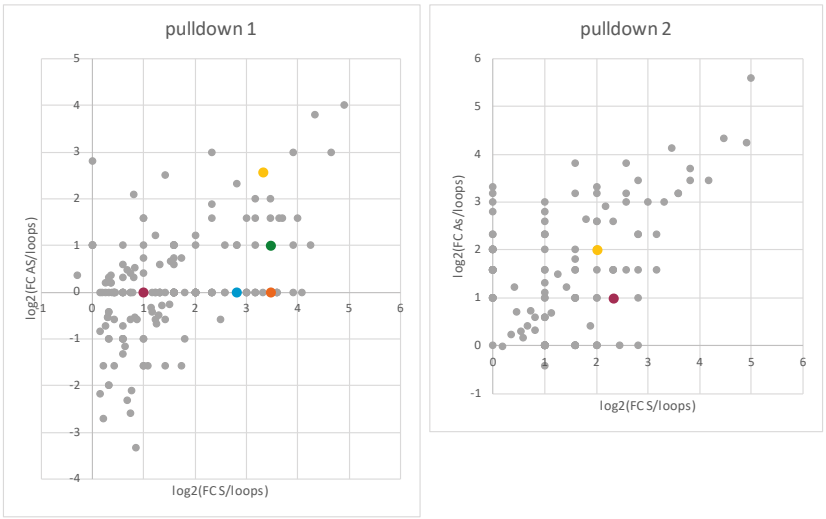

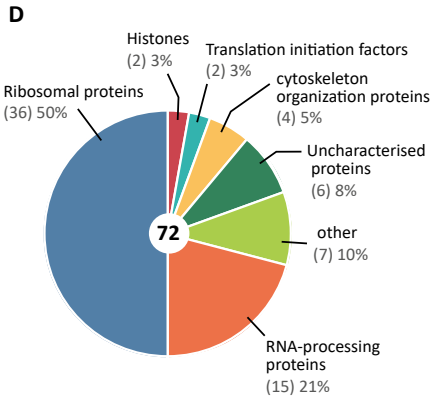

E

	1st Pulldown			2nd Pulldown			
	sat III S	sat III AS	loops only	sat III S	sat III AS	hsr omega	loops only
Centagon 1	7	1	1	0	0	0	0
Centagon 2	11	2	0	0	0	0	0
Centagon 3	10	6	0	12	12	10	3
Centagon 4	11	1	1	0	0	0	0
CG12128	2	0	0	5	2	2	0

Figure 8: Sat III transcripts pull down uncharacterised proteins

A. Number of proteins identified in the pulldown and filtering steps applied.

B. Overlap of the proteins identified in both pulldowns.

C. Fold change log2 values of the peptide count enrichment of the sat III pulldowns over the loops only pulldown. The peptide count enrichment of the sat III sense pulldown are plotted on the X-axis and the peptide count enrichment of the sat III antisense pulldown are plotted on the Y-axis. Each dot corresponds to one protein found in both pulldowns. The Centagon complex proteins and CG12128 are indicated in colour. In the first pulldown, some Centagon proteins are located on the X-axis because they were only enriched in the sat III sense pulldown.

D. Functions of the proteins found in both pulldowns. The absolute number is placed in brackets.

E. Peptide count numbers of the uncharacterised proteins of interest.

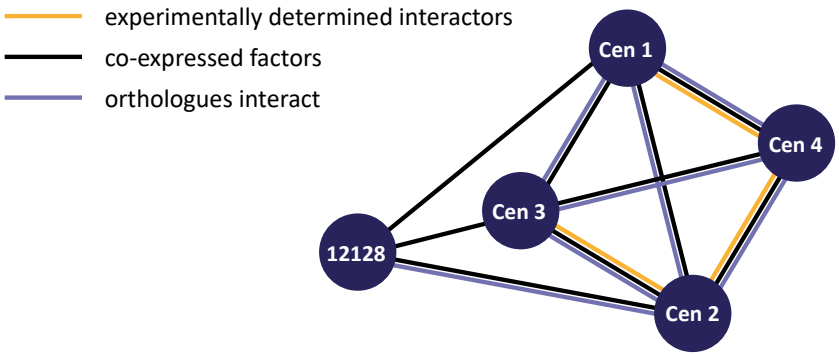

	Putative function	Human orthologue	*Identity*	*Similarity*
Centagon 1	Nucleolar protein	NOC3L	*35%*	*55%*
Centagon 2	RNA-methyltransferase	NOP2	*41%*	*55%*
Centagon 3	Ribosomal protein	RSL1D1	*23%*	*42%*
Centagon 4	RNA-helicase	DDX54	*42%*	*58%*
CG12128	RNA-methyltransferase	SPOUT1 (CENP-32)	*49%*	*69%*

Figure 9: The Centagon proteins may form a complex
Schematic view of interactions between the Centagon proteins according to STRING analysis (https://string-db.org/). Putative functions and human orthologues are detailed below, together with the percentage of identical and similar amino acids in *Drosophila melanogaster* and Human.

analysis (Fig. 9). Although other factors had an even higher peptide count enrichment in the sat III RNA pulldown, we focused on the four mentioned candidates because they had not been characterised before, were predicted to be in a complex and all had a link to the centromere or satellite RNA in the literature.

During the course of my experiments, CG12128 turned out to not have the same effects on the female reproductive tract as the other candidates (Fig. 21). Since the protein is very similar to the other candidates (found in the same RNA-pulldown and localising to the nucleolus) and has putative centromeric and mitotic functions, it served as a negative control in some experiments, and is introduced as well. Most experiments, however, were only conducted with CG13096, CG1234, CG8545 and CG32344. In my experiments, these four factors turned out to be essential for gonad development, which is why we termed the complex CENtromeric Transcript-Associated GONadal (Centagon) complex and the factors Centagon 1 (CG1234), Centagon 2 (CG8545), Centagon 3 (CG13096), and Centagon 4 (CG32344).

2.1.3 Centagon 1 (CG1234)

Centagon 1 is predicted to be a nuclear protein with chromatin binding properties (https://flybase.org/). Looking at the predicted domains (Fig. 10), the CCAAT-binding domain binds to a DNA consensus-sequence upstream of transcription initiation sites. It is present in proteins involved in 60S ribosomal subunit biogenesis. The armadillo-type fold is a structure that accommodates binding to large substrates such as proteins or nucleic acids (https://www.ebi.ac.uk/interpro/). Furthermore, it has a sequence reminiscent of the human Nucleolar Complex Protein 3 Homolog (NOC3L) protein. The yeast orthologue, NOC3p is important for replication initiation (Zhang et al. 2002) and 60S ribosomal subunit biogenesis (Milkereit et al. 2001). The human NOC3L has predominantly been researched in the context of adipocyte differentiation. There it has been shown that NOC3L promotes adipocyte differentiation by controlling DNA replication (Johmura et al. 2008). Interestingly, KD of Drosophila Centagon 1 has been identified in a screen to cause shorter mitotic spindles (Somma et al. 2008).

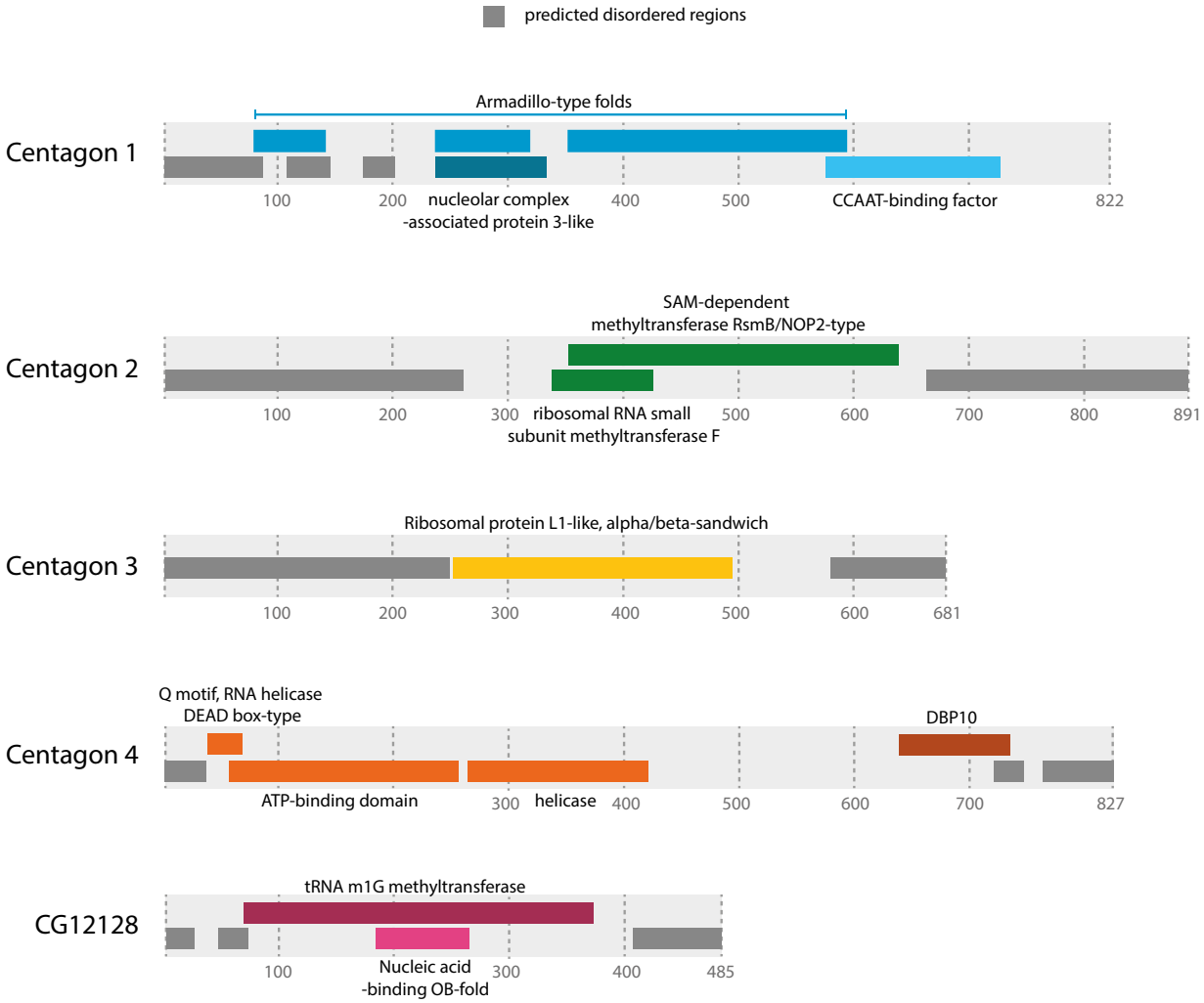

Figure 10: Predicted domains of the Centagon proteins and CG12128
According to https://www.ebi.ac.uk/interpro/

2.1.4 CENTAGON 2 (CG8545)

Inferred from its predicted domains (Fig. 10) and orthologues, Centagon 2 is a putative rRNA methyltransferase possibly involved in LSU-rRNA maturation (https://flybase.org/). Its human orthologue is the Nucleolar Protein 2 Homolog (NOP2) that is necessary for active cell proliferation (FONAGY et al. 1992) and is involved in the maturation of the large ribosomal subunit (SLOAN et al. 2013). In yeast, NOP2 has been reported to methylate a cytosine residue of 25S rRNA and was shown to be essential for proper rRNA processing (SHARMA et al. 2013). Furthermore, human NOP2 has been shown to act together with a lncRNA in the liver regulating nucleolar activity, cell proliferation and stem cell-like features (WANG et al. 2014). However, it can also interact with repetitive RNAs as it has been shown to bind the telomerase RNA component (TERC) thereby activating transcription of the cyclin D1 gene together with telomerase and regulating the cell cycle (HONG et al. 2016). Importantly, NOP2 also has been found in a human alpha satellite RNA-pulldown (ZHU et al. 2018), suggesting a conserved interaction with centromeric RNAs. Additionally, Centagon 2 was co-immunoprecipitated with CID in our lab (unpublished data, Sarah Doppler), emphasizing a possible role at the centromere.

2.1.5 CENTAGON 3 (CG13096)

Centagon 3 is predicted to be a ribosomal-like protein and an orthologue to the human RSL1D1. They share the ribosomal protein L1 alpha/beta-sandwich domain (Fig. 10), which binds to RNA (TISHCHENKO et al. 2007). Human RSL1D1 has been shown to regulate the nucleolar localisation of nucleostemin, which promotes continuous proliferation of stem cells and cancer cells (MENG et al. 2006). It also has been found to influence cell proliferation by binding to and repressing the translation of PTEN mRNA, a factor important for replicative senescence (MA et al. 2008). However, upon DNA-damage RSL1D1 has been suggested to promote apoptosis (LI et al. 2012), indicating that it may be involved in pathways with opposing functions. Interestingly, RSL1D1 also has been found as a top hit in a human alpha-satellite pulldown but no further experiments or validation has been conducted in this context (ZHU et al. 2018).

2.1.6 CENTAGON 4 (CG32344)

The predicted domains show that Centagon 4 probably belongs to the DEAD box RNA helicase family (Fig. 10), whose members are involved in RNA metabolism in several ways. In the nucleus their functions include transcription, mRNA-splicing and ribosome biogenesis (LINDER AND JANKOWSKY 2011). Its human orthologue, DDX54, has been categorized as a protein involved in ribosomal biogenesis, but also has been shown to repress transcription

by binding to nuclear receptors (Rajendran et al. 2003). Furthermore, it has been implicated to act in the early DNA damage response by splicing genotoxic stress-responsive transcripts (Milek et al. 2017). Although DDX54 itself has not been found in the human alpha-satellite RNA-pulldown, several other DEAD box helicases have (Zhu et al. 2018). Additionally, DEAH and DEAD box RNA helicases have been shown to bind the human satellite I ncRNA which is important for proper chromosome segregation (Nishimura et al. 2019). This suggests a more general centromeric RNA-binding capacity of the DEAD box RNA helicase family. Centagon 4 also has been identified in a CID pulldown of associated factors in Drosophila S2 cells (Barth et al. 2015).

2.1.7 CG12128

CG12128 has a tRNA (guanine-N1-)-methyltransferase domain (Fig. 10) with a rare alpha/beta knot structure, which is conserved in the SPOUT family (https://www.ebi.ac.uk/interpro/). It's human orthologue, SPOUT1, has been identified to bind mRNA (Baltz et al. 2012) as well as the miR-145 hairpin (Treiber et al. 2017). However, Ohta et al. renamed it centromere protein 32 (CENP-32) upon proteomics analysis that predicted mitotic chromosome association of CENP-32. Streptavidin-binding peptide–tagged CENP-32 accumulated on mitotic spindles and at kinetochores (Ohta et al. 2010). In addition, CENP-32 was necessary for tethering the centrosome to the spindle poles (Ohta et al. 2015).

2.2 Validation of novel sat III RNA binding partners

2.2.1 Centagon 1, 2, 3 and 4 interact in a Yeast-two-Hybrid (Y2H) assay

To assess whether the aforementioned proteins can indeed form interactions, as was suggested by STRING analysis (Fig. 9), I performed a Y2H assay. To this end, the four proteins with the strongest indication of interaction were cloned into the pMM5-LexADNA and pMM6-Gal4pTA plasmids, tagging the protein sequences with a DNA-binding domain (LexA) or a transactivation domain (Gal4p). When joined, these two domains activate reporter genes under the control of GAL4-UAS, in this case β-galactosidase. These plasmids were co-transformed in different combinations into competent yeast cells and left to grow 3 days at 30 degrees on agar plates. Three colonies of each combination were dissolved into YPD medium and pipetted onto a new plate, which was covered with an X-Gal-containing overlay the next day. Yeast cells whose tagged proteins interacted turned blue, because the expressed β-galactosidase hydrolyses X-Gal thereby releasing a blue dye.

The Y2H assay was repeated 3 times (Fig. 11A) and showed that Centagon 2 interacted with Centagon 1, 3 and 4 in the assay consistently (red circles). The conversed plasmid combinations

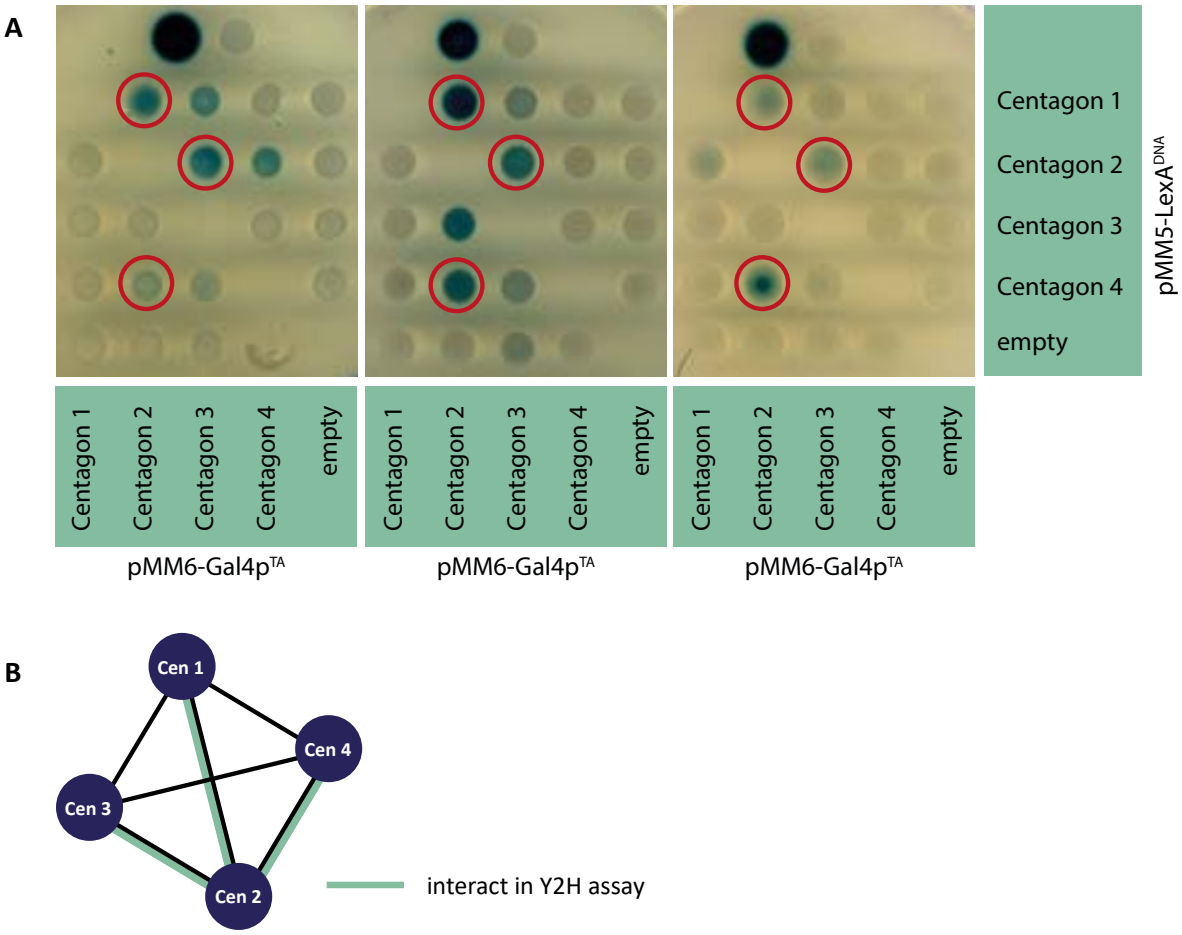

Figure 11: The Centagon proteins interact in a Yeast-Two-Hybrid assay
A. Three replicates of the Y2H assay. The positive control (Rdx and Cal1) and negative control (empty plasmids) are found in the first row. Combinations positive in all three repeats are encircled in red. B. Schematic representation of the interactions found in the Y2H assay.

only gave positive results in one of the three assays. Furthermore, combinations with pMM6-Gal4p-Centagon 3 gave false positives in the second repeat as seen by the blue colour of the yeast cells co-transformed with an empty pMM5-LexA control plasmid. However, the staining of the yeast cells containing the combination with pMM5-LexA-Centagon 2 is clearly brighter than the false positives and was the only one repeatedly positive. Therefore, I concluded that a direct interaction between Centagon 1, 2, 3 and 4 seems likely, with Centagon 2 being at the center of these interactions (Fig. 11B).

2.2.2 Centagon 3 is an RNA-binding protein as shown by EMSA

In order to validate the RNA-protein interactions, İzlem Su Akan, who was a master student in our lab, performed an Electromobility Shift Assay (EMSA). Because Centagon 3 was one of the candidates found in both pulldowns and the only one we were able to purify in sufficient amounts and purity, we decided to use this protein as an example. To this end, a GST-tagged version of Centagon 3 was purified from E. coli and incubated with in vitro transcribed sat

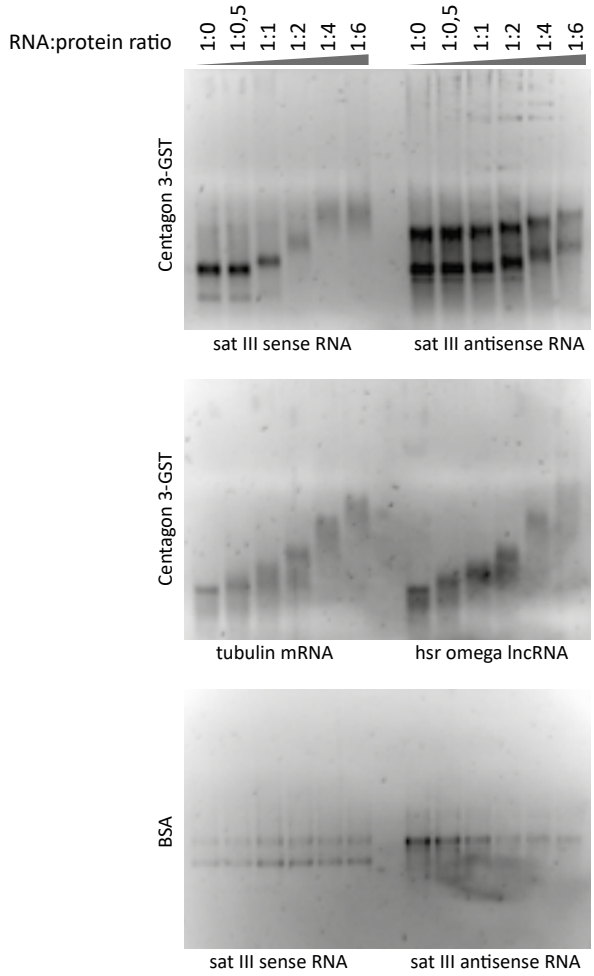

Figure 12: Centagon 3 interacts with sat III RNA in vitro
Non-denaturing RNA gel with different Electromobility Shift Assays. The molar ratio of RNA and protein is shown on top. The experiment was performed by İzlem Su Akan and was also published in her master thesis.

III transcripts as well as a tubulin mRNA control and the hsr omega lncRNA of a similar length. All transcripts were heated to 65˚C for 10 min and left at RT to cool down and refold before use. RNA and protein were mixed at different molar ratios (Fig. 12) and incubated 1 hour on ice before loading on a non-denaturing RNA gel, which was stained with ethidium bromide afterwards. As seen in Fig. 12, addition of GST-Centagon 3 lead to a shift of all four transcripts. Interestingly, the gel with sat III antisense RNA looked different from the other three EMSAs, with only a small shift visible at the bottom, but higher bands appearing in the upper region. All other transcripts behaved similarly upon addition of GST-Centagon 3 with a gradual shift upon increasing protein:RNA molar ratios. As can be seen on the gel images, sat III transcripts form two bands in the EMSA, also without addition of protein. Since these bands are not visible under denaturing conditions, they must be the result of secondary structures. Control EMSAs with bovine serum albumin did not lead to any shifts of the transcripts. In conclusion, we showed that Centagon 3 is a bona fide RNA-binding protein, albeit not specific for sat III.

2.3 Characterisation of the Centagon proteins in S2 cells

2.3.1 Protein localisation in S2 cells

In order to assess the localisation of the Centagon complex, S2 cells were transfected with constructs containing N-terminally GFP-tagged protein sequences of the Centagon members with a copia promoter and stable cell lines were made. The cells were fixed and stained with α-tubulin antibody to mark the spindles. Interestingly, all four Centagon proteins localised to the nucleolus during interphase and to the spindles adjacent to the metaphase plate during mitosis (Fig. 13A). During anaphase the signal was distributed more broadly on the spindles, while during telophase the tagged Centagon proteins were found close to the newly forming nuclei, to be eventually incorporated into the new nucleoli again. These findings were

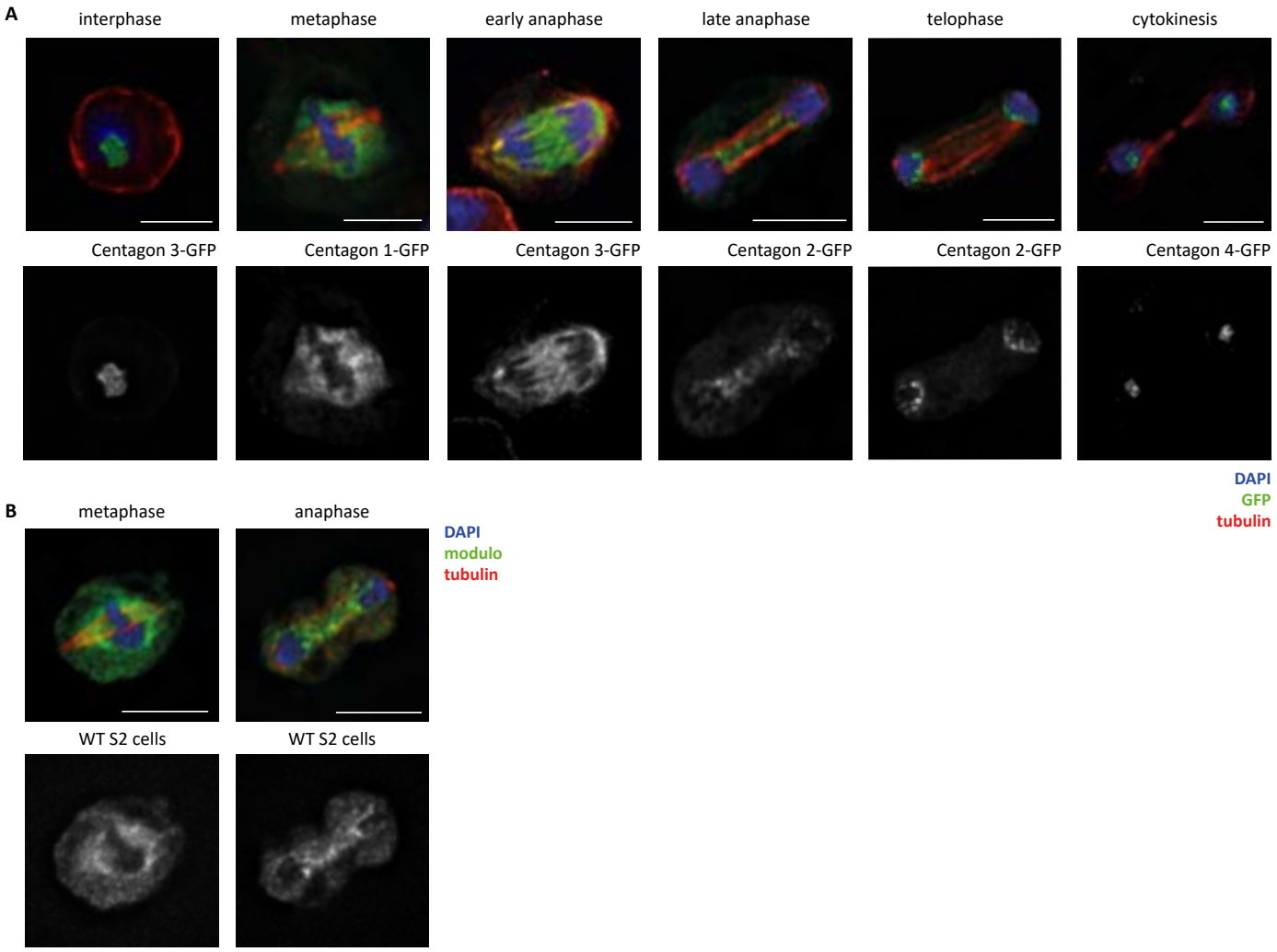

Figure 13: Localization of the Centagon complex during mitosis in S2 cells

A. Pictures show S2 cells expressing pLAP constructs with GFP-tagged proteins. The cells were fixated and co-stained with α-tubulin antibody (red) and DAPI (blue). The scale bar indicates 5 µm.

B. Fixed S2 cells stained with α-modulo (green) and α-tubulin (red) antibody and DAPI (blue). The scale bar indicates 5 µm.

validated with cells carrying inducible C-terminally-tagged V5-His constructs of the four Centagon proteins (not shown). IF staining with antibodies against Modulo (also a nucleolar protein) showed a similar distribution during mitosis (Fig. 13B), indicating that it might be a general feature of nucleolar proteins. Indeed, nucleolar proteins like fibrillarin and nucleolin, several ribosomal proteins, snoRNAs and pre-rRNAs are found in the perichromosomal compartment during mitosis, which surrounds the condensed chromosomes (Hernandez-Verdun 2011).

2.3.2 Knockdown of the Centagon proteins in S2 cells was inconclusive

Because KD of sat III RNA results in mitotic defects (Rošić et al. 2014), we wondered whether the Centagon proteins would show a similar effect. RNAi was performed by transfecting dsRNA complementary to the Centagon mRNAs. After four days, the cells were harvested for immunofluorescent staining and qPCR analysis. Unfortunately, the KD efficiency in S2 cells was not consistent and none of the monitored parameters (number of lagging chromosomes, mitotic index, spindle length, Cenp-C signal intensity) showed a promising difference in preliminary studies. Because RNAi experiments in Drosophila ovaries gave a clear phenotype that we could monitor and quantify well, the S2 cell experiments were abandoned without further analysis.

2.3.3 Sat III localization in S2 cells

Since the Centagon protein localization differs per cell cycle stage, we also monitored the localization of sat III RNA foci during mitosis. Lili Kenéz, a master student in our lab, performed sat III RNA FISH on S2 cells and assessed number and intensity of sat III RNA foci per cell cycle stage (Fig. 14A, B). During interphase most S2 cells contain 2-3 sat III foci, which are generally found in the nucleus. At the onset of mitosis the number of sat III foci increases drastically to 9-10 foci on average. The number of sat III foci increases to on average 13 during anaphase and is then distributed over the two daughter cells with on average 6-7 foci during telophase, slightly decreasing to 4-5 during cytokinesis. This could either be the result of fluctuating sat III RNA levels or a declustering of sat III RNA during mitosis. To assess the sat III RNA quantity, swe also analysed the signal intensity of the foci. This showed, that the mitotic foci had a significantly lower signal intensity compared to interphase cells (Fig. 14C). Unfortunately, it was not possible to quantify the total sat III signal intensity per cell, because the fluctuating foci intensities could not be captured with a single threshold setting. However, we can conclude that during mitosis, sat III transcripts have a different distribution compared to interphase. Interestingly, while almost all sat III

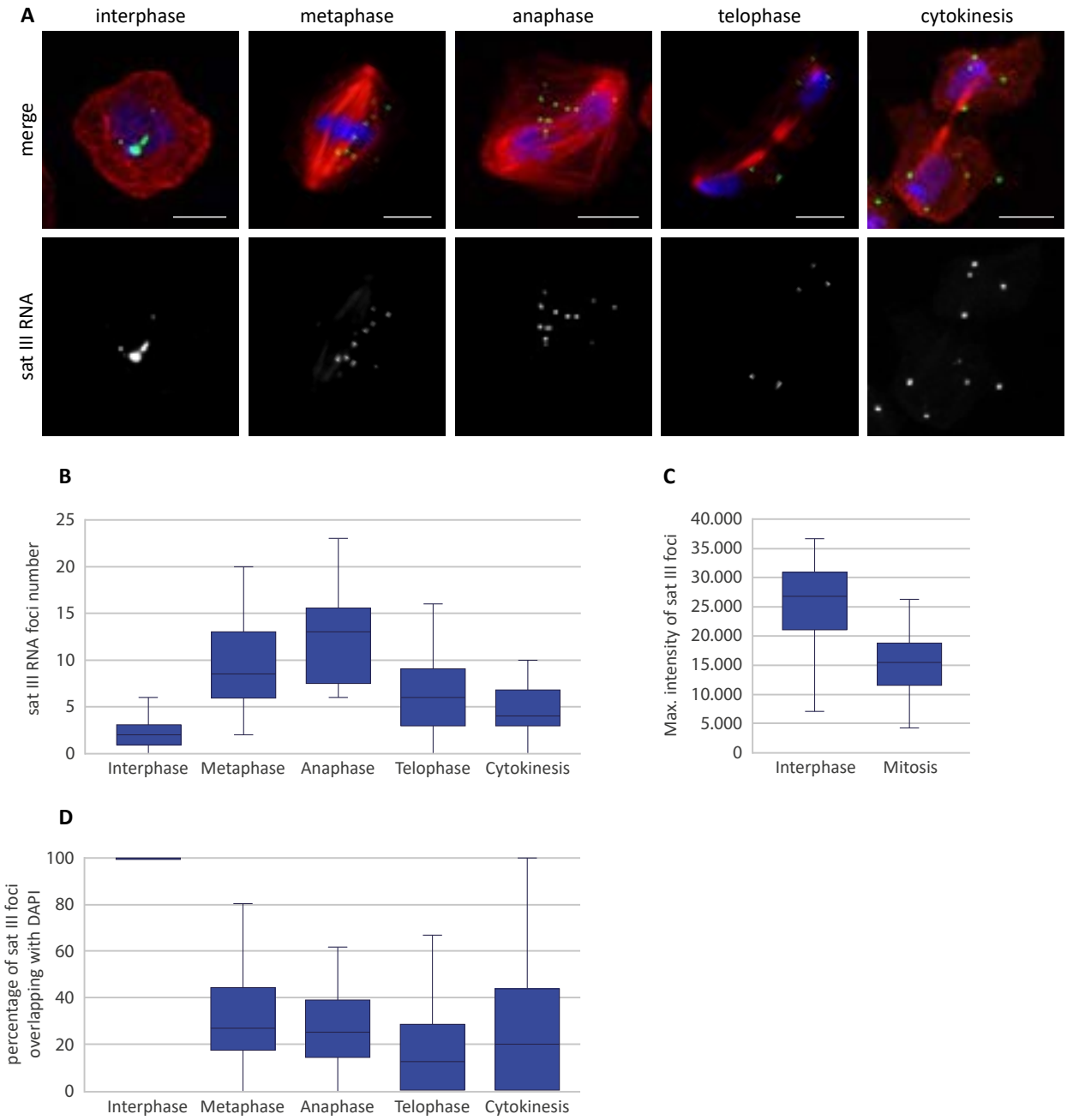

Figure 14: sat III RNA localization during mitosis

A. Examples of sat III RNA FISH in S2 cells during different cell cycle stages. Co-staining with α-tubulin (red) and DAPI (blue), sat III RNA signal in green. Scale bar = 5 µm, z-projection.

B. Quantification of the number of sat III RNA foci per cell cycle stage.

C. Max. intensity of the foci counted in B.

D. Percentage of the sat III RNA foci (same as in B.) co-localizing with DAPI.

Two independent experiments were combined into one graph.

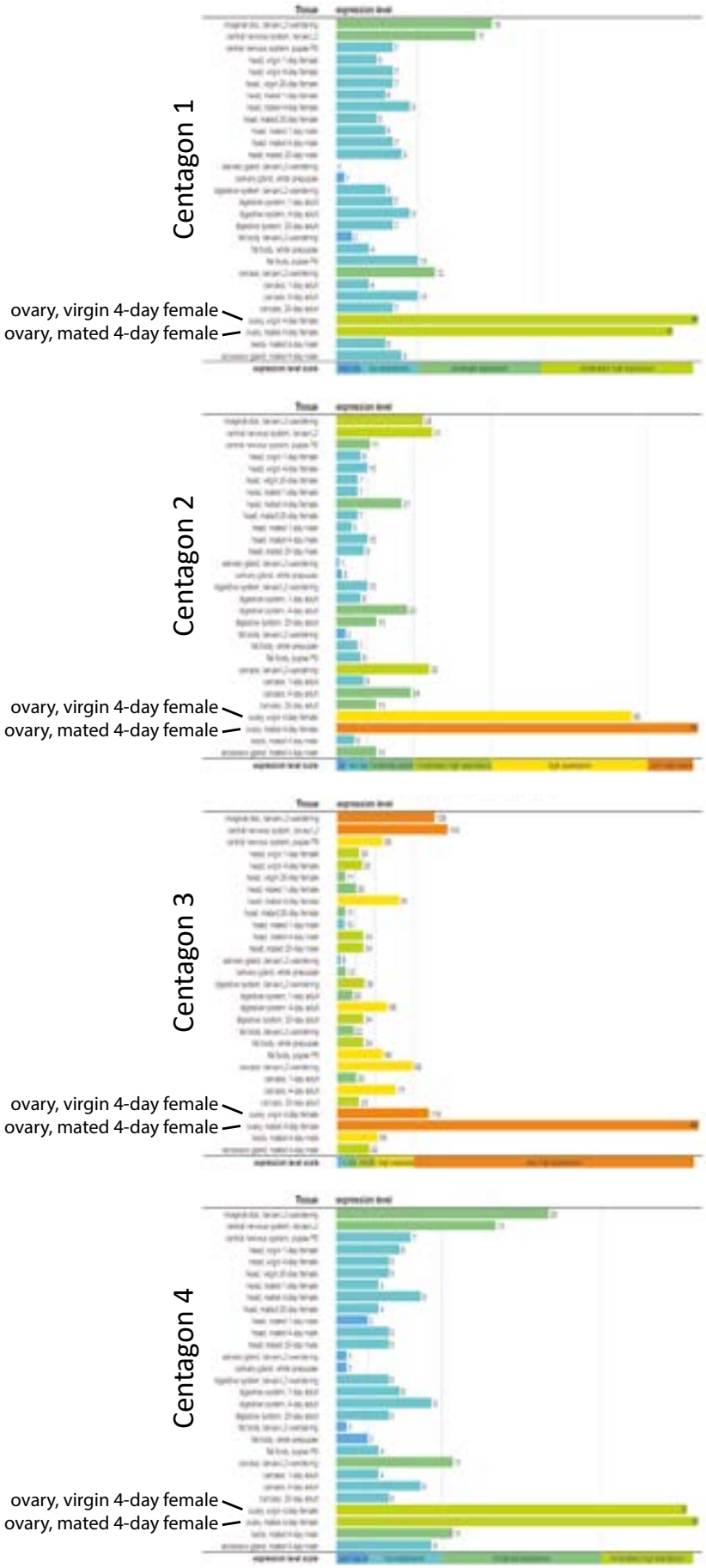

Figure 15: Expression levels of the Centagon members in fly tissues
Source: https://flybase.org/

foci co-localized with chromatin during interphase, this percentage drastically reduced to 20-30% during mitosis (Fig. 14D). Whether this is a sign for changing chromatin associations or merely a consequence of disturbing a local accumulation of sat III transcripts by the forces applied during mitosis, will have to be adressed in future experiments. When comparing the localization to the Centagon proteins, the sat III transcripts could interact with the complex especially during interphase and early mitosis, because of their similar distribution patterns.

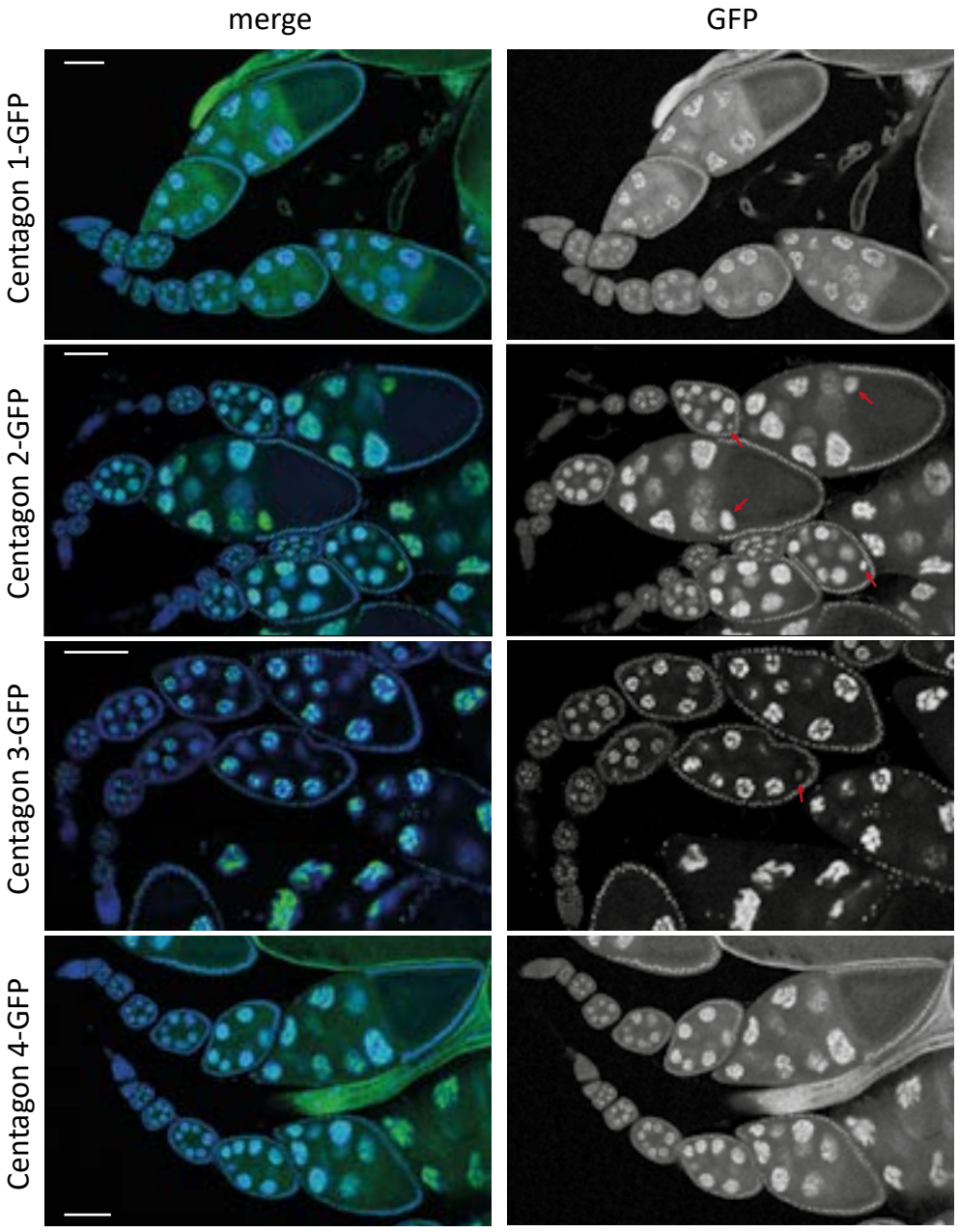

Figure 16: Localization of the Centagon complex in Drosophila ovaries
Pictures show fixed ovaries with endogenously GFP-tagged proteins co-stained with DAPI (blue). Red arrows point to oocyte nuclei with GFP signal. The scale bar indicates 50 µm.

2.4 Characterisation of the Centagon complex in Drosophila gonads

2.4.1 Localisation in the ovary

Because we had no reliable antibodies for all four Centagon proteins, we had made CRISPR-engineered flies where the four Centagon proteins were endogenously tagged with GFP. Since the expression of these proteins seemed to be highest in the ovary (Fig. 15), I dissected

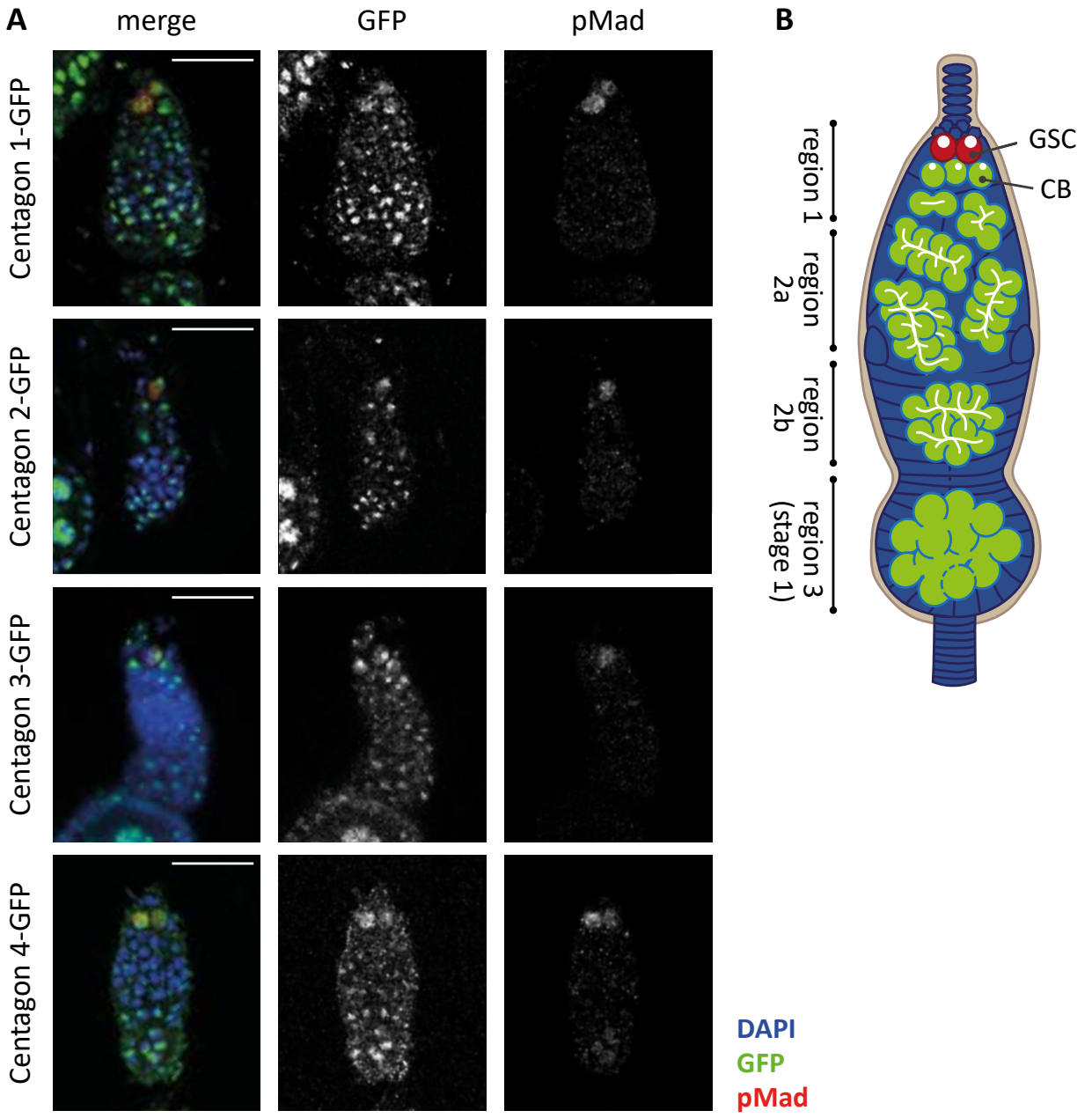

Figure 17: The Centagon proteis are expressed in GSCs

A. Pictures of germaria with endogenously GFP-tagged proteins co-stained with the GSC marker α-pMad (red) and DAPI (blue). The scale bar indicates 20 µm.

B. Schematic overview of the germarium.

ovaries and counterstained them with DAPI. The Centagon complex were clearly expressed in the developing germ line, as well as in somatic follicle cells (Fig. 16). Similar to S2 cells, most of the GFP signal localised to a sub-compartment of the nucleus, probably the nucleolus. In the nurse cells, the GFP-tagged Centagon proteins surrounded the chromatin and formed an irregular pattern throughout the nucleus. Centagon 2-GFP and Centagon 3-GFP were also found in the oocyte nucleus (red arrows). The fact that the Centagon expression seems to be quite tissue-specific, may explain why we did not observe any defects in KDs in S2 cells. Possibly, the proteins have a cell type-specific function that can only be monitored in vivo.

In the germarium, the protein localisation and expression levels changed during the development of the germ cells. In germ line stem cells marked with pMad antibody, the GFP signal was generally strong and not only found in the nucleolus, but distributed throughout the whole nucleus for all Centagon proteins (Fig. 17A). Although often there was still a

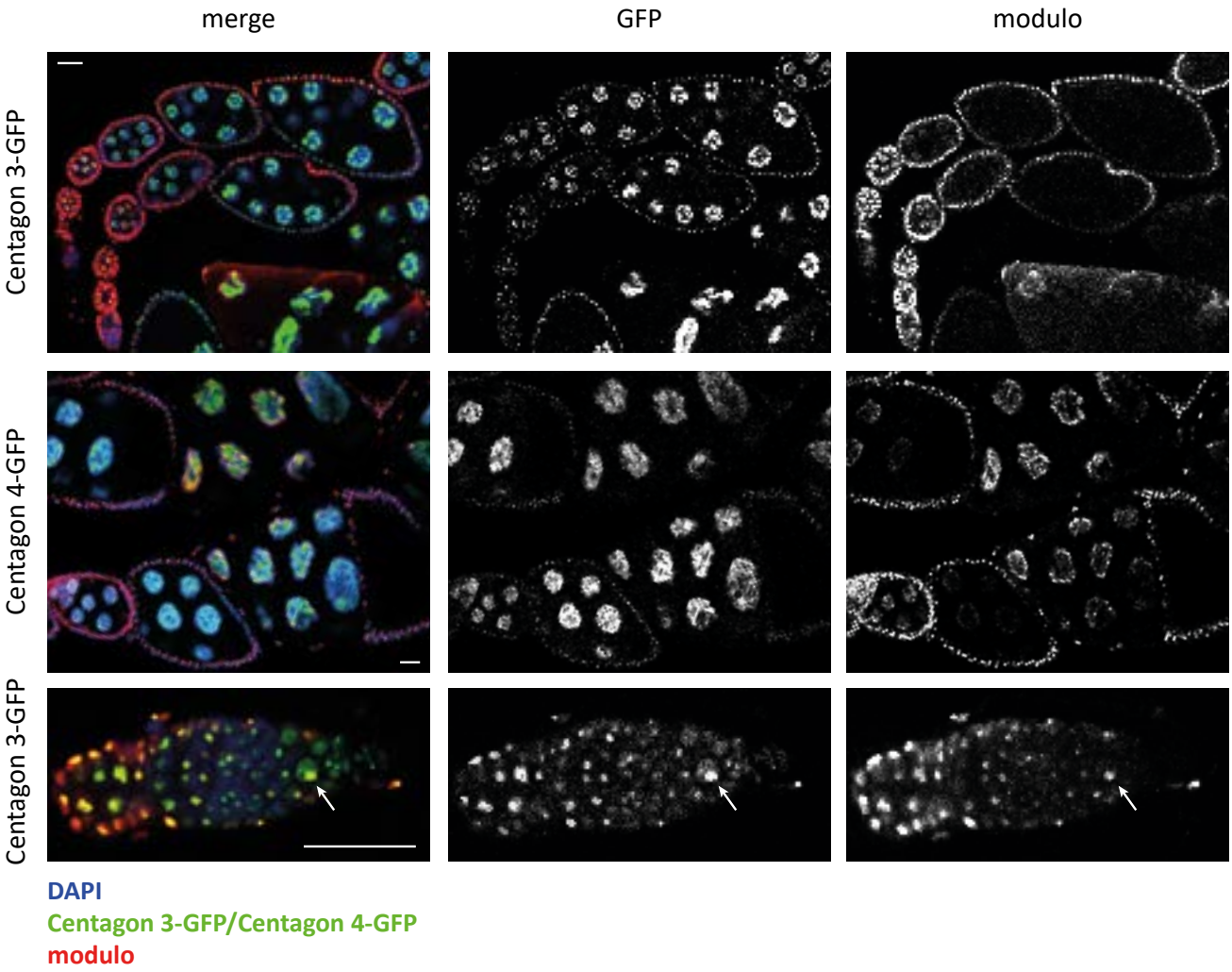

Figure 18: The Centagon proteins are expressed in the nucleolus
Pictures show fixed ovaries with GFP-tagged proteins co-stained with the nucleolus marker α-modulo(red) and DAPI (blue). Arrows point towards a GSC. The scale bar indicates 20 µm.

stronger GFP signal in the nucleolus. The first cystoblasts showed varying levels of GFP in individual germaria, sometimes the four Centagon proteins seemed to be not present at this stage, but in other cases their GFP signal was indistinguishable from the GSCs and relatively strong. In region 2a of the germarium (Fig. 17B), the GFP signal clearly diminished for all proteins and in region 2b, the Centagon proteins were re-expressed and localised to the nucleolus. On a similar note, pMad which marks GSCs was sometimes also detected in early cystoblasts and the germ cells of the first egg chamber, albeit at lower levels.

To assess whether this localization matches the nucleolus, I immunofluorescently labelled the ovaries of the GFP-tagged fly lines with a Modulo antibody (Fig. 18). Indeed, the signal of the GFP-tagged Centagon proteins and modulo overlapped, both in somatic and germ cells. In nurse cells, the nucleolus is not restricted to a single sub-location in the nucleus, but takes on a lobulated form throughout the whole nucleus (Dapples and King 1970). The GFP-tagged Centagon complex takes on a typical nucleolar localization for nurse cells, which is also seen in immunostainings with the nucleolus marker Fibrillarin (Liu et al. 2006). Unfortunately, our Fibrillarin antibody did not penetrate the ovary very well, which is why I used Modulo as

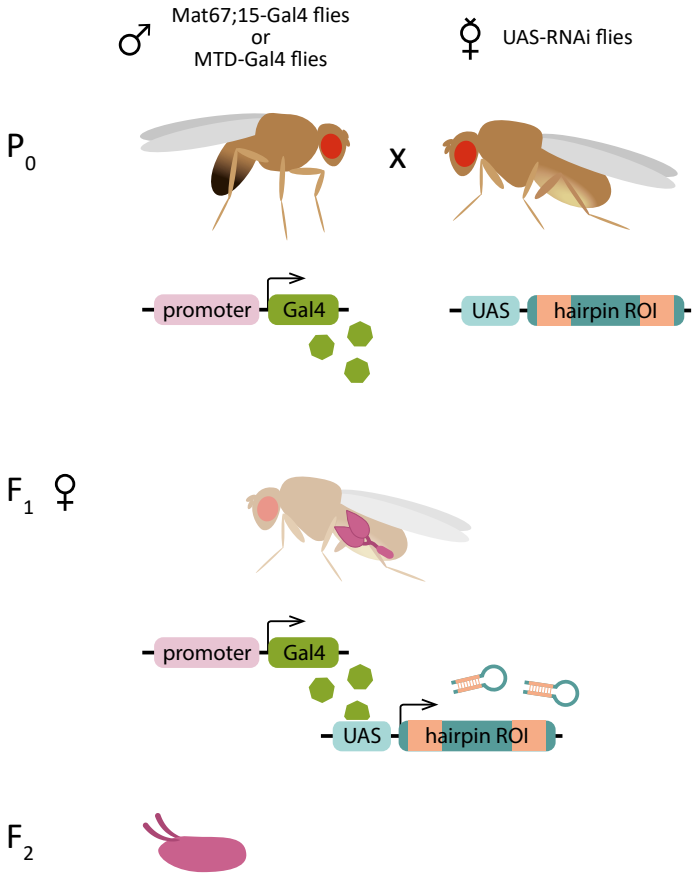

Figure 19: Crossing scheme of RNAi trip flies
For the experiments, ovary-specific drivers where used. Tissues affected by the knockdown are coloured pink. The knockdown was induced by the Gal4-UAS system.

a nucleolus marker instead. Modulo seems to have a slightly different nucleolar localization. A similar observation has been made for the human orthologue Nucleolin, which localises to the outer granular component and the dense fibrillar component (Ma et al. 2007), while Fibrillarin is found at the dense fibrillar component and fibrillary center (Amin et al. 2007). Therefore, I presume that Modulo is located at the outer nucleolus, while the Centagon proteins are found at the centre. Moreover, there seems to be an inverted expression pattern. While the Modulo signal is more pronounced in early egg chambers, the GFP signal of the Centagon complex increases with egg chamber maturation. Furthermore, the diffuse nuclear localization in GSCs does not seem to be standard for all nucleolar proteins as Modulo can only be found in the nucleolus (bottom panel).

2.4.2 Knockdown phenotypes in the ovary

To assess the function of the Centagon complex in ovaries, I performed knockdowns (KD) in the germ cells using two different Gal4 driver lines and trip RNAi fly lines of the respective proteins. The trip lines harbour an upstream activation sequence (UAS)-controlled inverted sequence which is complementary to the mRNA sequence of the protein of interest and will form a hairpin RNA when expressed (Fig. 19). Only when the RNAi flies are crossed with a fly expressing Gal4, the UAS will be activated and hairpin RNAs are expressed which will be

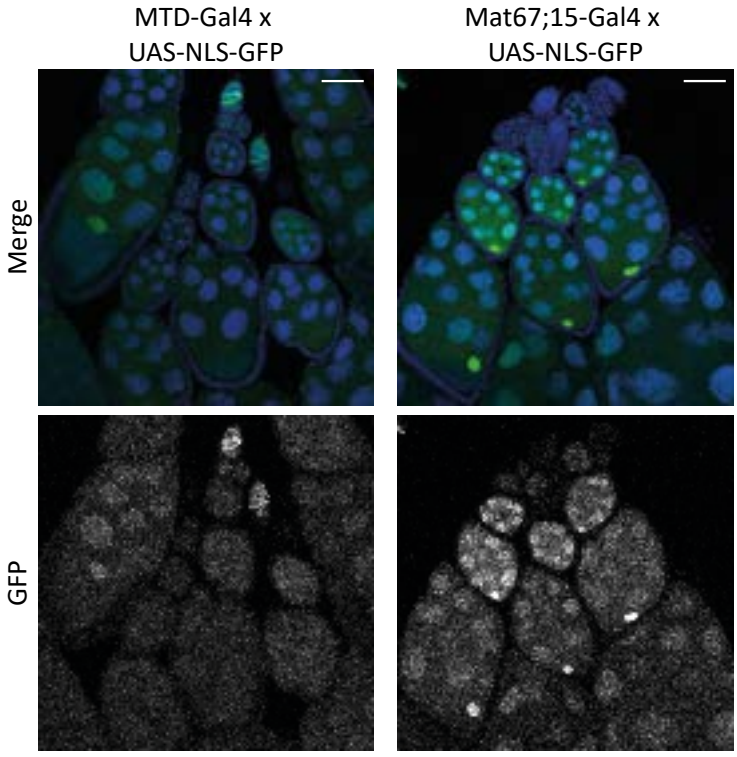

Figure 20: Expression pattern of the Mat67.15-Gal4 and MTD-Gal4 drivers
The Gal4-driver lines were crossed with flies that express a GFP-tagged nuclear localization sequence (NLS) under UAS control. The ovaries of the F1 females were fixed and co-stained with DAPI (blue). The scale bar indicates 50 µm.

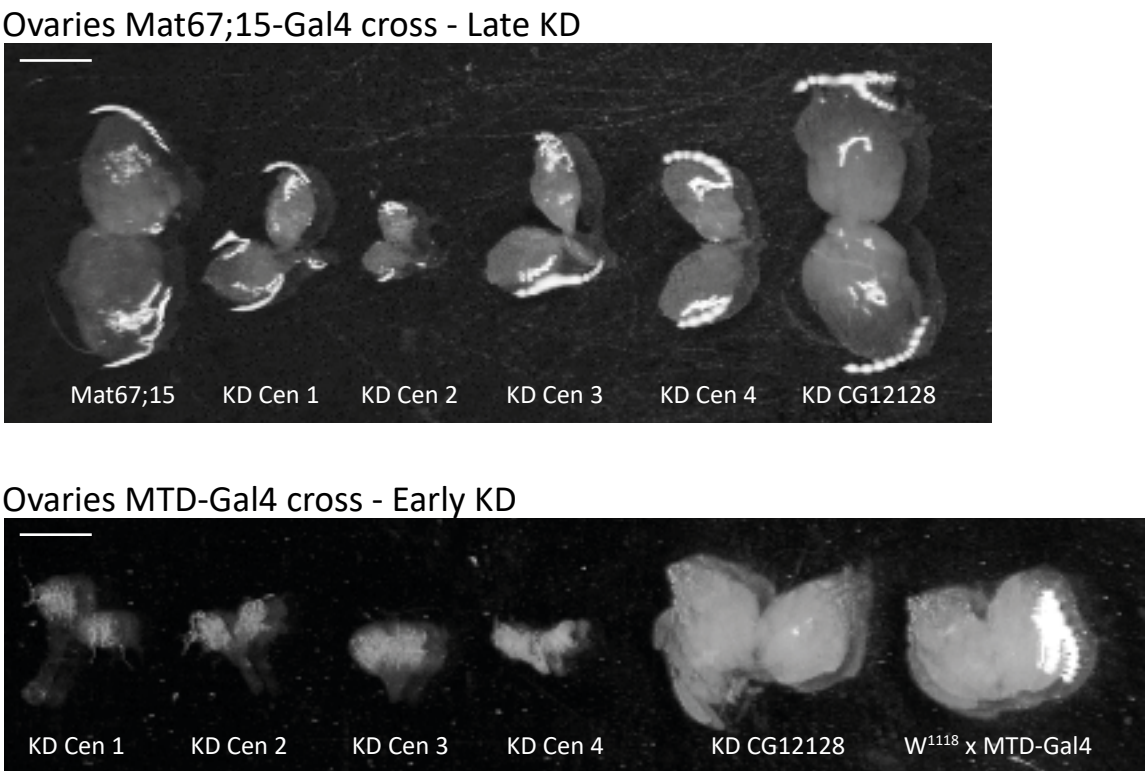

Figure 21: KD of the Centagon members leads to smaller ovaries
Ovaries of the KD cross F1 females were dissected and arranged on a glass slide.
The scalebar indicates approximately 0,5 mm.

processed by the RISC machinery leading to RNAi. For my experiments, I used the Maternal Triple Driver Gal4 line (MTD-Gal4), which has a Gal4 sequence on chromosome 2 and 3 with a nos promoter and on chromosome X with an otu promoter, and the Mat67.15-Gal4 line which expresses Gal4 under the control of the tubulin promoter on chromosomes 2 and 3. By crossing the respective driver lines with a UAS-NLS-GFP line, I assessed the onset of Gal4-activated expression in the ovary (Fig. 20). While MTD-Gal4-induced expression is already apparent in the germarium, Mat67.15-Gal4-induced expression only starts in early egg chambers. Additionally, Mat67.15-Gal4 seems to drive stronger expression in the oocyte nucleus compared to MTD-Gal4. Henceforth, I will refer to the crosses as early (MTD-GAl4) and late (Mat67.15-GAl4) KD of the Centagon complex.

Both crosses were kept at 25˚C and the offspring was kept for 2-3 days with fresh yeast paste before dissection of the ovaries. Already during dissections with a binocular microscope (magnification: 4x), a clear morphological difference could be seen for the early and late KD (Fig. 21). All affected ovaries appeared smaller and had less mature eggs, with the strongest effect in the early KDs. This was not the case for CG12128, where neither early nor late KD affected the ovaries. To assess the KD efficiency, RNA was isolated from late KD ovaries, because they provided enough tissue. The qPCR data showed a significant downregulation

of the Centagon mRNA levels in the respective KD ovaries compared to control knockdowns (Fig. 22), also for CG12128. Therefore, the lack of a phenotype in CG12128 KD ovaries cannot be attributed to an inefficient KD. Importantly, for the remaining four Centagon proteins a compensatory mechanism was detected: when one of the Centagon proteins was depleted by RNAi, the other three were upregulated, suggesting a form of coregulation or compensation mechanism. Especially Centagon 1 and 2 were upregulated upon KD of other factors, while both also had more severe phenotypes than Centagon 3 and 4 in the late KD. In general, the reduction of Centagon 2 had the greatest effect on oogenesis and Centagon 4 had the least penetrant phenotype in the germline.

MTD-Gal4-driven knockdown in larval gonads

To assess the phenotypes in more detail, the ovaries were fixed and immunostained with the germline marker α-vasa antibody (Hay et al. 1988) and counterstained with DAPI. The phenotype of the early KD turned out to be so strong, that only very sporadically germ cells were detectable. This result clearly showed that the Centagon proteins are essential for germ cell maintenance, however, the observation of an almost complete loss of germ cells was less

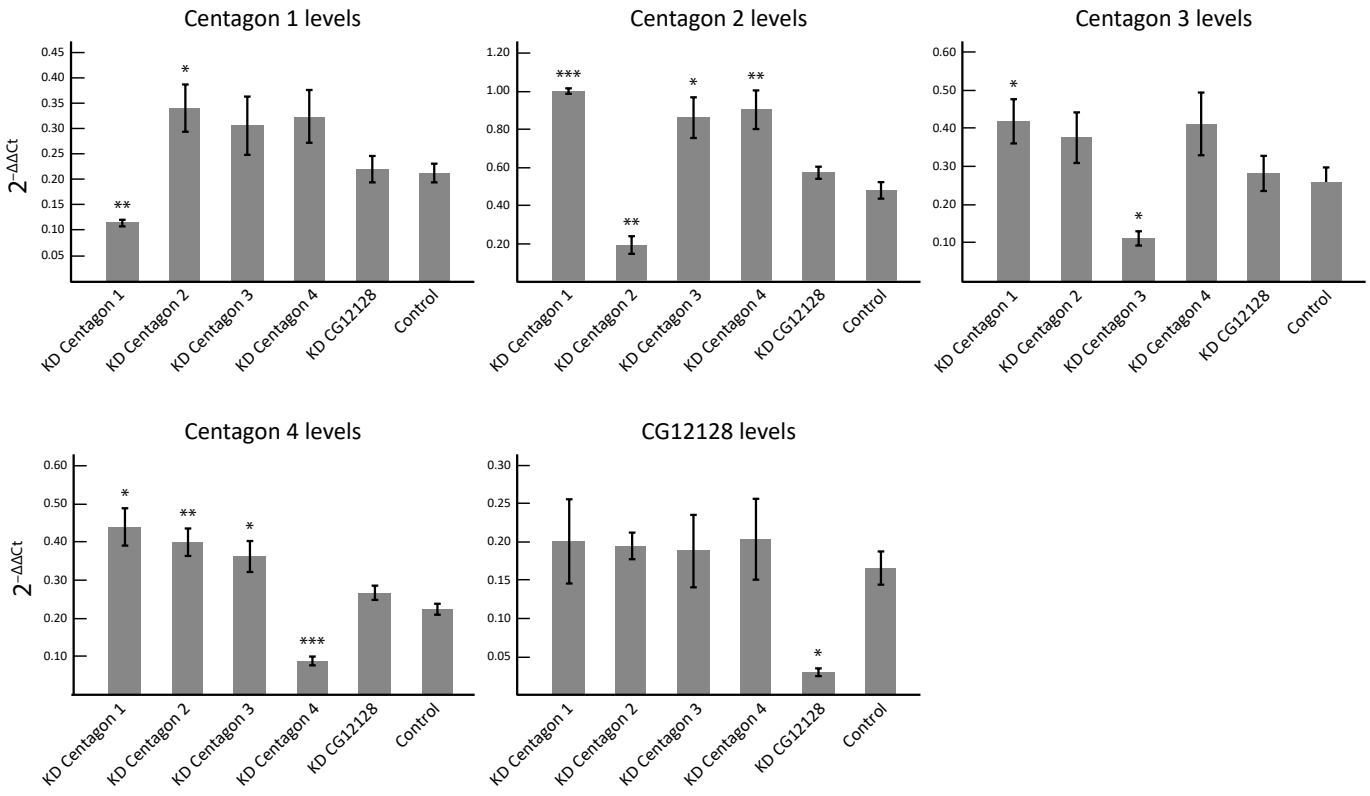

Figure 22: Centagon knockdown efficiency in the ovaries

Average RNA levels in the KD ovaries, normalized to housekeeping genes. For each triplicate, RNA was isolated from 10-15 ovaries. * indicate statistically significant differences compared to the control (w^{1118} x Mat67.15) calculated with a Student's t-test.

informative as to the underlying mechanism and function. Therefore, I proceeded to look at an earlier stage of ovary development, the 3rd instar larval ovaries. At this age, male and female larvae can only be distinguished by the size of their developing gonads (M. DEMEREC 1950). I sorted the 3rd instar larvae by gonadal size, dissected the developing ovaries and immunostained them with α-vasa and α-hts (marks somatic cells and spectrosomes) antibodies (DENG AND LIN 1997) and DAPI. As can be seen in Fig. 23, the female gonads did not show any striking defects. The different shapes of the KD larval ovaries were also seen in the control. No quantifications for gonad size or germ cell number are available, because the dissected larvae were not exactly the same age and the vasa immunostaining did not penetrate the whole tissue, preventing precise germ cell counting. Because the larval ovaries had a normal morphology and many germ cells, this strongly suggests that the KD flies start off with a normal amount of germ cells but loose them during subsequent development.

During imaging, it turned out that some larval testes were small enough that I mistook them for ovaries (Fig. 23). The larval testes can be distinguished by its elongated shape and the two chromatin-dense poles, with the anterior one harbouring the hub, GSCs and cyst progenitor cells and the posterior pole harbouring the male-specific somatic gonadal precursors. In between, the dividing gonialblasts, spermatogonia and spermatocytes are

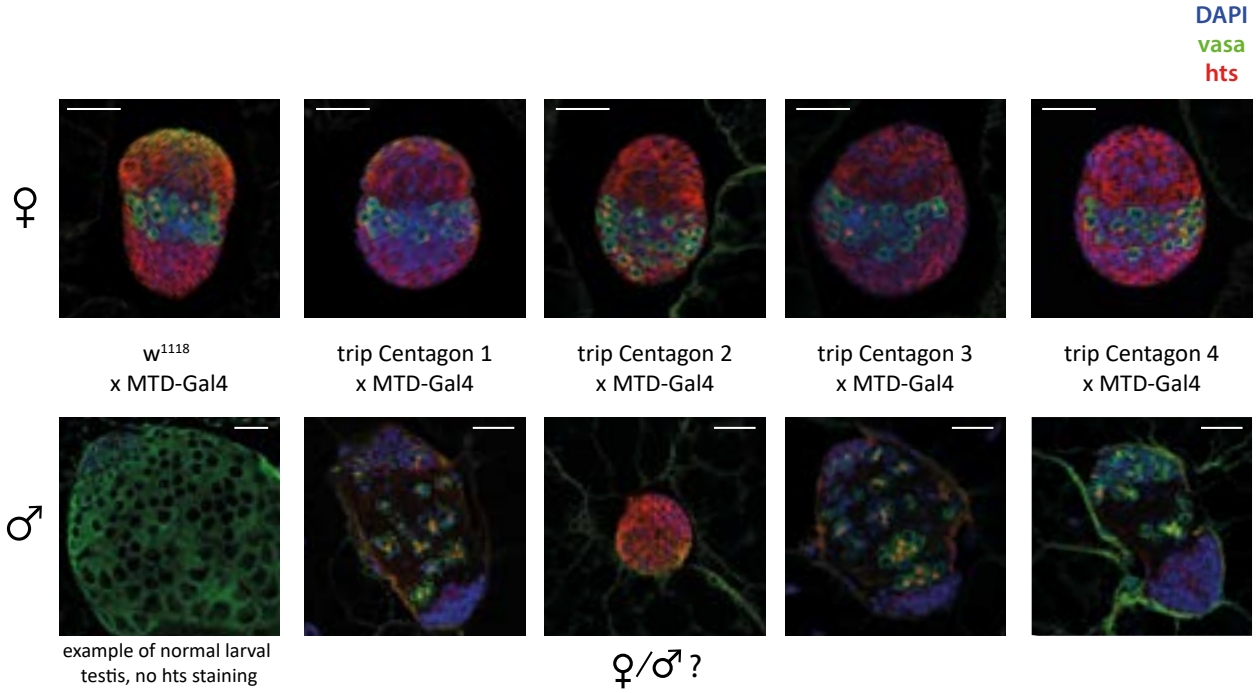

Figure 23: Only larval testis are affected by the Centagon KDs
Larval gonads were dissected from 3rd instar larvae and stained with germ cell marker α-vasa (green) and spectrosome marker α-hts (red) antibodies and DAPI (blue). Larval oavries are depicted in the upper row and (presumable) larval testis in the lower row. The scale bar indicates 20 µm.

found, which fill up the entire 3rd instar larval testis (M. DEMEREC 1950) (Fig. 23, lower left panel). In comparison, the KD testes appear significantly smaller (approx. 90 µm long vs. 200 µm long in w^{1118} larvae) and only have a few spermatogonia with aberrant vasa signal. This indicates the Centagon complex is not only important for the female germline, but also has a strong effect in male gonad development, as will also be discussed later. Notably, the Centagon proteins are expressed at much lower levels in testes compared to ovaries (Fig. 15, row below the ovaries), but this may differ in larval testes. Possibly, the defects occur earlier in male gonads, because they differentiate already in the embryo, whereas differentiation of the female gonads only starts in the third instar larva (see 2.1.2). This would argue for a differentiation defect upon KD of the Centagon complex. Additionally, I found small gonads without vasa-positive cells in larvae of the Centagon 2 KD. The trip RNAi fly line for Centagon 2 is heterozygous and balanced over CyO. Therefore, I can distinguish the trip Centagon 2-harbouring flies in adults by the absence of curly wings, but in larvae this is not possible. Stochastically, 50% of the larvae should be affected, with half being female and half being male. Unfortunately, since I did not count the male larvae, I cannot estimate whether the germ cell-less gonads are more likely male or female. Subsequently, I also cannot be sure whether the larval ovary in Fig. 23 has indeed reduced Centagon 2 levels. Seeing that the downregulation of the other Centagon members only affected male gonads and I was able to preserve some germ cells in the Centagon 2 KD ovaries later on, I would argue however that the germ cell-less gonads are most likely male.

MTD-Gal4-driven knockdown in young ovaries

My second approach to obtain ovaries which still have germ tissue left was to reduce the strength of the MTD-Gal4 driver by keeping the crosses at 18˚C, since Gal4 activity is temperature sensitive (DUFFY 2002). Additionally, younger females were dissected (0-4 hours old for the control and 0-1 day old for the KDs to obtain enough females). The ovaries were stained with the antibodies α-vasa and α-pMad (GSC marker) as well as DAPI (Fig. 24A, Fig. S1). Although the KD ovaries were still severely affected, a group of vasa-positive cells could be seen at the tip of the developing germarium together with two or three pMad-positive GSCs. Furthermore, several germ cell cysts were present, some even reaching the stage of early egg chamber (white arrows). Compared to the w^{1118} cross, the KD ovaries were clearly less developed, even when dissected from females which had aged a few more hours. Next to the slower development, the early KD ovaries had fewer cysts with improper shapes and aberrant vasa staining (Fig. 24A). The background signal in the green channel of the KD ovaries is caused by the fact that more connective tissue surrounds the germ cells. This is also visible with fully developed ovaries, but less apparent, because the ovarioles take

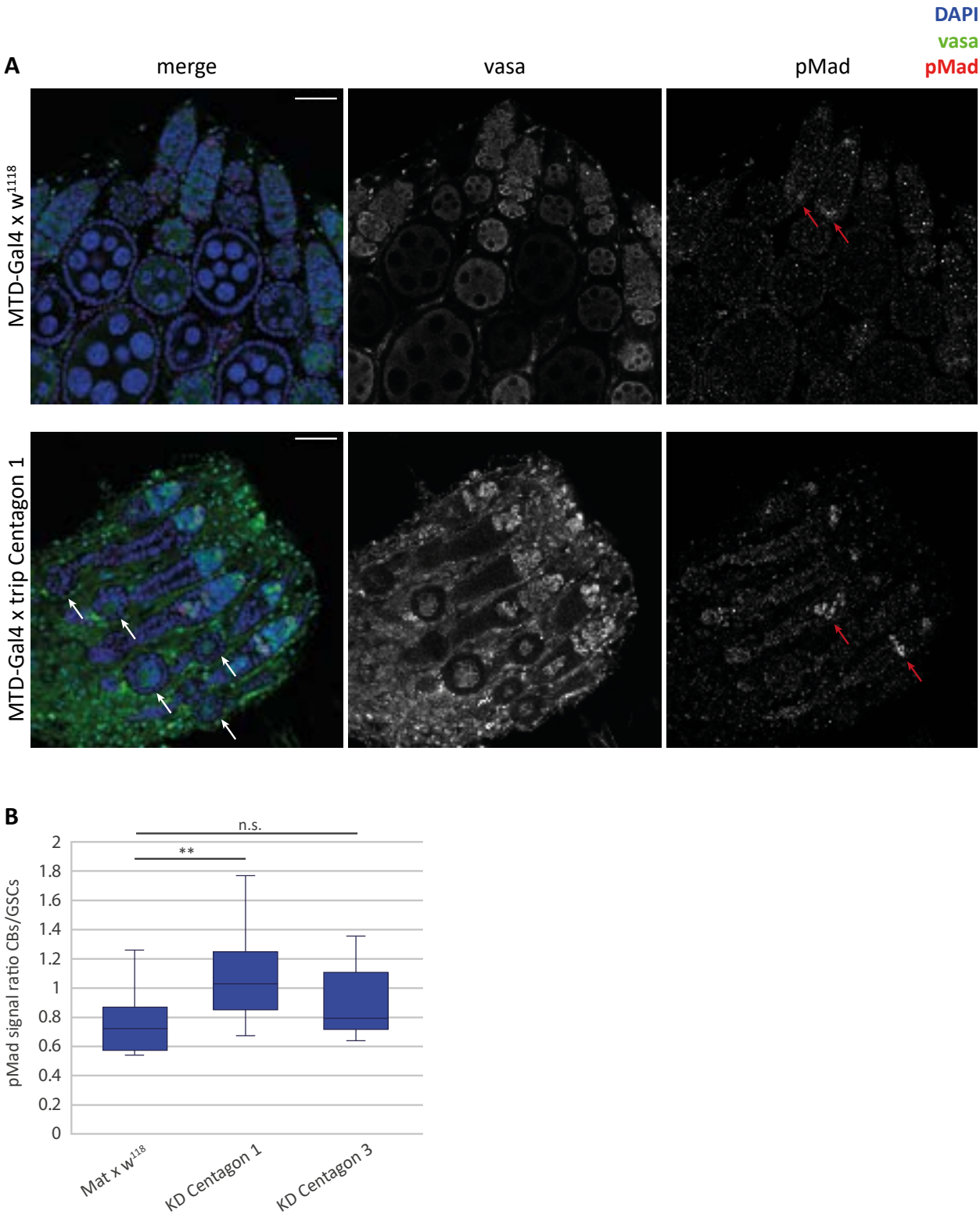

Figure 24: KDs in the germarium lead to loss of germ cells and no egg chamber formation

A. The trip UAS RNAi lines and w^{1118} were crossed with MTD-Gal4 and kept at 18°C. The F1 females were dissected shortly after hatching (0-4h for the w^{1118} control cross and 0-1 day for the KD crosses). The ovaries were fixed and stained with the germ cell marker α-vasa (green) and GSC marker α-pMad (red) antibodies and DAPI (blue). Red arrows point to pMad signal outside of the GSCs. The scale bar indicates 25 µm.

B. Quantification of the pMad signal intensity ratio of CBs/GSCs.

up most of the space. The pMad staining, which is usually highest in the GSCs, was also observed at later stages in the KD ovaries (red arrows). If this signal is specific, it could mean that pMad is re-expressed in differentiated cystoblasts and that maybe some form of dedifferentiation occurs. The pMad signal in cystoblasts was most consistently seen in the Centagon 1 KD ovaries (100% of the ovaries), followed by the w^{1118} cross and the Centagon 3 KD ovaries (approximately 66%). I calculated the ratio of pMad signal per cell of CBs vs. GSCs in the ovaries which showed the highest percentage of later pMad expression (Fig. 24B). In the w^{1118} cross, the CB/GSC pMad ratio was 0,76 on average, in the Centagon 1 KD ovaries the ratio was on average 1 and in the Centagon 3 KD ovaries the ratio was 0,9. Although the pMad levels in CBs were higher in both KD ovaries, only the difference of the Centagon 1 KD was significant ($p = 0,01$). These calculations show that GSCs and the affected CBs have equally high pMad levels in the Centagon 1 KD ovaries. Future experiments will have address whether this is caused by dedifferentiation of CBs. All in all, the germ cells in the early KD are still able to divide and differentiate, but have an aberrant morphology and fail to form egg chambers beyond stage 1, which could be caused by a differentiation defect.

Mat67.15-driven knockdown in ovaries

As stated before, the Mat67.15-Gal4 driver starts expression in early egg chambers. Therefore, the GSCs and early cystoblasts are unaffected, and egg chambers are able to form. The first phenotypes are seen in stage five egg chambers, where the nurse cell chromatin fails to disperse. Instead, the five-blob chromatin is maintained in depleted egg chambers. Consequently, many egg chambers arrest in development and die (Fig. 25A, Fig. S3). The phenotype is most prominent in younger females (2-4 days old), where 67-86% of ovarioles have only fragmented nurse cells and only 17-33% of the ovarioles also contain a normal-looking egg chamber (Fig. 25B). With increasing age (up to 7 days old) the ovaries partially overcome these defects, with nurse cells being less fragmented and some maturing into viable eggs (Fig 25A, right panel). This effect can also be seen in the survival assay (Fig. 26). For the survival assay, 30 virgins of the late KD were crossed with 20 males of the late KD and kept in cages with fresh yeast paste for two days, before eggs were collected from a staged overnight (15h) plate. While young KD females (2-4 days old) barely lay any eggs, after 3-6 days, up to 350 eggs were laid overnight by the Centagon 3 KD females (Fig. 26A). These numbers differed greatly between the crosses, with the other KDs laying 0-180 eggs. In general, the number of eggs laid by KD females was very low and the eggs themselves were smaller with shorter dorsal filaments. Some showed discolouration with an aberrant shape and no filaments at all. I categorised the eggs into normal, medium (smaller, but still recognisable as egg) and small (clearly deformed without dorsal filaments) (Fig. 26C). These

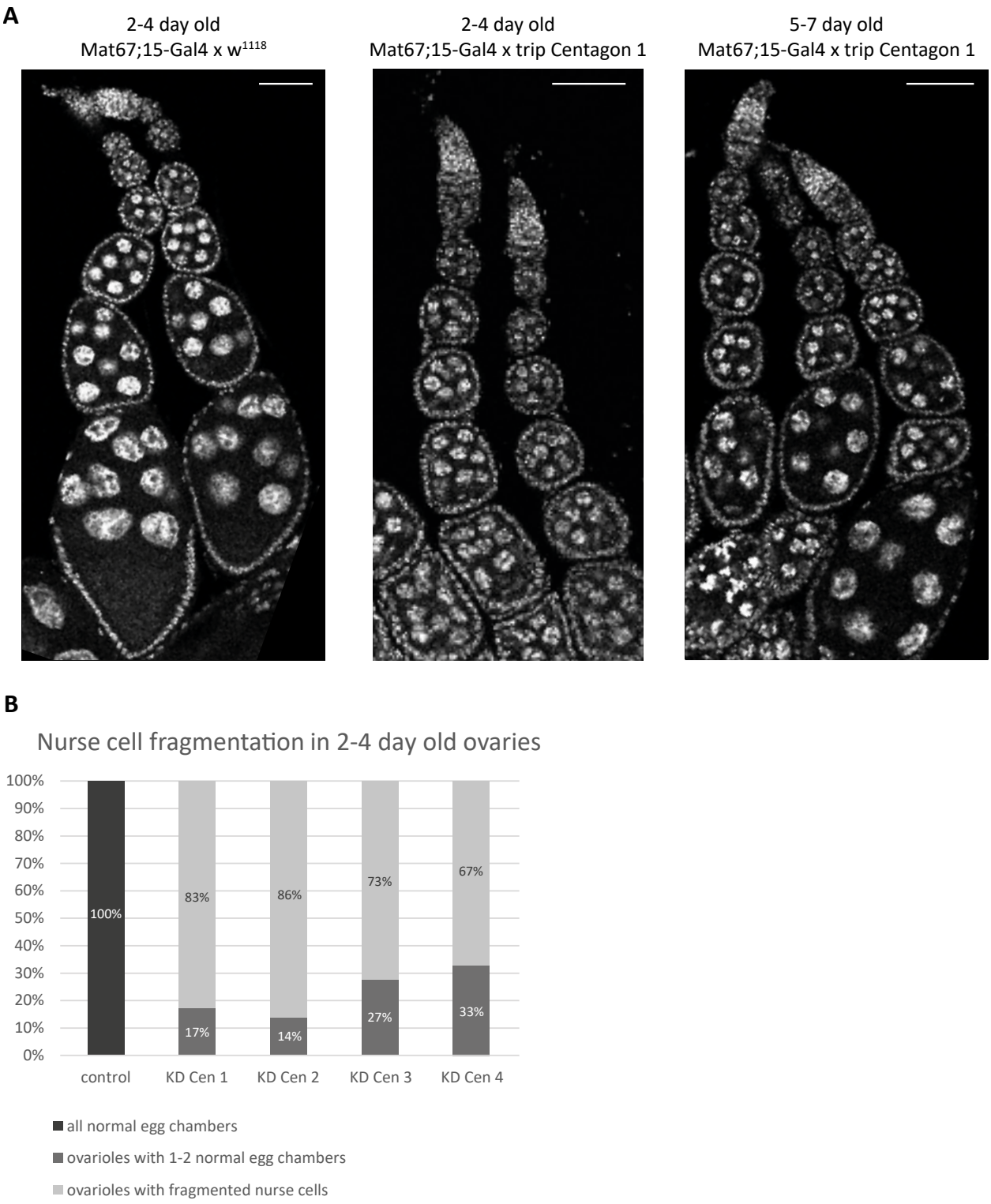

Figure 25: KDs in egg chambers lead to fragmented nurse cell nuclei and impaired egg chamber maturation

A. The trip UAS RNAi lines and w^{1118} were crossed with Mat67.15-Gal4 and kept at 25˚C. The F1 ovaries were dissected 2-4 days and 5-7 days after hatching and stained with DAPI (blue). The scale bar indicates 50 µm. A grey background was added to pictures which were rotated.

B. Quantification of the number of ovarioles harbouring no/all but few/only egg chambers with fragmented nurse cells. Early egg chambers (stage 1-5) with naturally occurring fragmented nurse cells were not included. At least 120 ovarioles were assessed per condition.

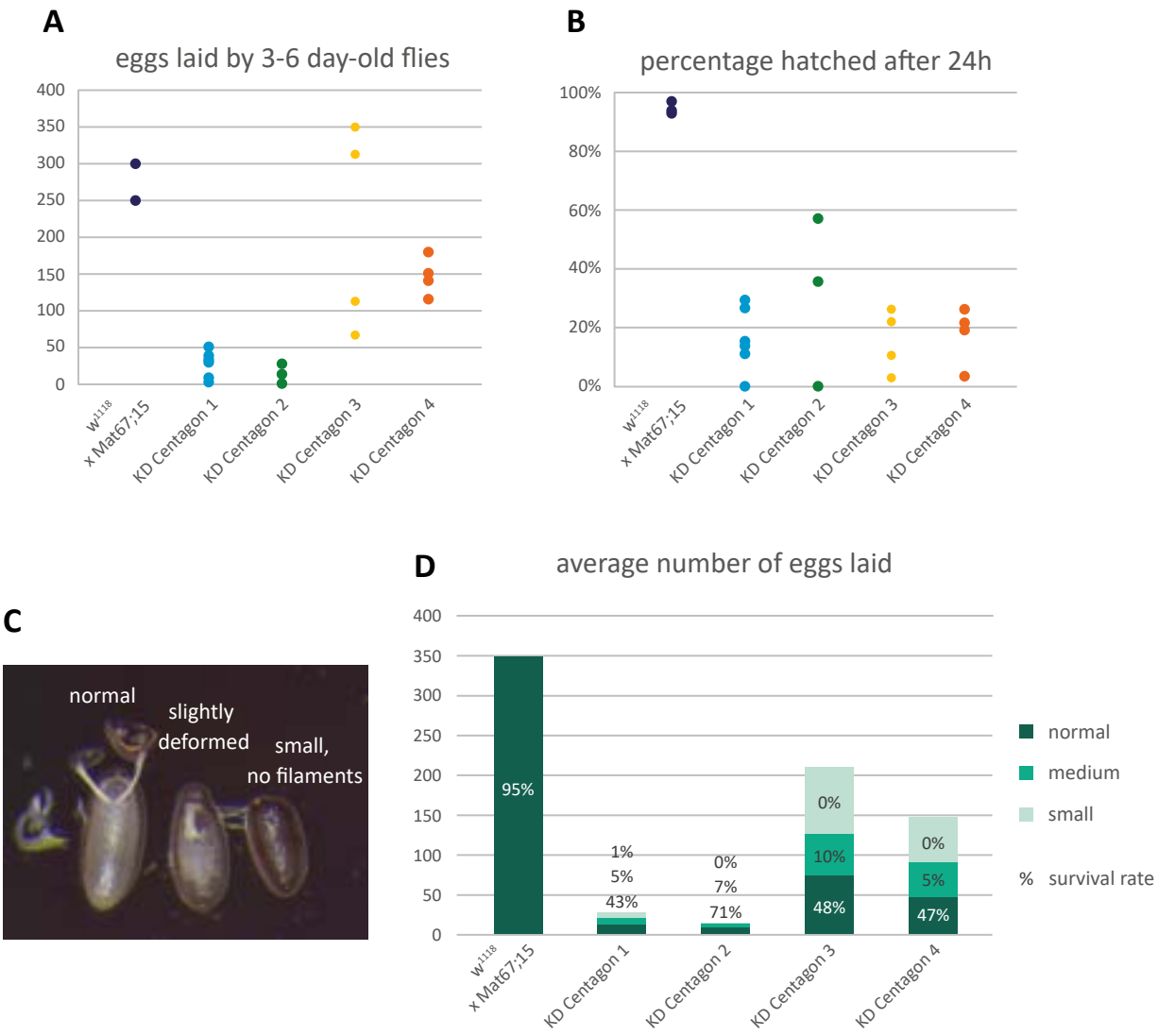

Figure 26: KD flies lay fewer eggs with aberrant morphology

A. Number of eggs laid by F1 females of Mat67.15-Gal4 crosses in a 15h period overnight. The cages were set up with 30 female virgins and 20 males. Each dot represents one survival assay.

B. Hatching rate of the eggs collected in A.

C. Egg phenotype examples of the KD flies. Phenotypes range from normal (left) to small deformed and discoloured eggs (righ).

D. Average number of eggs laid in A., categorised into the phenotypes shown in C, with survival rate per egg phenotype.

were arranged on a fresh agar plate with yeast paste and kept at 25˚C for 24h more hours to assess the hatching rate of the eggs. As can be seen in Fig. 26B, the hatching rate of the eggs laid by KD females was usually not higher than 30% compared to 95% in the control. This number is slightly misleading, since it does not take the reduced number of eggs laid by the Centagon KD flies in to account. In Fig. 26D, the average number and hatching rate of the eggs are shown, categorised by egg phenotype. A clear correlation is seen between the severity of egg malformation and the hatching rate with the small eggs never hatching and the highest hatching rate in the normal looking egg group. As was already observed

during ovary dissections, the KD of Centagon 1 and 2 produced the strongest phenotypes. In the KD of Centagon 3 and 4, where more eggs were laid, approximately 1/3 of the eggs was categorised as normal looking, while 2/3 belonged to the categories medium and small. However, also the eggs that had a normal morphology had lower hatching rates (43-71%), showing that these eggs were also affected by the KD of the Centagon proteins.

These experiments show that the identified sat III RNA interacting factors are not only important for germ cell survival in the germarium, they also influence chromatin formation in nurse cells and the formation of egg chambers during oogenesis.

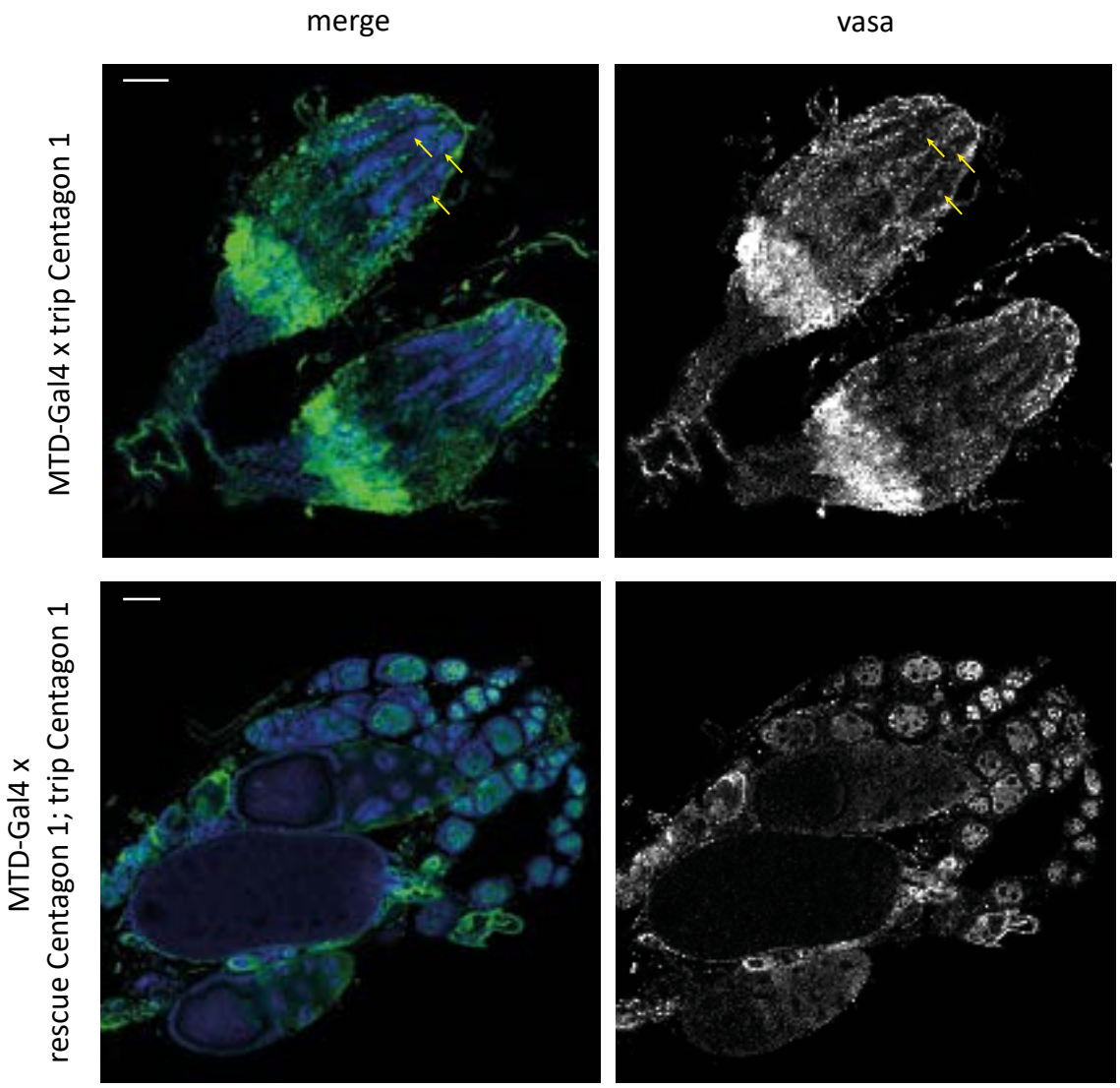

Figure 27: The phenotype of the Centagon 1 KD can be partially rescued by re-expression of Centagon 1

Trip Centagon 1 flies with and without the RNAi-resistant Centagon 1 expressing construct were crossed with MTD-Gal4 flies. Ovaries of F1 females aged 2-3 days were dissected and stained with germ cell marker α-vasa (green) and DAPI (blue). Arrows point to left-over germ cells. The scale bar indicates 50 µm.

2.4.3 Rescue of the KD phenotype (Centagon 1)

In order to show that the observed phenotype was indeed caused by the downregulation of the Centagon proteins, I performed a rescue experiment with Centagon 1 as an example. The Centagon 1 sequence including its upstream and downstream regions was cloned into the pATTB vector, with the change that the region targeted by the dsRNA of the trip Centagon 1 fly line was designed with alternative codons. This way, the ectopically expressed Centagon 1 was not susceptible to KD. The plasmid was injected into vas-int;attp40 embryos, where the construct was inserted on chromosome 2. In the end, two identical fly lines were obtained, originating from two different injected embryos. Consequently, the ubiquitously expressed Centagon 1 rescue construct was crossed into the trip Centagon 1 RNAi (chr. 3) line. Both trip Centagon 1 RNAi lines, with and without rescue construct, were crossed with the early MTD-Gal4 driver and kept at 25˚C. After a few days of aging, the F1 females were dissected and the ovaries were stained with α-vasa antibody, to mark the germ line, and DAPI (Fig. 27). The bright signal at the base of the ovaries in the GFP channel (upper panel) is probably background signal. As can be seen in Fig. 27, the ovaries expressing RNAi-resistant Centagon 1 are clearly more developed. In contrast to the original KD ovaries which only have a few germ cells left (arrows), they have many vasa-positive cells and are able to form egg chambers and even eggs. I performed this rescue cross with both rescue construct-expressing fly lines and found that 100% of the rescue cross flies (N=5 and N=6) had ovaries with vasa-positive developing egg chambers, compared to 0% in the normal Centagon 1 KD ovaries (N=4). As there are still many more early-stage egg chambers than late-stage and many nurse cells with five-blob chromatin, the oogenesis does not seem to be fully rescued.

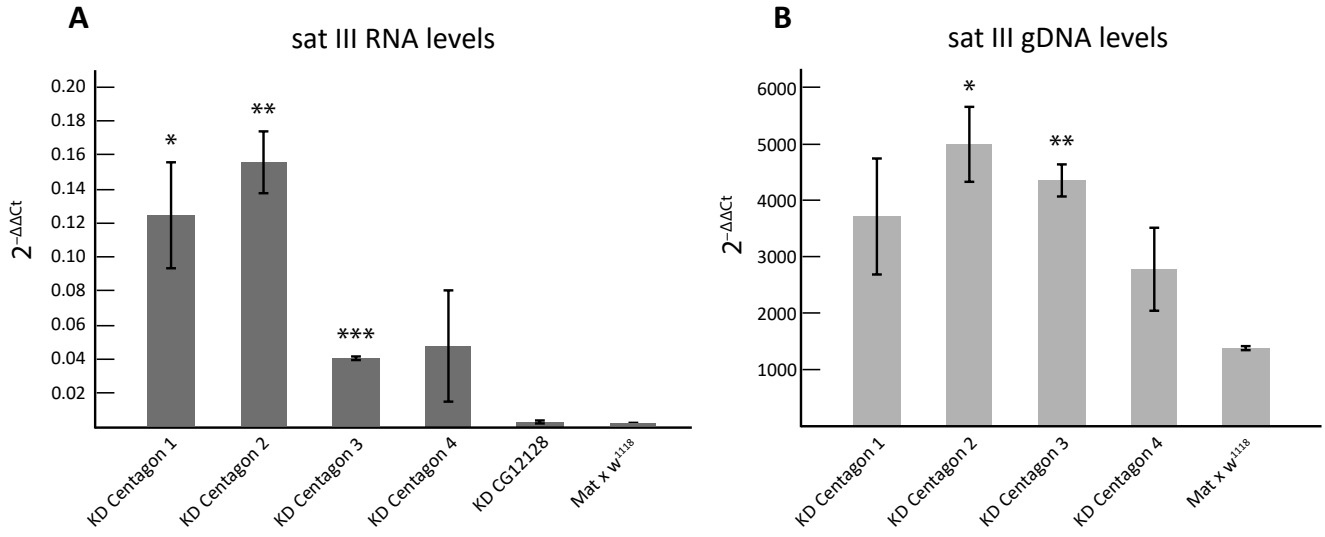

Figure 28: Sat III RNA is upregulated in the KD ovaries

Sat III RNA (A) and gDNA (B) levels were measured by qPCR and normalized to housekeeping genes. * indicate statistically significant differences compared to the control (w^{1118} x Mat67.15) calculated with a Student's t-test.

However, with ectopic expression of the RNAi-resistant Centagon 1, ovaries improved from having no germ cell structures at all, to having mature ovarioles and producing eggs. Therefore, the KD phenotype is definitely caused by the downregulation of Centagon 1 and not by an off-target effect.

2.5 Sat III RNA in ovaries

2.5.1 Sat III RNA levels in KD ovaries

When assessing the RNA expression levels in late KD ovaries (4.2.3), we also monitored SATIII RNA levels and noticed that sat III RNA levels were massively upregulated (Fig. 28A). Especially in the Centagon 1 and 2 KD ovaries, which also had the strongest phenotypes, sat III levels were more than 50 times higher compared to the w^{1118} control cross. In the CG12128 KD ovaries, which did not have a germline phenotype, sat III RNA levels were comparable to the levels of the control cross. Because early nurse cells still endoreduplicate their whole genome and switch to only reduplicating chromosome arms during the transition from S5 (five-blob chromatin) to G6 (dispersed chromatin) (Dej and Spradling 1999), the overall chromatin composition of KD ovaries with predominantly early egg chambers will be different from the w^{1118} cross with more mature eggs. Therefore, it is possible, that the increase in the pericentric sat III RNA levels is caused by a higher sat III DNA content in the KD ovaries. To assess this, I isolated genomic DNA from the KD ovaries and performed a qPCR (Fig. 28B). The KD ovaries had 2-3,5-fold higher sat III DNA levels than the control. However, this was far lower than the up to 50-fold increase of sat III RNA and cannot fully explain the effect.

2.5.2 Sat III RNA localization in late KD ovaries

Possibly, sat III expression is restricted to a specific developmental window during oogenesis, eg. sat III may be mainly expressed in early egg chambers and an accumulation of early egg chambers in KD ovaries could explain the high sat III RNA levels. To characterise the sat III RNA localisation, I performed single-molecule RNA Fluorescent In Situ Hybridization (smFISH). First of all, I tested the Hulu DNA probes for sense or antisense sat III transcripts on w^{1118} flies with zhr^{1} flies, which have lost the majority of the pericentric sat III DNA block through a translocation (Fig. 6), as a negative control. To give a better overview of the total sat III RNA signal in the ovaries depicted, I added a panel with a z-projection next to the single z-slice picture. Both probes produced multiple foci in w^{1118} nurse cells and a signal in the oocyte nucleus, with the strongest signal in the samples with sat III sense probes (Fig. 29A,B). Unfortunately, the sense sat III probe also produced a signal in zhr^{1} flies. With

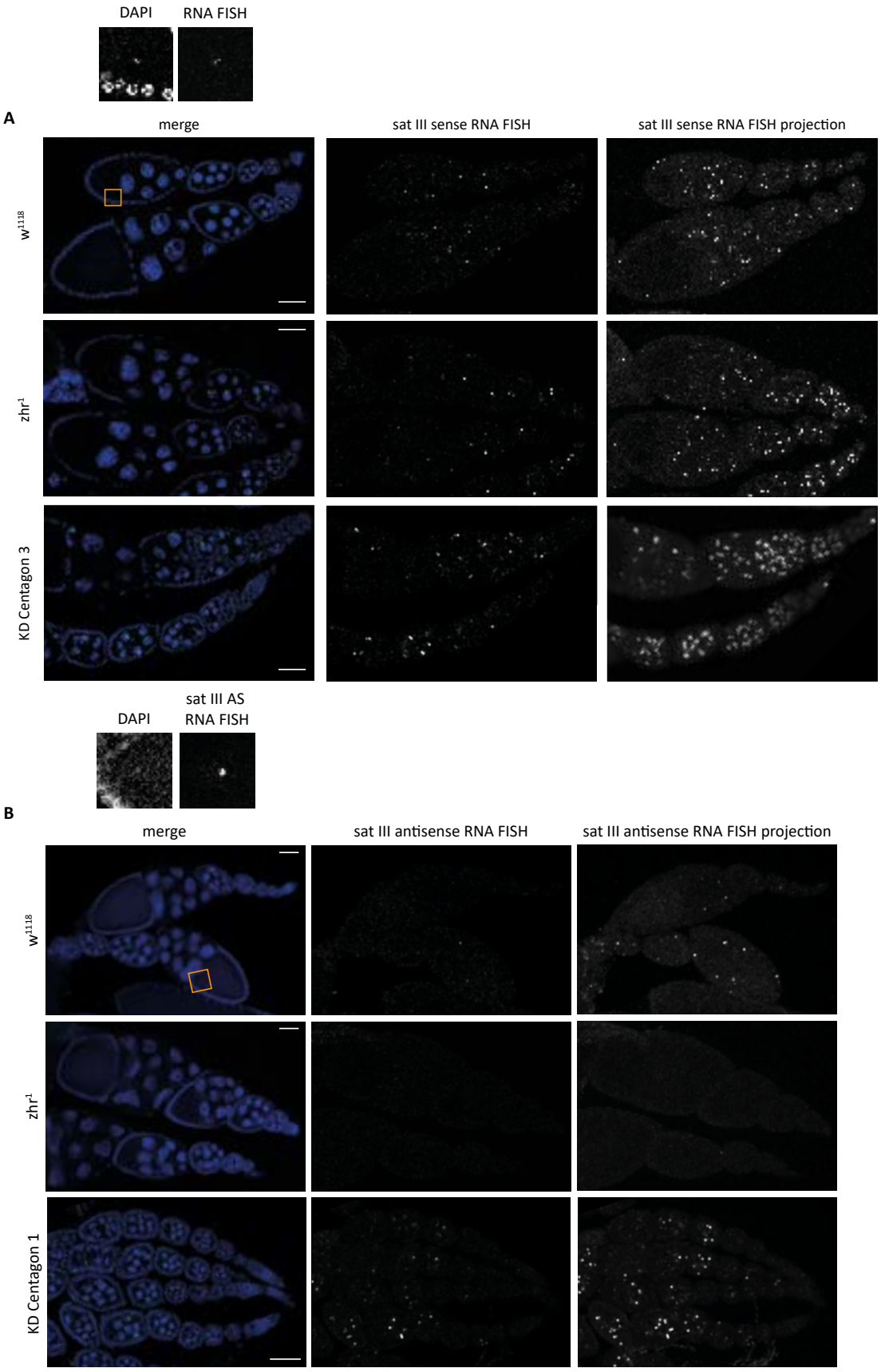

Figure 29: Sat III RNA is expressed in the nurse cells and oocyte nucleus of the ovary
A. Sat III sense and antisense (B) RNA FISH and on $w^{1118,}$ zhr^{1} and KD ovaries. In the first and second row one z- slice (2 µm) is shown, but to improve visibility of the sat III RNA signal a projection of all slices is shown to the right. The orange square is enlarged on top, showing sat III RNA signal at the oocyte nucleus. The scale bar indicates 50 µm. A grey background was added to pictures which were rotated.

the antisense probe there was no detectable signal in zhr[1] flies, indicating that it detected the sat III sequence specifically and not any of the other satellite repeats. Because it is not known how much sat III DNA is left in zhr[1] flies and whether there are also some sat III sequences found outside the major region on chromosome X, we cannot rule out that the sat III sense probe is specific as well, but targets a sequence that is still expressed in zhr[1] flies.

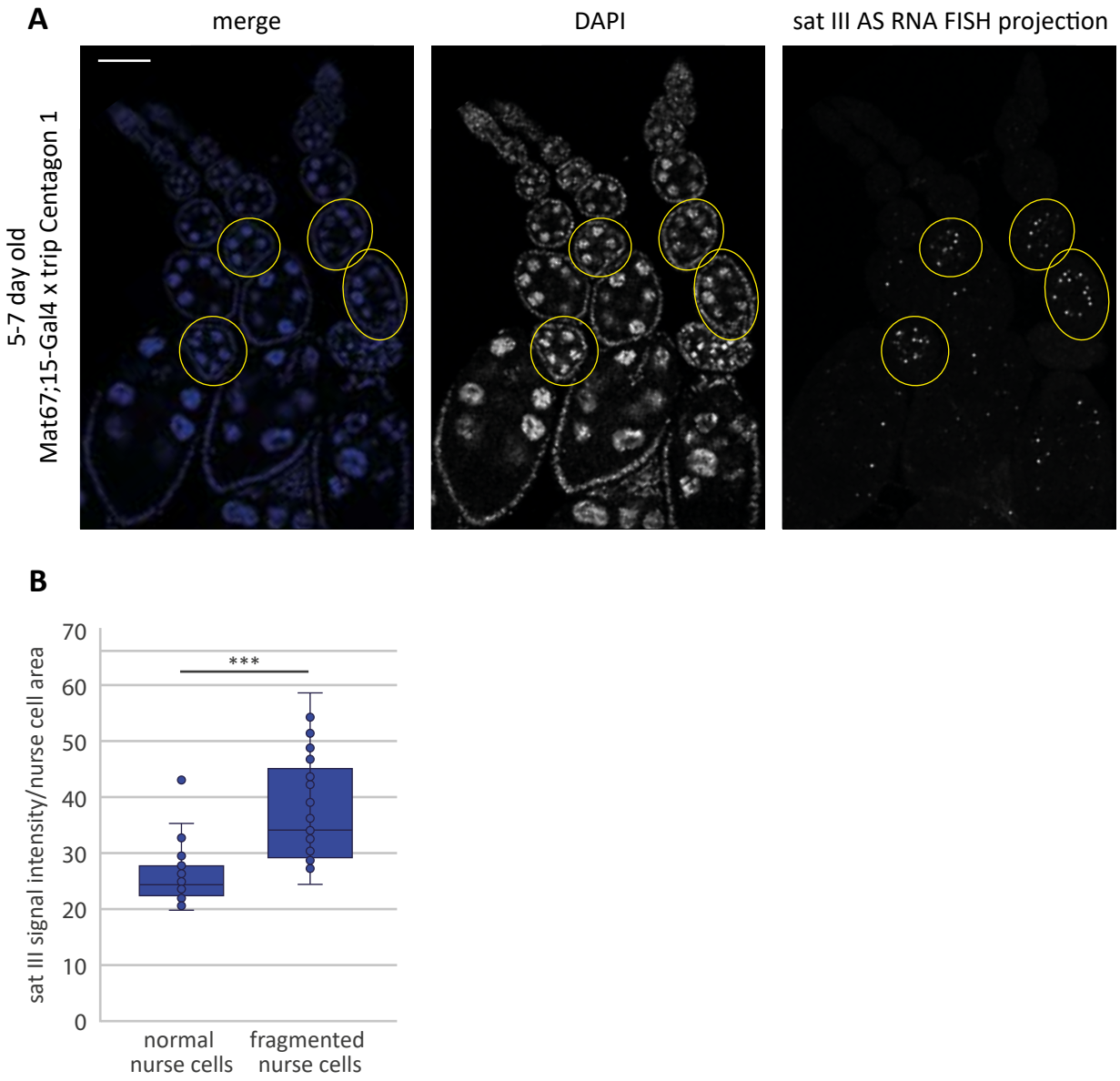

Figure 30: Sat III RNA FISH signal is highest in egg chambers with fragmented nurse cells

A. Example of egg chambers with fragmented nurse cells and high sat III levels (encircled) in 5–7-day-old ovaries of the trip Centagon 1 x Mat67.15-Gal4 cross. The scale bar indicates 50 µm. A grey background was added to pictures which were rotated.

B. Quantification of sat III levels in egg chambers with normal nurse cells and fragmented nurse cells. For each group, 33 egg chambers of 11 ovaries were assessed. The nurse cell region was selected by hand by looking at the DAPI staining and the projected sat III signals were measured in the selected areas. The sat III signal intensity was normalized to the area. * indicates a statistically significant difference calculated with a Student's t-test.

I also included an example of the Mat67.15-induced late KD ovaries with upregulated sat III RNA levels. As can be seen in Fig. 29, KD nurse cells have more and stronger sat III foci than in the w^{1118} cross. It also is apparent that sat III is expressed in all WT egg chambers, as well as in all KD egg chambers, indicating that sat III expression is not stage-specific and the upregulation or stabilization of sat III is not a secondary effect of failed egg chamber maturation. Rather, sat III RNA foci increased in size in growing WT nurse cells.

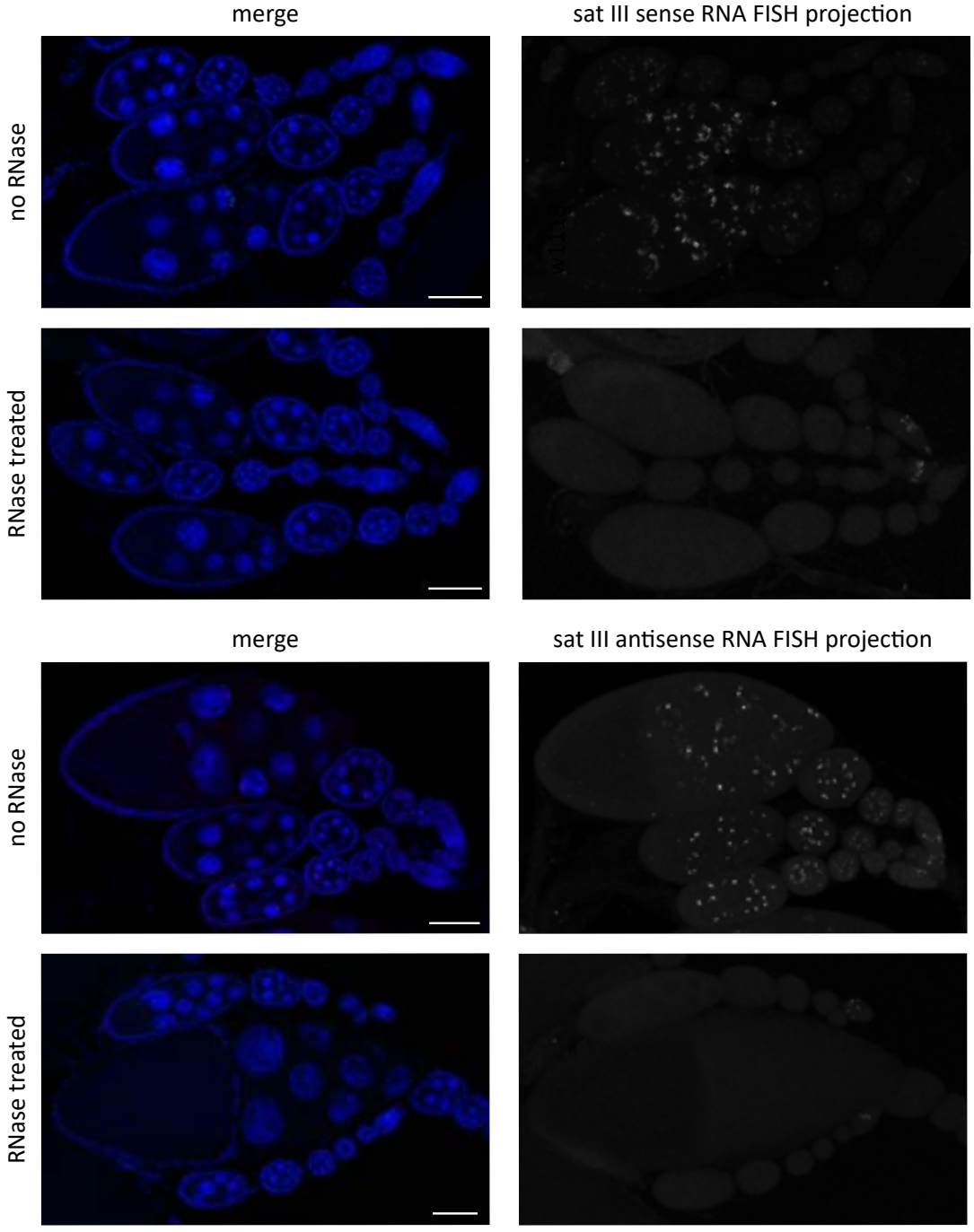

Figure 31: The sat III RNA FISH signal disappears after RNase treatment
Sat III sense and antisense RNA FISH was performed on w^{1118} ovaries with and without RNase treatment. A projection of all z-slices with sat III RNA signal is shown to the right. The scale bar indicates 50 µm. A grey background was added to pictures which were rotated.

Because the egg chambers are impossible to stage in the late KD phenotype, it is difficult to make a direct comparison between the control and KD sat III RNA FISH levels. Instead, I used 5-7 day old KD ovaries with a less penetrant phenotype to compare egg chambers with fragmented nurse cells to normal egg chambers within the same ovary (Fig. 30A). When quantifying the sat III signal intensity in egg chambers with normal and with fragmented nurse cell nuclei, the fragmented egg chambers had a 46% increase in sat III RNA levels ($p = 5{,}6 \times 10\text{-}8$)(Fig. 30B). Therefore, the sat III upregulation seems to be correlated to nurse cell chromatin formation. This may either be caused by impaired expression inhibition, or because sat III RNA breakdown is malfunctioning.

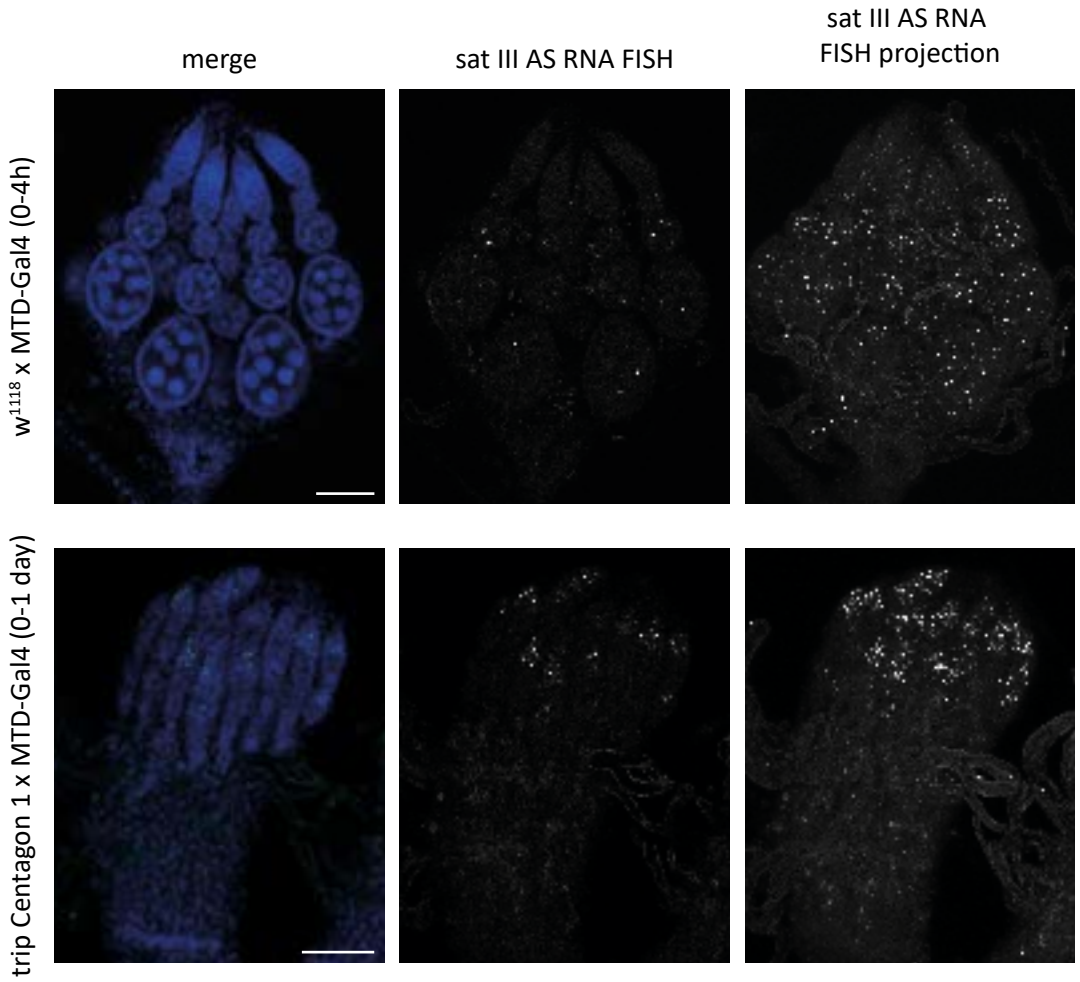

Figure 32: Sat III RNA may also be upregulated in the early KD ovaries
The trip UAS RNAi lines and w^{1118} were crossed with MTD-Gal4 and kept at 18˚C. The F1 females were dissected shortly after hatching (0-4h for the w^{1118} control cross and 0-1 day for the KD crosses) for sat III AS RNA FISH (green) and DAPI (blue) staining. In the first and second row one z- slice (2 µm) is shown, but to improve visibility of the sat III RNA signal a projection of all slices is shown to the right. The scale bar indicates 50 µm.

2.5.3 RNase control for the sat III RNA FISH

To ensure that the sat III RNA FISH detected RNA and not DNA, I performed an RNase digestion on the fixed ovaries before adding the HULU DNA probes. The control samples were incubated with RNase inhibitor in PBS for the same time period and at the same temperature. For both sat III sense and antisense the RNA FISH signal was absent when the ovaries were treated with RNase A, showing that the sat III RNA FISH probes indeed detect RNA (Fig. 31). Interestingly, a localized sat III RNA FISH signal remained in the germaria of RNase-treated ovaries. This means that either not all RNA is digested or the FISH probes bind to another structure when the target RNA has been digested away.

2.5.4 Sat III RNA localization in early KD

Subsequently, I performed sat III antisense RNA FISH on the early KD ovaries of Centagon 1. Again, crosses were kept at 18°C and females were dissected at the ages 0-4 hours for the control and 0-1 day for the KDs. In the w^{1118} control cross, sat III signal was seen in the young nurse cells with only very faint signal in the germaria (Fig. 32, Fig. S2). In the KD ovaries, bright sat III signals were specifically seen in the tips of the rudimentary ovarioles, where remaining germ cells can be found (see Fig. 24). This means that sat III RNA levels also seem to be elevated when the Centagon complex is knocked down in the germaria. This was not validated by qPCR, because so little germ tissue is left in the early KD ovaries that

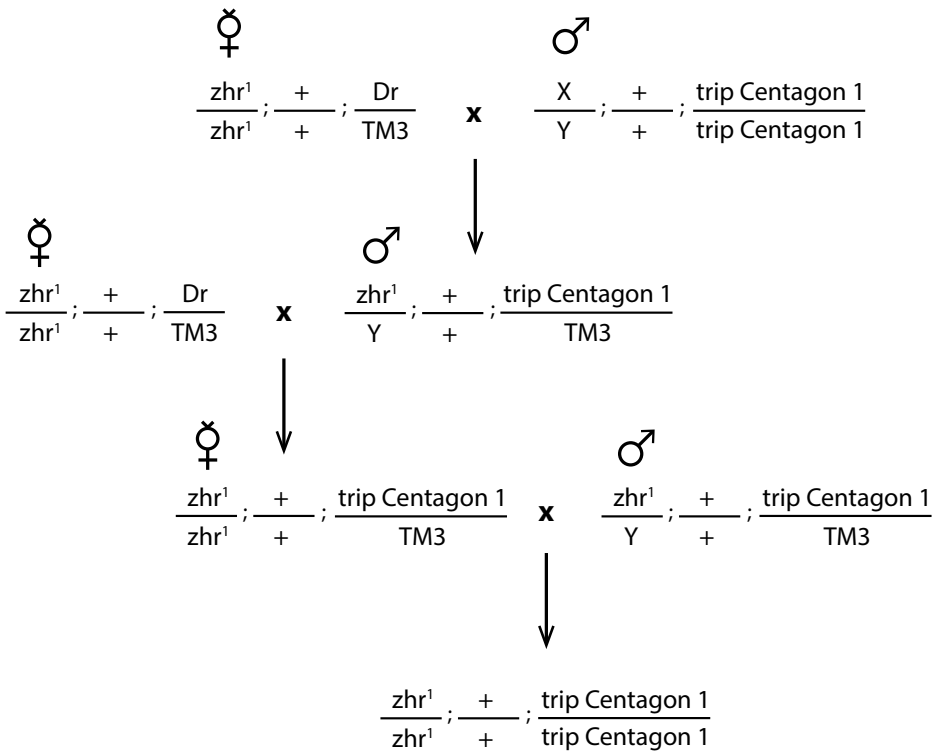

Figure 33: Crossing scheme for introducing the zhr^1 X chromosome
The same crossing scheme was used with the Mat67.15-Gal-4 driver line

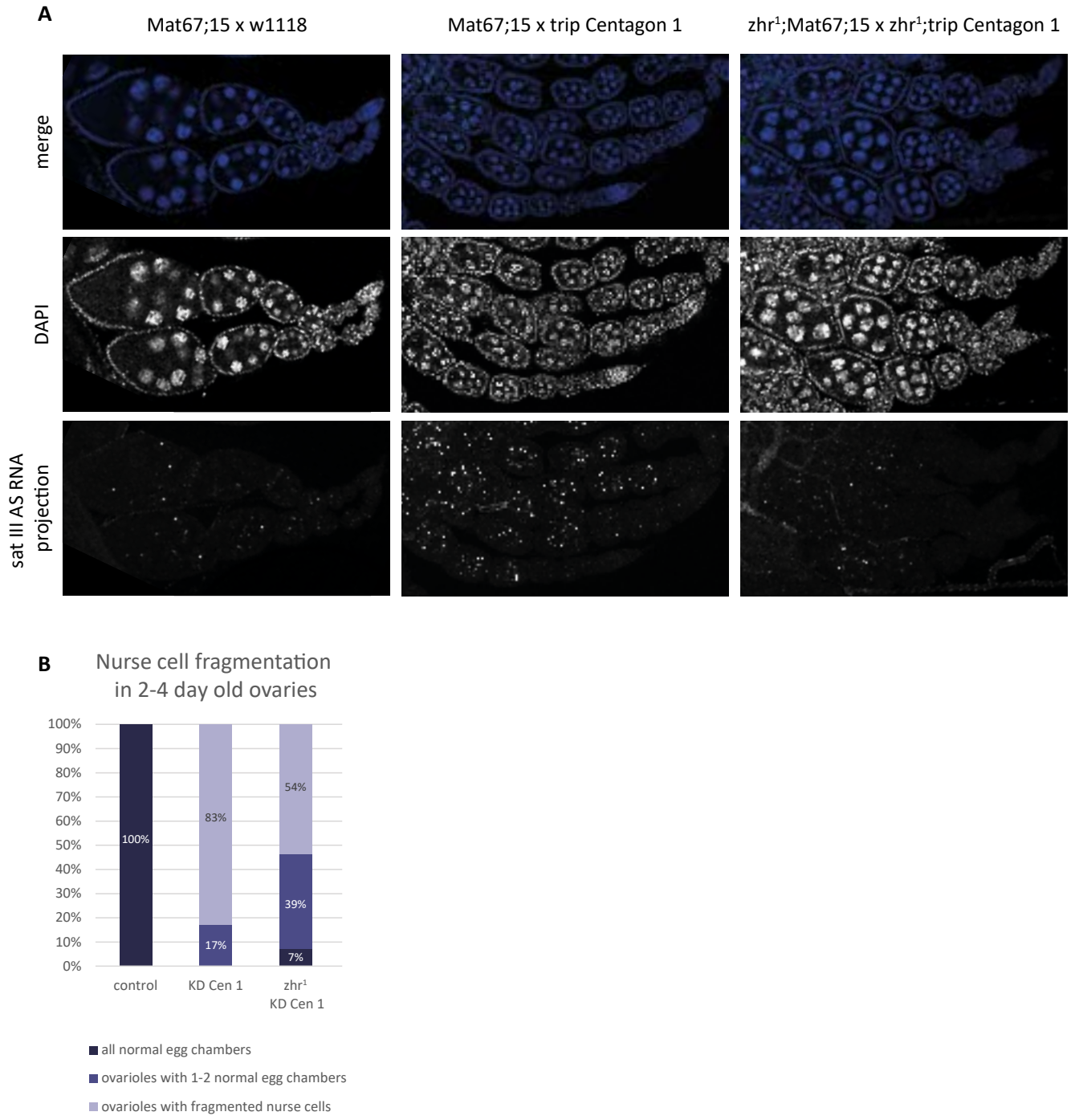

Figure 34: Removal of sat III reduces nurse cell fragmentation in the Centagon 1 KD phenotype

A. Pictures of 2-4-day-old ovaries of the indicated crosses with sat III RNA FISH (green) and DAPI (blue) staining. The sat III signal is a projection of all z-slices. The scale bar indicates 50 µm. A grey background was added to pictures which were rotated.

B. Quantification of the number of ovarioles harbouring no/all but few/only egg chambers with fragmented nurse cells. Early egg chambers (stage 1-5) with naturally occurring fragmented nurse cells were not included. The w^{1118} x Mat67.15-Gal4 and trip Centagon 1 x Mat67.15-Gal4 numbers are the same as in Fig. 24. At least 165 ovarioles were assessed per condition.

most of the RNA isolated would originate from somatic cells. Also, we cannot clearly state whether the sat III RNA foci are found in the germ cells or the follicle cells, since these cell types cannot be distinguished without an additional immunofluorescent staining with a germ cell or follicle cell marker. It is worth mentioning that the localization of the sat III foci is reminiscent of the signals seen in RNase treated w^{1118} ovaries (see Fig. 31). The signal is clearly stronger in the early KD ovaries, but it is possible that due to lack of specific RNA targets the sat III FISH probe binds something unspecific in the germarium. To address this, an RNase digestion has to be performed, which was left out due to time limitations. Until then, this result should be treated with caution.

2.6 Partial Centagon 1 KD rescue in sat III-deficient zhr^1 ovaries

2.6.1 Reduced nurse cell fragmentation in sat III-deficient zhr^1 ovaries

The striking upregulation of sat III RNA in both the early and the late KD, made us wonder whether the high sat III RNA levels play a functional role in the formation of the phenotypes. To address this question, the zhr^1 X chromosomes were crossed into the trip Centagon 1 RNAi line and the Mat67.15-Gal4 driver line for KD experiments (Fig. 33). The crosses w^{1118} x Mat67.15-Gal4 and trip Centagon 1 x Mat67.15-Gal4 were used as controls. I dissected F1 females aged both 2-4 days and 5-7 days old, because my previous experiments had shown that the phenotype ameliorates with aging. Interestingly and importantly, the ovaries with zhr^1 X-chromosomes were less affected (Fig. 34A). The fraction of ovarioles with all normal nurse cells increased from 0% to 7% and the fraction of ovarioles with at least one normal egg chamber increased from 17% to 39% compared to the KD ovaries with sat III RNA (Fig. 34B). Although no sat III RNA signal was detected with the antisense probes in zhr^1 flies before, a weak signal was observed in the KD ovaries with the zhr^1 X-chromosomes, indicating that a few sat III repeats may be left in zhr^1 flies.

To ensure that the KD of Centagon 1 was comparable in the flies with and without sat III, expression levels were monitored by qPCR (Fig. 35). Centagon 1 levels were approximately 50% reduced in the KD ovaries, with the levels of young zhr^1 X-chromosome-carrying flies being slightly higher. I also assessed the expression levels of Centagon 2 and sat III since both were upregulated in my previous experiment. Again, Centagon 2 levels almost doubled in both KD ovaries, but sat III levels only increased in the Centagon 1 KD ovaries (approximately 30-fold), with no sat III increase in flies with zhr^1 X-chromosomes. In the KD

flies with the zhr[1] X-chromosome, sat III levels were comparable to the w[1118] cross, similar to the observations with sat III RNA FISH. Either there is a low level of sat III left on the zhr[1] X-chromosome or the qPCR primers for sat III also recognise a similar sequence which may be upregulated in KD ovaries as well.

When looking at the older flies, the Centagon 1 KD was more efficient, but both the upregulation of Centagon 2 and sat III RNA were less strong (67% and 14-fold), especially for the zhr[1] X-chromosome harbouring flies. The latter showed only 17% upregulation of Centagon 2 levels and sat III levels were reduced to 30% compared to the w[1118] cross. This finding fits the observation that with increased age the phenotype tends to be less severe. However, both in young and old females, the zhr[1] X-chromosome harbouring flies, seem to fare better. Overall, this shows that the high sat III levels partially cause or maintain

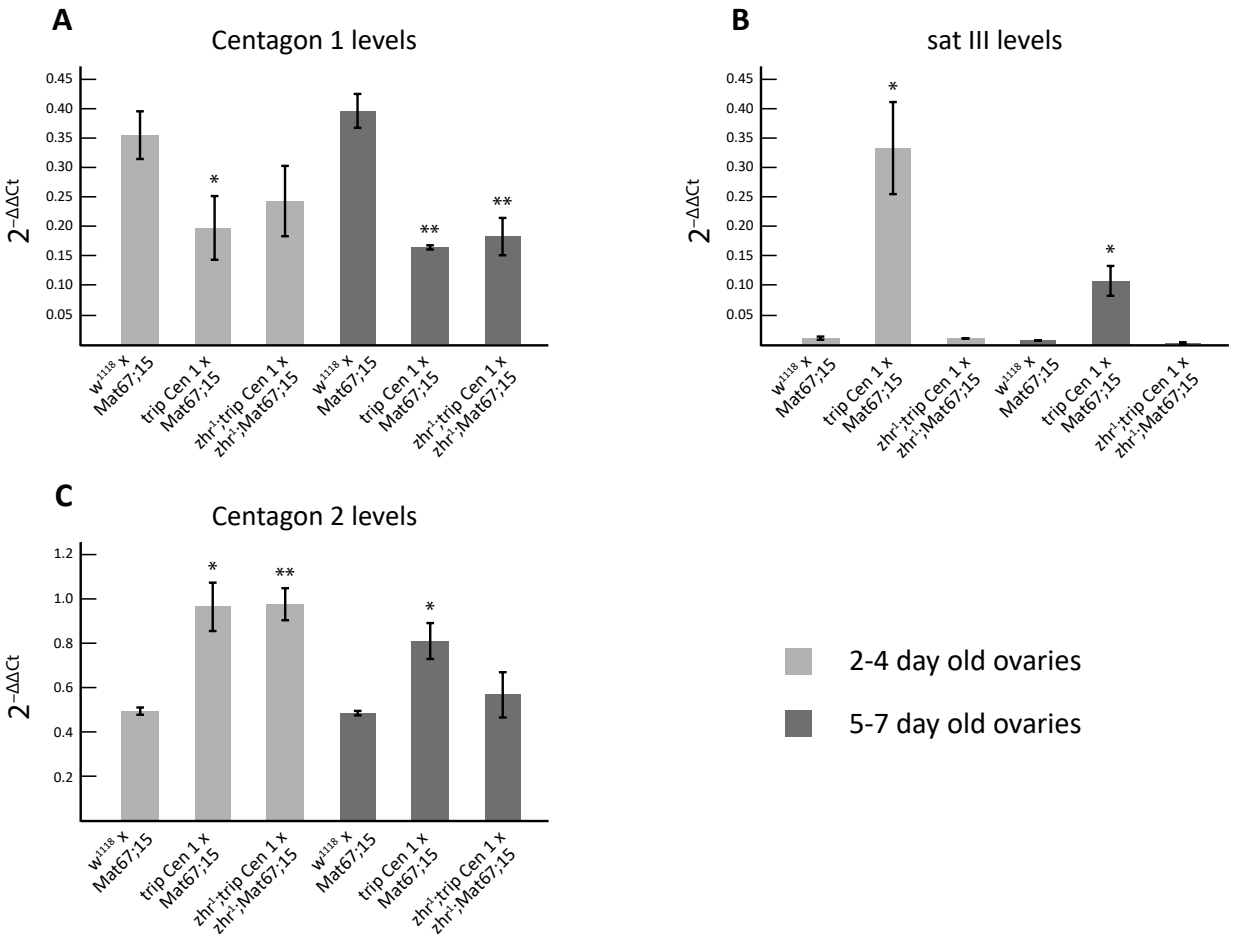

Figure 35: KD efficiency in the zhr[1];trip Centagon 1 ovaries

RNA levels were assessed by qPCR and normalized to housekeeping genes. Different colours indicate the age of the dissected F1 females. Centagon 1 (A), sat III (B) and Centagon 2 (C) ovary expression levels were measured in females of the w[1118] x Mat67.15-Gal4 cross, the trip Centagon 1 x Mat67.15-Gal4 cross and the zhr[1]; trip Centagon 1 x zhr[1]; Mat67.15-Gal4 cross.

For each triplicate, RNA was isolated from 10-15 ovaries.

* indicate statistically significant differences compared to the control (w[1118] x Mat67.15) calculated with a Student's t-test.

the nurse cell fragmentation upon Centagon 1 KD and that without sat III expression the phenotype is less severe.

2.6.2 Higher survival rate in sat III-deficient zhr^1 ovaries

To quantify the positive effect of having low sat III levels, I performed another survival assay with these crosses (Fig. 36). To be precise, I crossed the F1 females of Mat67.15-Gal4-induced KD crosses to w^{1118} males and monitored the F2 eggs. To control for the zhr^1 background, I also used F1 females of a zhr^1 x zhr^1; Mat67.15 cross. I monitored the flies from age 2-3 days until 6-7 days old. At first, no difference between the two Centagon 1 KD crosses was

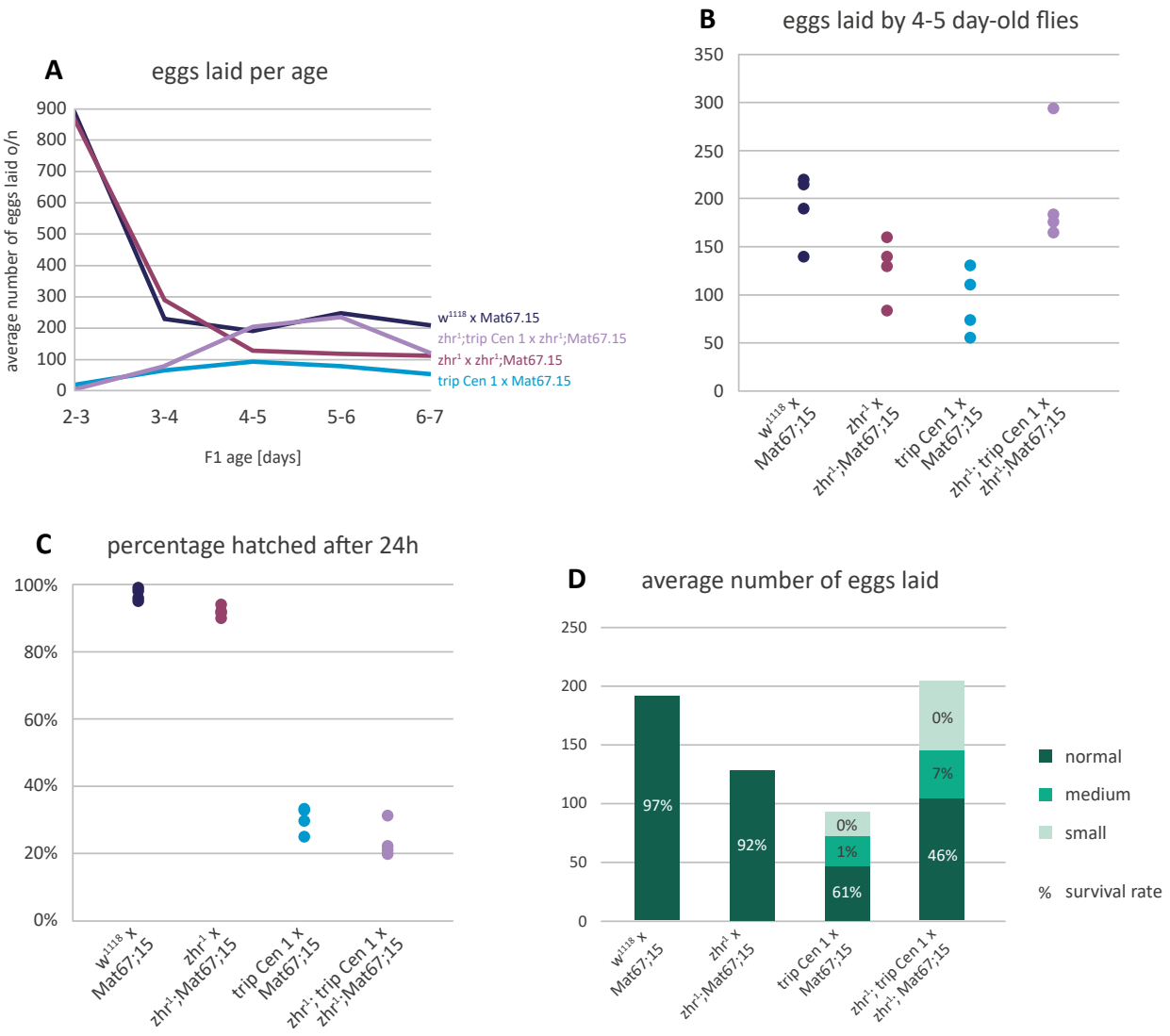

Figure 36: Centagon 1 KD flies without sat III upregulation lay more eggs

A. Average number of eggs laid by the indicated crosses at different ages.

B. Number of eggs laid at the age of 4-5 days. Each dot represents one survival assay.

C. Hatching percentage of the eggs laid in B.

D. Average number of eggs laid in B, categorised into the phenotypes normal/medium/small (see Fig. 25), with survival rate per egg phenotype.

observed, but from the age of 4-5 days old on, the flies with the zhr^1 X-chromosome started laying more eggs compared to the KD females with normal sat III (Fig. 36A). At the age of 4-5 days, the difference was even 3-fold. The opposite effect was seen in the controls, where the F1 females of the zhr^1 x zhr^1;Mat67.15 cross laid approximately 50% less eggs compared to the F1 of the w^{1118} cross. The zhr^1 X-chromosome even rescued egg laying of the KD females to the level of the w^{1118} cross, performing better than the zhr^1 x zhr^1;Mat67.15 control. However, the quality of the eggs remained poor and the hatching rate of the F2 generation remained around 30% upon sat III removal (Fig. 36B-D). In both Centagon 1 KDs, around 50% of the eggs were categorised as medium or small and had a very low hatching rate (0-7%) and also the hatching rate of normal looking eggs did not improve. In conclusion, the removal of sat III DNA and therefore RNA results in a partial rescue of the Centagon 1 KD phenotype in ovaries, with less nurse cell fragmentation and higher egg production.

2.7 KD of the Centagon complex in other cell types and tissues

Since all Centagon members are also highly expressed in somatic follicle cells (Fig. 16) and we already observed phenotypes in larval testis (Fig. 23), we wondered whether and to what extent the KDs effects were specific for the female germline. Therefore, I also used two somatic cell drivers, traffic jam (tj)-Gal4 and GR1-Gal4 to cross with the trip UAS RNAi lines (Goentoro et al. 2006; Sahai-Hernandez and Nystul 2013). As can be seen in ovaries of a UAS-NLS-GFP cross, the tj-Gal4 driver is already active in the follicle cells in the germarium, whereas the GR1-Gal4 driver activates GFP expression in follicle cells in older egg chambers (Fig. 37A). When looking at the KD ovaries, the later GR1-induced RNAi led to ovaries with follicle cell gaps, compound egg chambers (fusion of egg chambers due to the scarcity of enveloping follicle cells) and aberrant egg chamber shapes (Fig. 37B). Even more striking, tj-Gal4-induced KDs predominantly led to loss of all ovary tissue. Only in two cases ovary remnants could be recovered, 1 out of 5 Centagon 2 KD ovaries and 1 out of 5 Centagon 3 KD ovaries (Fig. 37B). This clearly shows that the Centagon complex is also essential for somatic cell survival in ovaries.

Furthermore, in collaboration with Dr. Kerem Yildirim, we dissected and stained adult testis of MTD-Gal4 x trip Centagon 1 and trip Centagon 3 flies (Fig. 38, Fig. S4). The staining included the germ cell marker α-vasa, the hub marker α-fasciclin III and the follicle cell marker α-traffic jam. In contrast to the w^{1118} cross (upper panel) with a fully developed testis filled with vasa-positive spermatogonia and spermatocytes, the KD testes did not develop properly. They are smaller in size, the GSC-anchoring hub is mislocalized, there are far too

many tj-positive cells and no sperm. As seen before in the larval testis, the KD of two of the Centagon proteins also drastically changed testis development and lead to sterile males. Therefore, the sat III-interacting proteins may be involved in a general pathway important for cell differentiation and proliferation in the male and female germline and beyond.

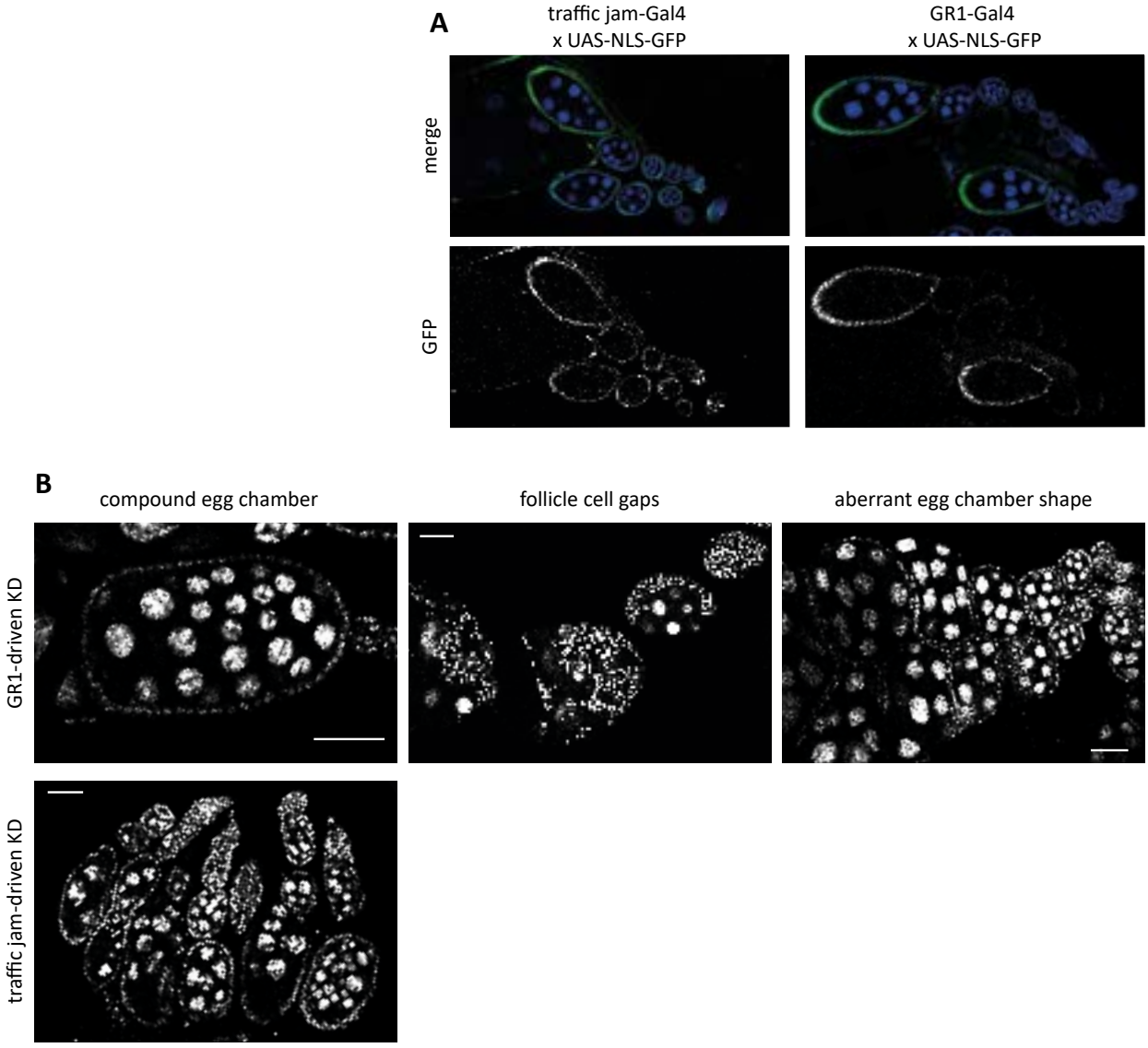

Figure 37: The Centagon complex is also essential for survival of somatic follicle cells.
A. Ovaries of the crosses UAS-NLS-GFP with traffic-jam-Gal4 or GR1-Gal4. The GFP signal shows where the driver starts expressing. The scale bar indicates 50 µm.
B. Examples of the tj-Gal4 and GR1-Gal4 induced KD ovaries with DAPI staining. For the GR1 cross a compound egg chamber, follicle cell gaps and aberrant egg chamber morphology are seen from left to right. For the tj-Gal4 cross one of the two only remaining ovaries is shown. For the rest, no ovary tissue remained after KD of the candidates. The scale bar indicates 50 µm. A grey background was added to pictures which were rotated.

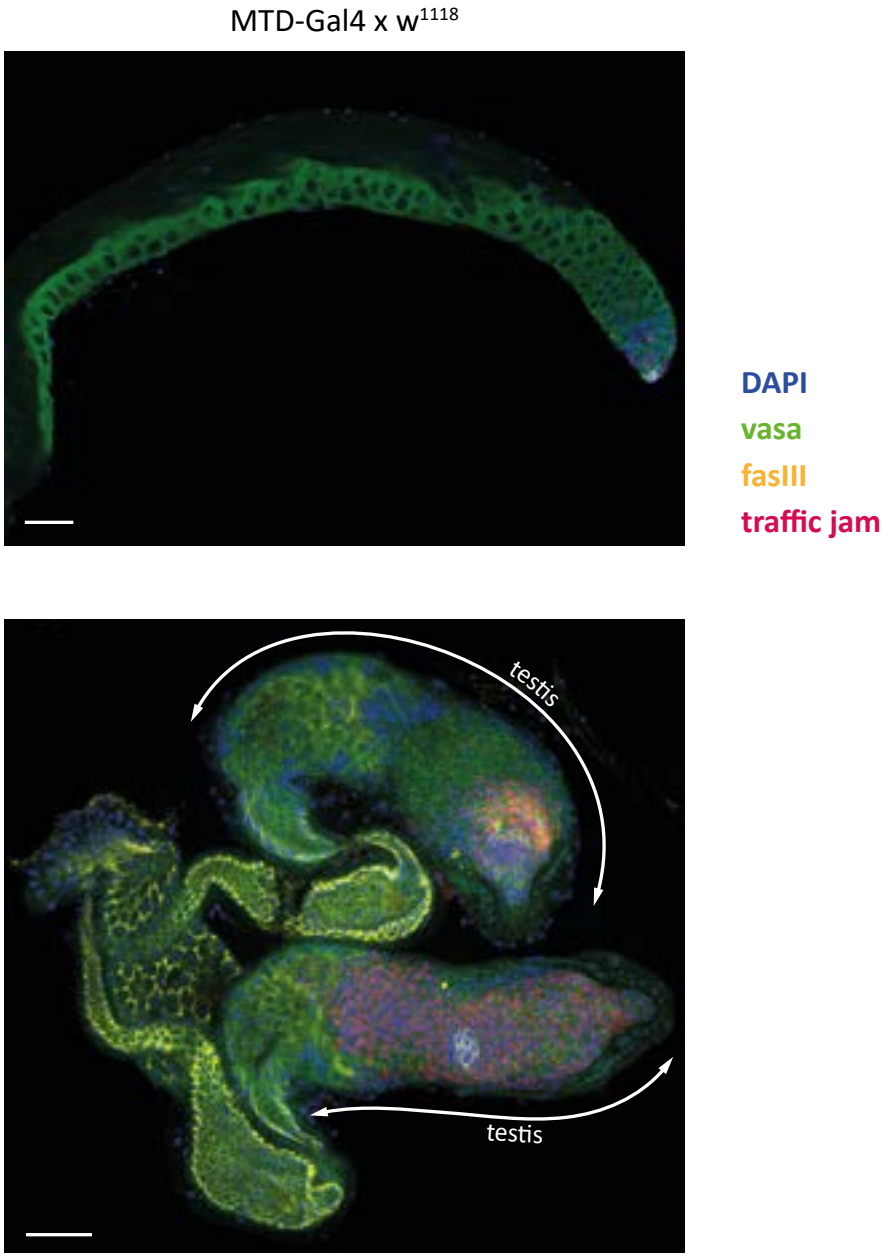

Figure 38: KD of the Centagon members leads to testis malformations
Control (w^{1118} x MTD-Gal4) testis and trip Centagon 3 x MTD-Gal4 testis, aged 1 week, stained with germ cell marker α-vasa (green), the hub marker α-fasciclin III (yellow), the follicle cell marker α-traffic jam (magenta) and DAPI (blue). Dissection, staining and imaging was performed by Dr. Kerem Yildirim. The scale bar indicates 50 µm.

3. Discussion

The Drosophila ncRNA sat III has been shown to stabilize newly incorporated CENP-A at the centromere and to facilitate correct chromosome segregation during mitosis (Rošić et al. 2014; Bobkov et al. 2018). The focus of this study was to identify new roles of sat III RNA by identifying new sat III RNA-binding proteins and characterizing their function in relation to sat III RNA. I found a complex of four previously uncharacterised nucleolar proteins in a sat III RNA-pulldown that were highly expressed in *Drosophila melanogaster* ovaries. RNAi experiments showed that the candidates were essential for gonad development in males and females and KD of the candidates resulted in germ cell loss in ovaries, persistent fragmentation of nurse cell nuclei and arrest of egg chamber development. Furthermore, sat III RNA levels were elevated in KD ovaries and depletion of sat III RNA partially rescued the phenotype. We, therefore, termed the complex Centromeric Transcript Associated Gonadal complex (Centagon). In conclusion, high sat III RNA levels seem to promote germ cell loss in ovaries when one of the four Centagon members is depleted. This emphasizes the importance of satellite RNA and its regulation for cell survival in the female germline and possibly in other tissues and cell types as well.

3.1 Sat III RNA potentially interacts with highly abundant proteins: coincidence or functional importance?

Half of the proteins pulled down consistently with sat III RNA (N=36, 50%) were ribosomal proteins, mostly localizing to the cytoplasm, while around 42% of the hits localized to the nucleus, including CG13096. Sat III RNA naturally is found in the nucleus during interphase and at the pericentric regions (Bobkov et al. 2018; Rošić et al. 2014), as well as in the spindle area during mitosis. Since I used whole cell lysate from cycling S2 cells with in vitro transcribed sat III RNA for the initial pull-downs, the experimental setup allows interactions that would not occur in vivo because of different localisation within the cell. Possibly, the ribosomal candidates were pulled down because they are a large class of RNA-binding proteins in general and highly abundant. The second largest class were RNA processing enzymes, particularly proteins involved in splicing (N=15, 21%). It is not known whether sat III is spliced or otherwise edited, except for a subset of sat III transcripts that have been shown to be polyadenylated in vivo (Wei et al. 2020). Also the sequences used in this study are polyadenylated in vivo, because they were found by 3’ rapid amplification of cDNA ends (RACE) by adding an adapter to poly(A) tails (Rošić et al. 2014). Other candidates found in the sat III RNA-pulldown were proteins involved in cytoskeleton organization, translation

initiation factors and histones. Apart from the histones (H3 and H4) which could interact with sat III during its localisation at the chromatin, there is no indication that sat III RNA binds these proteins in vivo. To our surprise, also 6 uncharacterised proteins were enriched in the sat III RNA pulldown. Their predicted functions and protein classes included the piRNA pathway, rRNA and tRNA processing, RNA splicing, a helicase and a ribosomal protein, mostly predicted to localise to the nucleus or nucleolus. This indicates that the uncharacterized proteins could predominantly fit within the RNA processing group. All in all, I identified mostly proteins that were known or predicted to interact with RNA, albeit with varying functions.

3.2 A COMPLEX OF UNCHARACTERIZED NUCLEOLAR PROTEINS BINDS SAT III RNA

Of all the proteins identified in the sat III RNA-pulldown I decided to focus on four hitherto uncharacterized proteins: Centagon 1 (human NOC3L), Centagon 2 (human NOP2), Centagon 3 (human RSL1D1) and Centagon 4 (human DDX54). The four candidates were predicted to form a complex, which I verified with a yeast-two-hybrid assay (Fig. 10). Importantly, when one of the Centagon proteins was depleted, the other three were upregulated. This shows that the members of the Centagon complex also interact on a functional level. Of the four Centagon members, only Centagon 3 was found in both pulldowns (Fig. 7), indicating that it may have the strongest association with sat III RNA within the complex or possibly the only one that has a direct association to sat III RNA. Coincidentally, it is also the only protein that we could purify in sufficient amounts and purity for an EMSA and, therefore, the only protein whose sat III RNA-binding capacity we validated. In the EMSA, Centagon 3 did not only bind to sat III RNA, but also to the control hsr omega (Fig. 11), which was already indicated in the mass spectrometry data of the hsr omega pulldown (Fig. 7) (12 peptide counts in the sat III pulldown sample vs 10 in the hsr omega sample). Because Centagon 3 also bound to the tubulin transcript in vitro, we concluded that it is probably a bona-fide RNA-binding protein. The other three candidates were not found in the second RNA pulldown, indicating that they either bind sat III RNA more loosely, or only indirectly through their interaction with Centagon 3. This could be further specified with RNA-EMSAs or RNA-IPs in future experiments. In theory, Centagon 1, 2 and 4 all have the capacity to bind RNAs, because of their domains and predicted homologues (Fig. 9). Centagon 1 has an armadillo-type fold which accommodates binding to large substrates such as proteins or nucleic acids (https://www.ebi.ac.uk/interpro/), Centagon 2 is a putative rRNA methyltransferase whose homologue NOP2 binds to long non-coding and repetitive RNAs (Hong et al. 2016; Wang et

al. 2014) and Centagon 4 is a putative DEAD box RNA helicase, whose family members have been shown to bind human satellite I RNA (Nishimura et al. 2019). On the other hand, I could only validate the interaction of Centagon 2 with all other Centagon members with the yeast-two-hybrid assay. Therefore, I propose a model where Centagon 2 forms the centre of the Centagon complex with Centagon 3 being the direct link to sat III RNA. Because sat III RNA and the Centagon members have a similar localisation during interphase and early mitosis (Fig. 12 and 13), their interaction may be stable throughout these stages.

3.3 The Centagon complex could contribute to multiple pathways

When assessing the predicted domains and functions of orthologues of the Centagon members, a few overlaps and common features can be found. These suggest a few possible functions of the nucleolar Centagon complex:

1. **Ribosomal biogenesis**: The yeast orthologue of Centagon 1 (Noc3p) is important for 60S ribosomal subunit maturation and export, and also has been implicated in rRNA maturation (Milkereit et al. 2001). Centagon 2 is a putative rRNA methyltransferase, possibly involved in rRNA maturation. The nucleolar protein fibrillarin, for example, is also an RNA methyltransferase and essential for methylation of pre-rRNAs, synthesis of both 18S and 25S rRNA and ribosome assembly (Tollervey et al. 1993). Also Centagon 3 seems to be an rRNA processing factor, whose KD leads to the accumulation of aberrant rRNA intermediates in S2 cells (Sanchez et al. 2016). Furthermore, Centagon 4 is a putative DEAD-box RNA helicase, which can unwind RNA duplexes and remove proteins from RNA. Because of these functions, DEAD-box RNA helicases are often found in large complexes involved in RNA metabolism, such as spliceosomes or the nascent ribosome (Linder and Jankowsky 2011).

2. **RNA-splicing**: The human orthologue of Centagon 1 (NOC3L/FAD24) has been suggested to have a role in pre-mRNA splicing (Tominaga et al. 2004) and as mentioned, above Centagon 4 is a putative DEAD-box RNA helicase which are often found in big complexes such as spliceosomes (Linder and Jankowsky 2011).

3. **S-phase and replication initiation**: The yeast orthologue of Centagon 1 (Noc3p) binds to chromatin constitutively and initiates S phase and replication (Zhang et al. 2002). Its human orthologue, Noc3L, initiates replication by recruiting

components of the pre-replicative complex to the origin of replication (Johmura et al. 2008; Cheung et al. 2019). Another cell cycle function has been found for the human orthologue of Centagon 2 (NOP2), which has been identified to bind to the promoter of cyclin D1, thereby activating its transcription. Cyclin D1 is important for G2 to S phase transition (Fonagy et al. 1992; Wang et al. 2020). Furthermore, the human orthologue of Centagon 3 (RSL1D1) promotes cell proliferation and overexpression increases the fraction of cells in S phase (Ma et al. 2008).

3.4 A possible role for the Centagon proteins in ribosome biogenesis and GSC differentiation

Considering that the Centagon proteins are highly expressed in the female germ line, there are several ways how their putative functions could contribute to oogenesis. As described in chapter 1.3.2, ribosome biogenesis is tightly linked to stem cell maintenance and defects in ribosome biogenesis can shift the balance in GSC division towards differentiation or impair differentiation. Accordingly, two screens identifying genes essential for GSC self-renewal and proper differentiation found many factors involved in ribosome biogenesis-associated processes such as rRNA transcription, rRNA processing and ribosome assembly (Yan et al. 2014; Sanchez et al. 2016). Notably, the role in splicing of some Centagon proteins may also occur in the context or rRNA maturation and, therefore, might be connected to a role in ribosome biosgenesis. If the Centagon complex functions in ribosome biogenesis, their depletion could affect the GSC self-renewal capabilities and promote aberrant differentiation. This would fit with the observation that germ cells are lost when the Centagon proteins are knocked down in germaria with the MTD-Gal4 driver (chapter 2.4.2). On the other hand, in a less penetrant KD at 18 ˚C, I still could identify pMad-positive germ cells (Fig. 23), not only in the stem cell niche, but also in later germ cell cysts. In the case of the Centagon 1 KD specifically, the pMad levels were equally high in the CBs and GSCs, arguing for a dedifferentiation defect. In that case, the failure of germ cells to properly differentiate and form egg chambers, could also be the cause for germ cell loss. Indeed, I observed that the young egg chambers of the MTD-Gal4-induced KDs, never matured and probably underwent apoptosis. Not all germ cell cysts expressed pMad, but all had an aberrant morphology as seen by the disorganized vasa signal.

A second finding pointing towards a differentiation defect, was the male-specific effect of the Centagon KD in larval gonads. At the time of dissection the larvae had reach the 3rd instar stage, when male gonad development has reached a far more advanced stage than

in females. While male gonads already start to differentiate in the embryo (Fig. 1), female gonads mainly proliferate and only start differentiating at the onset of the 3rd instar larval stage. If the Centagon complex is involved in germ cell differentiation, it is no surprise that the effects in the male gonad are visible at an earlier stage compared to females since the differentiation takes place at an earlier stage in the male germ line. Furthermore, one could argue that the spermatogonia or spermatocyte remnants in the larval testis would fit with a differentiation defect, since they do not develop properly, are too few and also show an aberrant vasa immunostaining. If stem cell-maintenance was affected, this would mostly affect stem cell number and not the morphology of differentiated cells.

Interestingly, all four Centagon proteins were identified in the screen by Sanchez et. al. mentioned earlier (Sanchez et al. 2016), of which Centagon 2 and 3 were further characterized. In their experimental setup with the nanos-Gal4 driver (also expressing in the germarium), the KD ovaries accumulated undifferentiated Bam-negative, interconnected germ cells in the tip of the germarium and had egg chambers without oocyte specification. Although this phenotype differs from my observations, they also describe a differentiation defect of the germ cells. Possibly, both phenotypes are the result of the same differentiation defects caused by ribosome biogenesis perturbation, but with different outcomes due to different timing, strength and specificity of the Gal4-driver used for the KD.

If the Centagon complex is involved in ribosome biogenesis, then why are the proteins expressed so highly in the Drosophila ovaries? It has been shown that GSCs express variant isoforms of general transcriptional components, translation initiation factors and ribosomal proteins, some even being GSC specific (Kai et al. 2005). These factors may help to transcribe, process and translate germ cell- or GSC-specific genes, thereby supporting the maintenance of cell identity. Therefore, it may not only be ribosome biogenesis itself that is important for GSC maintenance and differentiation but which ribosome biogenesis factors are expressed in the cell. In the case of the Centagon proteins, their expression is high in GSCs but diminishes in the subsequent stages (Fig. 16). However, upon KD of the Centagon proteins, I do not observe an accumulation of differentiated cells. On the other hand, we know that the other Centagon complex members are upregulated when one is depleted, so maybe the balance of the Centagon complex members is important for the cell identity in the germ line. It should be noted, that the Centagon complex was also expressed in somatic ovary cells, where depletion led to detrimental defects, especially when knocked down in the stem cell niche (Chapter 2.7). Furthermore, Centagon 4 has been found in a neuronal stem cell self-renewal screen (Neumüller et al. 2011) and the human orthologue of Centagon 1

is important for adipocyte differentiation (Tominaga et al. 2004). This indicates that the Centagon complex does not specifically function in the germ line, but may have a general role in stem cell biology, possibly through a role in ribosome biogenesis.

As mentioned above, the Centagon complex may also be involved in S phase and replication initiation. With the observed phenotypes in KD ovaries, this seems less likely to be the cause of germ cell loss. Assuming that Gal4 expression and, therefore, the KD of the Centagon proteins starts at the same time in male and female larvae, any defect impairing cell cycle progression should also affect the proliferation of germ cells in the female gonad. However, no major differences in the larval ovaries of the Centagon KD and the control cross were observed. Nonetheless, a role in replication initiation cannot be excluded. As described in chapter 1.3.1, asymmetry of the stem cell is already initiated during replication when either new or pre-existing histones are preferentially incorporated in one of the two DNA strands to be specifically inherited by one of the daughter cells during mitosis. It is conceivable that GSCs express a specific subset of genes involved in replication which are essential for creating asymmetry, thereby indirectly linking replication to differentiation. With such a role, a dysfunctioning Centagon complex would only become apparent during a time in development when the GSCs start to asymmetrically divide.

3.5 The Centagon members may be part of a bigger complex

Interestingly, the Centagon complex members may also interact with two other RNA helicases, as can be seen by STRING analysis (Fig. 38). These previously uncharacterized RNA helicases, CG5589 (Aramis) and CG9253 (Porthos) where shown to be involved in ribosome biogenesis and identified to cause the same undifferentiated germ cell cysts as were documented by Sanchez et. al. CG5589 (Aramis) seemed to be involved in translation of mRNAs harbouring a TOP motif, which included many ribosomal proteins and a p53 repressor Non1. Depletion of CG5589 (Aramis) inhibits translation of Non1 and thereby leads to elevated p53 levels and cell cycle arrest in GSCs (Martin et al. 2021). The connection of ribosome biogenesis deregulation and p53 increase has also been reported by other authors (Donati et al. 2013; Sloan et al. 2013). Among others, for the human orthologue of Centagon 2 (NOP2) whose depletion resulted in dramatically reduced levels of 28S and 5.8S rRNAs, as well as a slight reduction of S5 rRNA incorporation into the ribosome. p53 levels were clearly upregulated after NOP2 KD (Sloan et al. 2013), showing that the defects found after Centagon KD may also be mediated through p53. Therefore, it would be very informative to measure Non1 and p53 levels in Centagon-depleted ovaries to assess whether this pathway is affected. All in all,

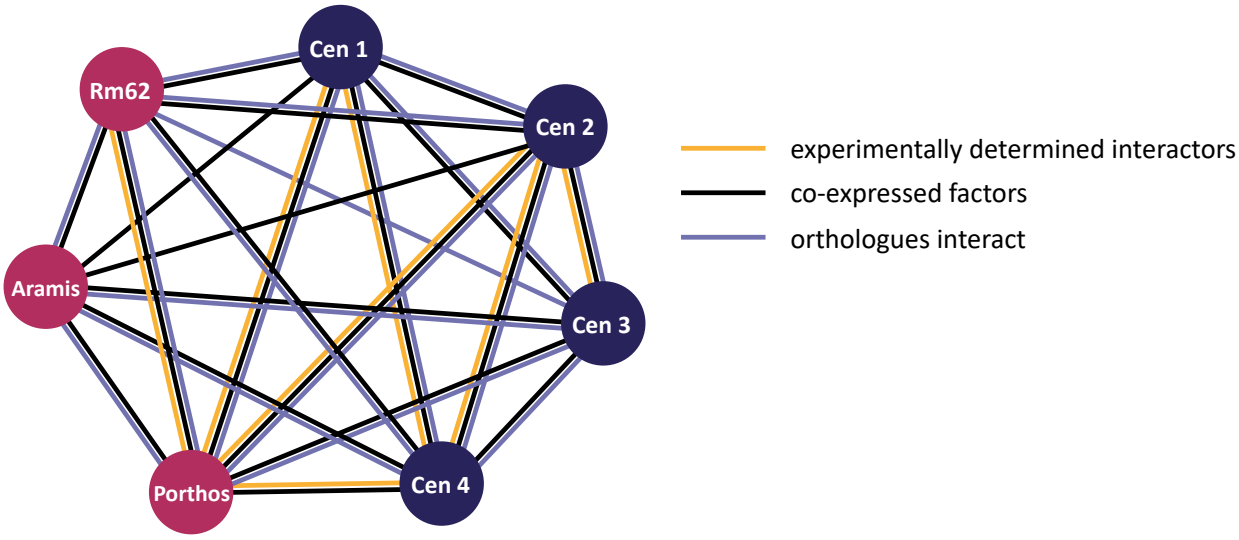

Figure 39: The Centagon proteins may be in a bigger complex
Schematic view of the interactions between the Centagon proteins and the DEAD/DEAH-box RNA helicases RM62, Aramis and Porthos according to STRING analysis (https://string-db.org/).

the Centagon members may be part of a bigger group of proteins affecting GSC maintenance through their ribosomal functions and p53 regulation.

The question remains what role the non-coding sat III RNA could have in a complex that may be involved in rRNA maturation. In general, ncRNAs have been shown to affect multiple aspects of gene expression, from epigenetic regulation, to transcription, transcript processing and translation (Zhang et al. 2019). In the context of rRNA maturation, sat III RNA hypothetically could influence splicing or other post-translational modification of rRNAs. Especially because the sat III locus is located next to the rDNA locus, their transcripts are likely to meet and such a process could have co-evolved. This is, however, speculative and more research is needed to identify a putative role of sat III RNA in the context of rRNA biology.

3.6 The Centagon complex affects nurse cell chromatin formation in ovaries

3.6.1 Ribosome biogenesis

When the Centagon complex was depleted at a later stage during oogenesis with the Mat67.15-Gal4 driver, the germ cells were affected in a different manner. Egg chambers arrested early in development during the five-blob chromatin stage and eventually underwent apoptosis (Fig. 24). Because the endocycles of the nurse cells are unique and not widely studied, it might be helpful to look at other genes with a similar phenotype to identify possible causes.

The first example is a ribosomal S2 protein, encoded by string of pearls, which received its name due to mutants with characteristic ovarioles harbouring arrested egg chambers of equal size (Cramton and Laski 1994). The ribosomal protein S2 is involved in assembly and nuclear export of the pre-ribosome (https://flybase.org/), indicating that also here ribosome assembly may be of importance. Just like ribosome biogenesis is connected to stem cell maintenance (Sanchez et al. 2016), it might also be essential in later stages of oogenesis. It has been hypothesized that restructuring of the nucleolus after nurse cell chromatin dispersal is necessary for rapid ribosome synthesis (Dej and Spradling 1999). In mutants of the chromatin insulator Su(Hw), however, the five-blob nurse cells had normal rRNA intermediate levels and normal oocyte production (Baxley et al. 2011), showing that the aberrant chromatin formation does not affect ribosome biogenesis on a quantitative level. On the other hand, nucleolus perturbation and faulty ribosome biogenesis could affect the nurse cell chromatin. Females with KDs of Centagon members lay considerably smaller and deformed eggs (Fig. 25), which could point towards a protein synthesis problem. Furthermore, egg chambers with fragmented nurse cells remain small (Fig. 24), which also suggest a halt in protein synthesis.

3.6.2 Splicing

Next, splicing seems to play a major role in the five-blob phenotype. Ovarian tumor (otu) mutants harbour the nurse cell chromatin dispersal defect (King et al. 1986), which is linked to the long 104 kDa isoform (Steinhauer and Kalfayan 1992). Consequently, genes which affect the splicing of otu transcripts, such as the splicing factor Half pint together with Hrp48 and Gloround, result in the five-blob phenotype when mutated (van Buskirk and Schüpbach 2002; Goodrich et al. 2004; Kalifa et al. 2009). Importantly, the nurse cell fragmentation defects can be rescued by supplying the right isoform of otu (van Buskirk and Schüpbach 2002). Also other proteins involved in splicing cause the five-blob phenotype when mutated, such as the DEAH-box helicase Pea (Klusza et al. 2013) and the DEAD-box RNA helicase Gemin3 (Cauchi 2012). In other mutants otu splicing is unaffected, but otu levels are reduced, as is the case for the HnRNP Squid (Goodrich et al. 2004). Also, the Centagon proteins may have roles in splicing and may affect nurse cell chromatin dispersal through an otu-dependent pathway. otu splice forms may be monitored by PCR or Northern blot to further address this in the future.

3.6.3 Cell cycle regulation

Mutations of E2F1/DP/mip120, important for cell cycle gene transcription and G2-M transition (Royzman et al. 2002; Cheng et al. 2017), also cause the five-blob phenotype, suggesting a connection of this phenotype to cell cycle progression. Knowing that the Centagon members seem to be important for entering S phase and initiating replication, it is very interesting to consider that nurse cells with the five-blob phenotype do not manage to disperse their chromosomes, which usually happens between S5 and G6. During this endocycle, S phase is shortened and the cells are thought to undergo some form of mitosis to separate the chromosomes (Dej and Spradling 1999). When the Centagon members are knocked down, an error in S phase could prevent the nurse cells from entering the next phase of endocycling. That the nurse cells are not affected earlier could be due to the timing of Gal4 expression with the Mat67.15-Gal driver. As visible in Fig. 19, Mat67.15-Gal4-driven expression of NLS-GFP starts around the egg chamber stage 4, just before chromatin dispersal. Alternatively, the Centagon complex has a specific role during the transition from endocycle 5 to 6. It is unclear whether DNA replication itself is impaired in the context of nurse cell dispersal defects. At least in one example, five-blob nurse cells did not show any differences in ploidy compared to egg chambers from heterozygous controls (Hartl et al. 2008). In our own experiments, I only assessed the gDNA levels of sat III in relation to actin and gapdh genes, but performed no absolute quantifications. Additionally, not all egg chambers with fragmented nurse cells arrest during development, as has been shown in several studies (van Buskirk and Schüpbach 2002; Motola and Neuman-Silberberg 2004; Baxley et al. 2011). In the case of Centagon KDs, nurse cell fragmentation usually coincided with a general halt of egg chamber growth. The egg chambers that developed further, had also less fragmented nurse cells. Whether these two mechanisms are indeed coupled needs to be seen in the future.

3.6.4 Transcriptional silencing and heterochromatin formation

Last but not least, DEAD-box RNA helicase Rm62 (p68) mutants have the characteristic fragmented nurse cells. Since Rm62 is involved in splicing, a plausible cause for the phenotype would be the loss of the right otu spliceform. However, Rm62 has also been shown to be important for RNA export from the nucleus and gene silencing. In Rm62 mutants, nascent transcripts are retained at the site of transcription for a longer time period, which presumably impairs gene shutoff. Targeting of Rm62 to loci at the onset of gene shutdown may increase the export of RNAs and clear the region for protein complexes inducing heterochromatin formation (Buszczak and Spradling 2006). Although it is not clear how this function contributes to the nurse cell chromatin dispersal defects, it is comprehensible that an alteration in endocycle and chromatin formation requires a change

in gene expression, and a defect in gene silencing could impair the transition. As Rm62 has been found in a complex with Ago2 (Ishizuka et al. 2002), it might additionally interact with the RNAi pathway, forming a potential link between RNA clearance and heterochromatin formation (Buszczak and Spradling 2006). The Centagon complex may have a functional connection to Rm62. Not only was Rm62 found in my sat III RNA pulldown (although not strongly enriched), STRING analysis also predicted that all Centagon members interact with the DEAD-box RNA helicase Rm62 (Fig. 38). Additionally, the human orthologue of CG32344 (DDX54) acts as a transcriptional repressor by interacting with nuclear receptors (Rajendran et al. 2003). Simultaneously, this may also be a putative pathway causing the differentiation defect in GSCs. It is known, that GSCs undergo transient transcriptional silencing when differentiating into CBs (Flora et al. 2018) and a defect in gene shutoff may impair differentiation. Indeed, in adipocytes, both orthologues of Rm62 (DDX5) and CG1234 (NOC3L) have been shown to promote differentiation (Ramanathan et al. 2015; Tominaga et al. 2004).

All the examples mentioned above demonstrate that the five-blob chromatin phenotype is caused by perturbations of many different pathways. I have proposed several mechanisms by which the Centagon complex could be involved in nurse cell chromatin dispersal, but further experiments are necessary to assess whether impaired RNA splicing, replication defects, RNA clearing and transcriptional silencing and/or ribosome biogenesis attribute to the imbalances in the cell.

3.7 Sat III RNA levels are elevated in KD ovaries

One important finding of my work is that upon KD of the Centagon complex in ovaries, sat III RNA levels were strongly elevated. I measured sat III RNA levels by qPCR in Mat67.15-Gal4-induced KD ovaries and detected up to 50-fold higher levels compared to the control. I also determined that the high sat III RNA levels were not solely caused by a higher sat III DNA content of the arrested nurse cells, but must be caused by higher transcription rates or increased stability of the transcripts. Subsequently, I performed sat III RNA FISH and observed that sat III expression is not limited to a specific oogenesis stage and that the transcripts are found in the nurse cell and oocyte nuclei. The latest experiments in S2 cells suggest that sat III RNA localizes in *cis* on the pericentromere of the X chromosome (Bobkov et al. 2018). In our sat III RNA FISH experiments in ovaries, there seems to be more than one foci per nurse cell, which could be due to the special chromosome arrangement or a localization in *trans* as observed before (Rošić et al. 2014). After S5, the nurse cell chromosomes disperse

into 32 pairs of two, therefore, multiple sat III RNA foci may still mean that the transcripts localize in *cis*. In depleted egg chambers with the five-blob phenotype, sat III levels were significantly higher compared to normal egg chambers within the same ovariole (Fig. 29).

I also detected high sat III RNA levels in the rudimentary ovaries of the MTD-Gal4-induced KD (Fig. 31). There, the transcripts localized to the stem cell niche, while usually the sat III foci are only visible in egg chambers. Interestingly, a similar pattern was observed in w^{1118} ovaries with RNase treatment, where all sat III RNA signals disappeared, apart from a region in the germarium. In ovaries without RNase treatment, no sat III RNA signal was found at this location, so it is specifically bound by sat III FISH probes after digesting the RNA. Since the sat III RNA FISH is performed at 30°C, the probes are very unlikely to bind dsDNA. However, maybe ssDNA or remaining RNA are bound in the RNase control ovaries. In my experiments I used RNase A, which specifically degrades the cytidines and uridines of single stranded RNA (Borkakoti 1983). If RNA-DNA triplex structures are present, the RNA could be protected from RNase A or ssDNA could be available for the FISH probes. Maybe this binding only occurs when no other, more readily available RNA strands are present. Alternatively, these signals are just completely unspecific binding of the probes, when no sat III RNA can be bound. Either way, an RNase control of the rudimentary MTD-Gal4 KD ovaries should be performed to confirm that the signals observed are RNase-sensitive. If so, depletion of our candidates in both early and late oogenesis result in upregulation of sat III RNA. If we consider the aforementioned functions of our candidates, several mechanisms can be proposed.

3.7.1 Disruption of the nucleolus and impaired heterochromatic silencing

First, the KD of the Centagon members may disturb the nucleolus integrity. This has already been shown in other genes, whose KD resulted in GSC maintenance defects (Martin et al. 2021; Sanchez et al. 2016). The nucleolus has an outer layer of perinucleolar heterochromatin where the nucleolus-associated chromatin domains (NADs) localize. NADs are gene poor, consist of many repetitive elements, harbor heterochromatic histone marks and are generally transcriptionally silent (Matheson and Kaufman 2016). It has been shown that localization of the centromeres to the perinucleolar heterochromatin is important for maintaining centromeric heterochromatin and the silencing of repetitive elements. In S2 cells, depletion of the chromatin insulator CTCF resulted in declustering of centromeres from the nucleolus and increased levels of repetitive element transcripts, including sat III. This led to increased double-strand breaks in the genome and mitotic defects (Padeken et

al. 2013). Also in human cells, centromere-nucleolus associations are important for silencing satellite repeats (Bury et al. 2020). Possibly, the depletion of Centagon members affects the nucleolar organization to a degree where the heterochromatic status of sat III repeats cannot be maintained. It should be noted, that the Drosophila rDNA genes are found on the X and Y chromosome and sat III repeats are adjacent to the rDNA locus on the pericentromere of chromosome X. However, also other chromosomes without rDNA loci cluster around the nucleolus, indicating that this is not merely a side-effect of the close genomic proximity of centromeres and rDNA (Padeken et al. 2013). It has even been suggested, that the localization of centromeres to the nucleolus is satellite RNA-dependent (Wong et al. 2007), which would fit with the notion that repetitive transcripts silence their own transcription (see 1.5.4). It seems, that with the depletion of Centagon proteins, the balance between sat III expression and silencing is disturbed. Considering that the Centagon proteins seem to be general RNA binders, maybe they are also involved in the regulation of other (satellite) RNAs. This may be mediated by the alteration of general heterochromatin organization in the nucleolus and relocalization of the centromeres. To validate this, more in-depth studies of nucleolus size and shape are necessary in our KD ovaries, to discern nucleolar aberrations, as well as immunostainings with heterochromatin and centromere markers to identify changes in heterochromatin amount or distribution, as well as centromere mislocalizations.

3.7.2 Defects in the piRNA pathway

Another pathway that possibly targets the regulation of sat III expression, is an involvement of the Centagon complex in the piRNA pathway. As discussed before, the piRNA pathway is vital in the Drosophila ovaries, because it silences transposable elements whose expression would be detrimental for the germ line. High centromeric RNA levels have been shown to cause mitotic defects in mice and human cells (Bouzinba-Segard et al. 2006; Chan et al. 2017) and even though sat III transcripts do not reintegrate in the genome, they may be sufficiently similar to transposable elements (because of their repetitive sequence and localization) to be regulated by the piRNA pathway. Supporting this hypothesis, is the finding that sat III RNA is bound by the piRNA proteins Piwi, Aub and Ago3 and some satellite RNAs of *Drosophila melanogaster* are processed into piRNAs (Wei et al. 2020). Also KD of rhino, involved in a pathway that licenses transcription of piRNA clusters, has been shown to induce the five-blob phenotype in nurse cells (Volpe et al. 2001). However, in a screen searching for factors involved in the piRNA pathway, the Centagon members were screened but not identified as piRNA associated factors (Handler et al. 2013). Therefore, this option seems less likely or less straightforward as discussed here.

3.7.3 Impaired cell cycle, transcript removal and breakdown

If the Centagon complex is indeed associated with the RNA helicase Rm62, the elevated sat III levels may be caused by a failure to remove nascent transcripts from the chromatin. As described before, the removal of transcripts is important for gene shutdown and heterochromatin formation. Mutation of Rm62 led to an accumulation of transcripts on the chromatin that were otherwise exported from the nucleus (Buszczak and Spradling 2006). In the case of sat III RNA, this defect is more difficult to assess since sat III RNA foci are always present on the chromatin, also in wildtype flies. Possibly, sat III transcripts only have a function at the chromatin and are rapidly degraded once removed. Since Rm62 also binds Ago2, a connection to the RNAi pathway has been suggested (Ishizuka et al. 2002). Interestingly, Rm62 and Ago2 were also enriched in my sat III RNA pulldown (see suppl. table 1, 2), suggesting that sat III may indeed be regulated by this pathway. The Centagon complex could be involved in RNA processing through RNA methylation and/or splicing, which might promote the breakdown of sat III RNA with or without the involvement of the RNA-induced silencing complex. This would explain the high sat III transcript levels in the KD ovaries.

Alternatively, an arrest in cell cycle could allow the nurse cells to keep synthesizing sat III RNA. It has been suggested that the (peri)centromere is transcribed only during M/G1 phase and not during S/G2 (Bobkov et al. 2018). As described before, the orthologues of Centagon members are implicated in S phase and replication initiation, therefore, a loss of these factors might arrest cells in G1, when sat III is transcribed.

3.8 The Centagon phenotype is dependent on sat III transcripts

The high levels of sat III RNA could easily be a secondary effect of the Centagon KD, without any consequences for GSC self-renewal or nurse cell endocycles. To our surprise, the opposite was observed. When I knocked down Centagon 1 with the Mat67.15-Gal4 driver in zhr^1 flies where (most of) the sat III repeats on the X-chromosome are lost, the 5-blob chromatin phenotype was partially rescued. In flies with the zhr^1 X-chromosomes, whole ovarioles with normal egg chambers could be recovered and the egg laying rate was restored. However, half of the eggs produced still looked abnormal and the hatching rate did not improve. This suggests that with low sat III RNA levels, more eggs are laid and therefore more eggs hatch, but the quality of eggs remains similarly poor to the ones with high sat III RNA levels. This means, that high sat III levels promote the five-blob phenotype and arrest of egg chamber development. I did not attempt to cross the zhr^1 X chromosome into the

MTD-Gal4 driver line and, therefore, do not know whether the early phenotype of germ cell loss can also be partially rescues by reducing sat III RNA levels. How high sat III RNA levels contribute to the phenotype of the nurse cells, remains unclear. Until now, satellite overexpression has mainly been researched in the context of mitosis, where it leads to segregation defects (Bouzinba-Segard et al. 2006; Chan et al. 2017). In murine cells, this was accompanied by the mislocalization of heterochromatin inducing factors, such as the histone methyl transferase Suv39h1 and HP1 (Bouzinba-Segard et al. 2006), suggesting a possible link between high satellite RNA levels and heterochromatin defects. In yeast, this link has been well established. There, centromeric transcripts are process by RISC and induce centromeric heterochromatin formation (Volpe et al. 2002). In flies meanwhile, multiple publications report that piRNA pathway proteins such as Aub, Piwi, Spn-E and Ago3 may be involved in heterochromatin formation by processing satellite transcripts (Usakin et al. 2007; Pal-Bhadra 2013; Wei et al. 2020). Most of the time, depleting or mutating the piRNA pathway proteins lead to derepression of the pericentric heterochromatin, but is not clear whether -vice versa- satellite RNA levels also affect heterochromatin formation and whether heterochromatin changes would affect the nurse cell dispersal.

Interestingly, the dispersal of nurse cell chromatin has been proposed to depend on an M-like cell cycle stage without the formation of a spindle (Dej and Spradling 1999). I have shown that high satellite III RNA levels impair the dispersal of nurse cell chromatin, since KD flies with reduced sat III levels, had less fragmented nurse cells. This means that high sat III RNA levels impair the mitosis-like dispersion phase. A similar effect may take place in the Rm62 mutants which accumulate transcripts on the chromatin (including rRNA) and also have a five-blob phenotype (Buszczak and Spradling 2006). Hypothetically, the accumulation of transcripts could tether the chromosomes together or form a physical barrier for factors necessary for nurse cell chromatin dispersal. To elucidate the involved mechanisms, more research is needed on how nurse cell chromosome dispersal functions and which factors are involved. Until then, it would be interesting to monitor sat III levels in ovaries where proteins with similar phenotypes have been knocked down to get a better overview and to monitor whether more transcripts are upregulated in the Centagon KD ovaries.

Furthermore, I observed major defects when knocking down Centagon members in somatic follicle cells. There, too few follicle cells were produced, which resulted in gaps in the follicle cell layer, whereas a KD in the stem cell niche resulted in no ovaries at all (Fig. 36). Coincidentally, ovary follicle cells also have polytene chromosomes. Unfortunately, I did not perform sat III RNA FISH on these ovaries and do not know whether sat III RNA is

upregulated here, as well. Further experiments will, therefore, be needed to show whether the detrimental effect of high sat III levels is connected to the polyploidy of cells.

Most likely, the KD of the Centagon complex does not only affect sat III, but also other heterochromatic loci. Therefore, we were surprised that the removal of sat III was already enough to partially rescue the development of egg chambers. Maybe, sat III repeats are sufficiently abundant (11 Mb on the X chromosome (Lohe et al. 1993) to produce the majority of aberrantly expressed RNAs with its 50-fold enrichment in the Centagon KD ovaries and their removal therefore sufficient to see an improvement. Maybe, removal of other upregulated transcripts could improve the rescue effect even further. RNA-seq experiments could provide more information on the upregulated RNA classes and also clarify what pathway the Centagon proteins may be involved in.

3.9 Open questions and future perspectives

In this thesis, I identified a new nucleolar complex (Centagon), which is important for germ cell survival, egg chamber development, nurse cell chromatin dispersal in Drosophila ovaries and regulation of sat III RNA levels. Moreover, I showed that sat III RNA misregulation upon KD of Centagon members causes the nurse cell chromatin dispersal defect and arrest in egg chamber development. As discussed, many pathways could contribute to the observed phenotypes, but further experiments are required to elucidate the mechanisms involved.
First of all, it would be helpful to determine whether the germ cell loss phenotype is indeed caused by a differentiation defect. Immunostainings with the CB marker Bam will help to identify the differentiation status of the leftover germ cells. Second, several immunostainings could be performed to narrow down the number of possible pathways involved. E.g. nucleolus, heterochromatin, centromere and p53 markers to assess quantitative and qualitative differences compared to wildtype ovaries. The Centagon members have also been implicated in rRNA processing. Therefore, rRNA intermediates from KD ovaries could be monitored by Northern Blot to reveal any defects in rRNA processing.

When I depleted the Centagon components in the early egg chambers, the egg chambers arrested in development and had a five-blob phenotype. Since the incorrect splicing of otu seems to be the cause in many cases, it would be interesting to assess the otu variants present in the Centagon KD ovaries. Preliminary experiments already indicated that the splicing may be affected. However, these findings need to be validated.

However, the most important question still remaining is how the Centagon complex regulates sat III levels. As discussed, the Centagon complex was identified in a sat III RNA pulldown and the interaction of one of the components, Centagon 3, was verified. Therefore, the Centagon complex may actively modify sat III RNA, for example by splicing or methylation by Centagon 2. To elucidate this, a Northern blot could be performed from KD ovary RNA to analyze sat III RNA transcript lengths. Furthermore, our lab is currently working at a method to identify centromeric RNA modifications, which will be also very useful in the context of the Centagon complex.

Then we do not know whether the Centagon complex regulates more transcripts. Centagon 3 is a bona-fide RNA binding protein and Centagon members have been implicated in splicing and rRNA processing, strongly suggesting that the complex does not specifically interact with sat III RNA. It would be interesting to assess which other RNAs are upregulated upon KD of the Centagon complex by performing RNA-seq. The ensuing pattern could be very helpful to elucidate the function of the Centagon complex.

Last, I identified a new effect of sat III RNA, namely its promotion of the five-blob phenotype defect and egg chamber arrest in Centagon-depleted ovaries. Why do the high sat III RNA levels impair nurse cell endocycle progression and is the germ cell loss in MTD-Gal4-driven KDs also caused by sat III RNA? These questions will have to be addressed in future experiments, e.g. by performing other rescue experiments with zhr^{1} flies.

All in all, I identified new interaction partners of sat III RNA in the form of a nucleolar complex, which regulates sat III levels in ovaries. Hereby, I contributed to the understanding of sat III RNA roles and opened up new directions for studying centromeric RNA function.

4. Methods

4.1 Molecular biology techniques

4.1.1 Cloning

Coding regions of genes were amplified by PCR with the Q5 polymerase (NEB) from S2 cell or Drosophila cDNA and cloned into vectors using GIBSON assembly. Basically, a 15 µl reaction with 7,5 µl Gibson Assembly Master Mix (Gibson et al. 2009), 0,03 pmol linearized plasmid and 0,06 pmol insert were incubated at 50°C for 15 min.

In case GIBSON cloning didn't work, the Circular Polymerase Extension Cloning (CPEC) (Quan and Tian 2009) method was used. For this, a Q5 polymerase reaction of 25 µl was set up with 200 ng of linearized plasmid and equimolar amounts of insert(s), but without primers. A standard PCR program was used with a Ta of 55°C and an elongation time of 30 sec./kbp of the ligated plasmid.

Subsequently the ligated plasmid was transformed into chemically competent E.coli by mixing the plasmid with 50 µl thawed E.coli and leaving it on ice for 20-30 min. After incubating the mixture 45 sec. at 42°C, it was placed on ice for 2 min. and supplemented with 250 µl LB medium. The bacteria were incubated 1 h on a shaker at 37°C (not necessary when transforming plasmids with ampicillin resistance), centrifuged 3 min. at 1.500 x g to settle the bacteria and remove excess medium before plating on agar plates with the corresponding antibiotic. Bacteria colonies were grown in LB medium at 37°C and the plasmids were isolated with the NucleoSpin Plasmid kit from Machery Nagel. The primers used for synthesizing the insert were designed with the NEBuilder Assembly Tool (https://nebuilder.neb.com/). All plasmid sequences were verified using Sanger sequencing.

The following plasmids were used:
pLAPcopia-GFP (Kan)
pMTpuro-V5-His (Amp)
pSP73-4xS1m
pGEX-GST
pATTB
pMM5-LexADNA
pMM6-Gal4pTA

4.1.2 gDNA extraction from ovaries

Depending on size, 5-10 ovaries were dissected, snapfrozen in 50 µl Squish buffer in a PCR tube and stored at -20°C. Upon thawing, the ovaries were grinded in the squish buffer using a pipet tip and dissolved by pipetting up and down. 10 mg/ml proteinase K was added and the following program was run on a thermocycler: 30 min. at 37°C for proteinase K digestion, followed by 2 min. at 95°C to deactivate the enzyme. The PCR tubes were filled up to 100 µl with squish buffer, followed by 200 µl Phenol/Chloroform/Isoamyl alcohol 25:24:1 (v/v). The samples were vortexed for 15 sec. and centrifuged 5 min. at 12.000 g. The upper aqueous layer was transferred to a new Eppendorf tube

and 1 volume chloroform was added. Again, the sample was vortexed for 15 sec. and centrifuged 5 min. at 12.000 g and the upper layer was transferred to a new Eppendorf tube. Subsequently, 0,1 volume NaOAc (pH 5.0) and 2 volumes 100% EtOH were added, the samples were mixed by pipetting up and down and stored at -20°C over-night or at -80°C for more than an hour. Afterwards the sample was centrifuged 30 min. at 18.000 g at 4°C and the pellet was washed with 75% ethanol, followed by 10 min. centrifugation at 18.000 g at 4°C. The ethanol wash was repeated and the residual ethanol was removed, followed by a brief drying step before resuspending the DNA pellet in 20-50 µl dH_2O, depending on pellet size.

Squish buffer
10 mM Tris-HCl pH 8.0
1 mM EDTA
25 mM NaCl
In dH_2O

4.1.3 RNA EXTRACTION

From S2 cells: harvested S2 cells were spun down and resuspended in an equivalent amount of Trizol or TriSure.
From Drosophila: whole flies, embryos or dissected tissues (in 20 µl PBS) were snapfrozen in liquid nitrogen and supplemented with Trizol (or TriSure) to a total of 100 µl (and stored at -20°C). Subsequently the tissue and Trizol were homogenized with a pistel in an 1,5 ml Eppendorf tube. More Trizol was added (up to 1ml) and the samples were centrifuged 10 min. at 12.000 x g at 4°C. The supernatant was transferred to a new Eppendorf tube.
RNA was extracted according to the manufacturer's protocol. RNA pellets were resuspended in RNase-free water according to the pellet size.

4.1.4 gDNA DIGESTION OF OVARY RNA

For the sat III RNA qPCR in ovaries an additional gDNA digestion step was performed:
10 µg ovary RNA was digested with Turbo DNase for 20 min. at 37°C (10 µg RNA, 1 µl Turbo DNase, 3 µl Turbo DNase buffer and 0,5 µl RNasin Plus in a 30 µl reaction). The reaction was placed on ice and mixed with 170 µl H_2O as well as 20 µl NaAc (3M, pH 5,2). Subsequently, 220 µl Phenol-Chloroform-Isoamyl was added, vortexed for 10 sec. and centrifuged 5 min. at 16.000 x g at RT. The upper phase was transferred to a new Eppendorf tube and supplemented with 200 µl chloroform. Again, the mixture was vortexed for 10 sec. and centrifuged 5 min. at 16.000 x g at RT, before transferring the upper phase to a new Eppendorf tube. 200 µl Isopropanol was added together with one 1 µl GlycoBlue and the tube was inverted a couple of times before incubating at -80°C for at least 1 h. The sample was centrifuged 30 min. at 18.000 x g at 4°C. The supernatant was removed and the pellet was washed with 750 µl 75% ethanol by vortexing until the pellet was afloat and centrifuging 5 min. at 18.000 x g at 4°C. The wash was repeated once and all ethanol was removed to air-dry the pellet, after which 15 µl H_2O was used for resuspension.

4.1.5 Reverse Transcription and qPCR

For reverse transcription the Quantitect kit (Qiagen) was used according to manufacturer's instructions. 2 µg RNA were used in a 14 µl gDNA digestion reaction. Half (7 µl) was used in a 20 µl reverse transcription reaction and half was supplemented with RNase-free H_2O up to 20 µl. Both + and -RT samples were incubated 30 min. at 42°C, followed by 3 min. at 95°C. The resulting cDNA was diluted 1:3 with RNase-free H_2O.

qPCRs were performed using LightCycler® 480 SYBR Green I Master Mix (2X) (Roche) with one reaction containing: 7,5 µl 2x Sybrgreen, 1 µl diluted cDNA, 1 µl each of forward and reverse primers (10 µM) and 4,5 µl H_2O. Each sample was measured in triplicate, with one triplicate consisting of a mastermix including cDNA which was divided over 3 wells of the 384-well plate (Roche). The following program was used on the LightCycler® 480 (Roche): 10 min. at 95°C, followed by 40 cycles of 15 sec. 95°C and 1 min. at 55°C.

4.1.6 RNA gel electrophoresis

RNA was run on a denaturing MOPS-formaldehyde agarose gel. 0,5 g Agarose were mixed with 5 ml 10x MOPS and 42,25 ml RNase-free H_2O and brought to a boil until the agarose was dissolved. The solution was cooled to 60°C, before 2,75 ml formaldehyde was added, quickly mixed and poured into a gel tray. RNA samples were supplemented with 1/5 volume RNA loading buffer and 2x the volume of RNA + loading buffer of RNA sample buffer. The RNA was heated 10 min. at 65°C to unfold, immediately placed on ice and loaded unto the solidified gel. The gel was run at 70 V in 1x MOPS (or 30 V o/n).

10x MOPS

0,2 M	MOPS pH 7,0
20 mM	sodium acetate
10 mM	EDTA

In RNase-free H_2O

RNA loading buffer

50% (v/v)	glycerol
1 mM	Na_2EDTA
0.4% (v/v)	bromophenol blue
40 µg/ml	ethidium bromide

in RNase-free H_2O

RNA sample buffer

10 ml	formamide
3.5 ml	37% formaldehyde
2 ml	5x MOPS

4.1.7 RNA Electrophoresis mobility Shift Assay (EMSA)

For the EMSA equal amounts of RNA (in vitro transcribed from PCR templates or linearized vectors with the T7 MegaScript kit, Invitrogen) were incubated with increasing amounts of protein. To this end, the RNA was folded by heating 10 min. at 68°C and incubating 10 min. at RT before placing on

ice. The RNA and protein were incubated for 30 min. on ice, RNA loading buffer (NEB) was added and the samples were loaded on a non-denaturing 1% agarose gel in TAE buffer and run at 120 V for a couple of hours. When the RNA had migrated through 2/3 of the gel, the gel was transferred to an ethidium bromide bath (with RNase-free TAE) and incubated for 20 min. The gel was rinsed a couple of times with TAE and imaged on the GelDoc from BioRad.

4.1.8 Yeast Two Hybrid (Y2H)

All Centagon sequences were cloned into the pMM5-LexADNA and pMM6-Gal4pTA vectors. As a positive control a combination of pMM5-Cal1 and pMM6-Rdx was used and as a negative control empty vectors. Subsequently, a combination of one pMM5 and one pMM6 plasmid was transformed into competent yeastS SGY37VIII cells (Knop et al. 1999), to introduce all Centagon protein combinations possible. This was achieved by adding 15 µl yeast to 500 ng (2 x 250 ng) plasmid and adding 100 µl LIPEG. The mixture was vortexed and incubated 20 min. at RT. 10 µl DMSO was added and the yeast was incubated 10 min. at 42°C. The yeast cells were spun down 3 min. at 3.000 g (20°C) and the yeast pellet was resuspended in 50 µl PBS. The yeast mixture was spread on an agar plate and incubated 3 days at 30°C.
From each transformation three colonies were picked and resuspended in 15 µl YP and incubated 1h at 30°C and 600 rpm. Afterwards the yeast mixture was carefully pipetted onto an agar plate as drops and incubated 1 day at 30°C.
The next day, the X-Gal overlay was prepared and carefully poured on top of the agar plate, followed by another day of incubation after which the positive (blue) yeast cells were assessed.
Yeast cells were always handled by an open flame or under a flow hood.

LiPEG

100 mM	lithiumacetate (Sigma)
10 mM	Tris-HCl pH8.0
1mM	EDTA (Sigma)
40%	PEG3350 (polyethyleneglycol, Sigma)

Filtersterilized

Agar plates

2x SC stock solution:

6,7 g	Bacto yeast nitrogen without amino acids
2 g	drop-out mix, lacking histidine and leucine
20 g	Glucose

Up to 500 ml ddH_2O, stirred and autoclaved

2x Agar stock:

20 g Bacto Agar
Up to 500 ml ddH_2O, stirred and autoclaved

The SC-X and Agar stock were combined when still warm, poured into plates under the hood, left to dry and stored at 4°C.

X-Gal overlay
7,8 ml 1M NaH_2PO_4 + 12,2 ml 1M Na_2HPO_4, adjusted to pH 7.0 with NaOH

1. 15 ml of the mixture above
   300 µl 10 % SDS
   3 ml 0,1 M KCl
   300 µl 0,1 M $MgCl_2$
   heated to 40°C

2. 120 mg agarose
   in 9 ml ddH_2O, boiled 30 sec.

3. 12 mg X-Gal
   in 300 µl DMF

Combined 1 and 2 while still warm and immediately added 3 before pouring on top of the agar plates.

4.2 BIOCHEMICAL TECHNIQUES

4.2.1 RNA-PULLDOWN

Blocking beads
Up to 200 µl of High Performance Streptavidin Sepharose beads (GE Healthcare) (in suspension) were washed twice with 1 ml WB-100 at 4°C on a rotator wheel. The beads were centrifuged 1 min. at 1.500 x g at 4°C to settle the beads and pipet of the buffer. Beads were blocked with 1 ml blocking buffer and incubated 2,5 h at 4°C on the rotator wheel. Afterwards the beads were washed 3x with WB-300 and stored in WB-150 in an Eppendorf tube at 4°C until use.

Cell lysis and preclearing
Pulldown 1
500 ml of S2 cells in medium were grown in suspension until a density of approximately 8 x 106 cells/ml was reached. Cells were washed 2x with cold PBS and centrifuged 10 min. at 6.000 x g. The pellet was resuspended in lysis buffer 150 (100 µl/106 cells) and kept on ice for 1 h. Subsequently the cells were lysed using the BioRuptor (NextGen) with 5 cycles of 30 sec. on/ 30 sec. off. The lysate was centrifuged for 15 min. at 16.000 x g at 4°C. The supernatant was precleared by incubating 10 ml with 200 µl blocked High Performance Streptavidin Sepharose beads for 3 h at 4°C on a rotator wheel. At this point, the protein concentration was measured using a Bradford Assay (Bio-Rad). For storage, the precleared lysate was snap frozen in liquid nitrogen and kept at -80°C.

Pulldown 2
650 ml of S2 cells in medium were grown in suspension until a density of approximately 8 x 106 cells/ml was reached. Cells were aliquoted in 50 ml steps, washed 1x with cold PBS and centrifuged 10 min. at 6.000 x g. The pellets were snapfrozen in liquid nitrogen and stored at -80°C. A pellet (4 x 108 cells) was thawed on ice under addition of 5 ml lysis buffer 500 and kept on ice for 30 min.

Afterwards the cells were lysed 2x 10 sec. with a 40% amplitude with a probe sonicator). The lysate was centrifuged for 15 min. at 16.000 x g at 4°C. The supernatant (4,8 ml) was diluted with 11,2 ml lysis buffer w/o NaCl to a final NaCl concentration of 150 mM. The protein concentration (3 mg/ml) was measured with the DC protein assay kit (Bio-rad). The lysate was snapfrozen in liquid nitrogen and kept at -80°C. After thawing, the lysate was incubated with 200 µl blocked High Performance Streptavidin Sepharose beads and 2,5 µl RNase inhibitor/ml lysate for 3 h at 4°C on a rotator wheel.

RNA-pulldown

The RNA-pulldown was carried out in duplicate. Per sample, 50 pmol of the in vitro transcribed RNA containing the 4x S1m loops was refolded by heating it 5 min. to 65°C and cooling it down 10 min. at RT before putting it back on ice. The precleared cell lysate (Pulldown 1 : 2 mg/sample, Pulldown 2: 1,5 mg/sample) was supplemented with 2,5 µl/ml RNase inhibitor and 0,1 µg/ml tRNA. RNA and cell lysate were combined and incubated 1 h at 4°C on a rotator wheel. At this point, a 20 µl sample (10 µl from each duplicate) for RNA extraction was taken (input). 35 µl (packed) blocked beads were added (= 70 µl beads in suspension) and the mixture was incubated for 1,5 h at 4°C on a rotator wheel. The beads were centrifuged 1 min. at 1.500 x g at 4°C and 20 µl (10 µl from each duplicate) of the supernatant was kept for RNA extraction (flow-through). The beads were washed 5x with WB-150 and 250 µl samples (125 µl from each duplicate) were taken from the supernatant of wash 1 and 3 for RNA extraction. After the washes, 20 µl bead slurry (10 µl from each duplicate) was taken for RNA extraction. The rest of the beads was incubated in 150 µl WB-150 with 50 µg/ml RNase A (Applichem) for 15 min. on ice, carefully vortexing the sample every 5 min. The eluates were combined in a new eppie and supplemented with 1,5 ml ice-cold acetone for protein precipitation and kept at -20°C o/n. The next day, the eluate was centrifuged 30 min. at 17.000 x g at RT. The supernatant was removed and the pellet was washed twice with 80% sterile Ethanol (RT). The pellet was air-dried and resuspended in 36 µl 1x SDS loading buffer.

Samples were denatured 5 min. at 95°C and kept on ice before loading onto a (10%) precast gel at the ZMBH MS-facility, where the samples were run at 80V until the samples had migrated 0,5 cm into the gel. The gel was stained with Coomassie and the samples were cut out for further processing.

Blocking buffer

1 mg/ml	BSA
200 µg/ml	Glycogen
200 µg/ml	Yeast tRNA
0,01% (v/v)	NP-40

In wash buffer-100

Lysis buffer 150/500

20 mM	Tris pH 7,5
150/500 mM	NaCl
1,5 mM	$MgCl_2$
2 mM	DTT
2 mM	RVC

With 1 mini complete proteinase inhibitor tablet (Roche)/10 ml

Wash buffer 100/150/300

20 mM	HEPES-KOH pH 7,9
100/150/300 mM	NaCl
10 mM	$MgCl_2$
0,01% (v/v)	NP-40
1 mM	DTT

4xS1m-tagged RNA synthesis

For in vitro transcription, the Megascript kits for SP6 and T7 (Invitrogen) were used. In a 40 ul reaction, 2 µg of linearized plasmid (pSP73-4xS1m with different inserts) was used as a template and the reaction was left at 37°C o/n. The next day, 1 µl Turbo DNase was added and the reaction was incubated 15 more min. at 37°C, followed by a clean-up with the mini quick spin columns (Roche).

4.2.2 Protein expression and purification

Protein coding sequences were cloned into pGEX vectors with a GST tag. The plasmids were transformed into BL21 bacteria and grown until the density of OD 0.6. Protein expression was induced by addition of IPTG (0.3 mM) and incubation for 16 h at 25°C. Cells were harvested, washed with PBS and snapfrozen. The pellet was thawed in addition of lysis buffer and the cells were incubated shortly on a rotator at 4°C. Subsequently, the cells were lysed in two cycles with the Avestin Emulsiflex Homogenizer and centrifuged at 20.000 rpm, 4°C for 30 min.

The lysate was filtered with a 0.45 µM filter and loaded onto the ÄKTA GST column chromatography system for purification. Two washes with 150 mM and 100 mM NaCl were performed before eluting with 30 mM Glutathione in PBS, pH 9.0. The eluate was loaded onto a PD-10 desalting column (GE Healthcare) and eluted with PBS to remove the salt. Further concentration was performed with a 10K centricon tube (Amnion). The loaded sample was centrifuged at 4000 rpm, 4°C for 10 min. and the concentration was assessed with the DC Protein Assay kit (Bio-Rad). The resulting 500 µl sample was supplemented with 10% glycerol and aliquoted before snapfreezing it in liquid nitrogen and storing it at -80°C.

Lysis buffer

500 mM	NaCl
0.1%	NP-40
2mM	PMSF

Protease inhibitor solution A (1:1000)
Protease inhibitor solution B (1:500)

1 mM	DTT

In 1x PBS

4.3 Cell biological techniques

4.3.1 Cell culture

Drosophila Schneider 2 (S2) cells were grown in Schneider's Drosophila medium supplemented with 10% (v/v) Fetal Bovine Serum and 200 µg/ml penicillin and streptomycin at 25°C. Cells were split twice a week and diluted according to the cell confluence (usually 1:10). Transfected cells were supplemented with additional selection antibiotics, Hygromcin (250 µg/ml) or Puromycin (50 µg/ml). For cell growth in suspension, 1:200 Heparin and 1:2000 Synperonic were added to the medium and cells were incubated at 25°C in an Erlenmeyer flask while shaking 80 min-1.

Cells were frozen by resuspending confluently grown cells of a T75 cell culture flask and transferring them to a 15 ml tube which was centrifuged for 3 min. at 800 x g. The supernatant was removed until 2,25 ml was left and 2,5 ml fresh serum medium was added. 500 µl DMSO was added, carefully mixed and the cells were quickly aliquoted in 5 cryotubes. These were placed in a Mr. Frosty freezing container (Thermo Fisher) with isopropanol and transferred to -80°C. For long time storage, the cryotubes were transferred to a liquid nitrogen container.

Cells were thawed by adding 1 ml of serum medium to the frozen cells. The mixture was carefully pipetted up and down to accelerate the thawing. The cells were transferred to a 15 ml tube with 5 ml serum medium and centrifuged for 3 min. at 800 x g. The supernatant was removed and the cells were resuspended in 3 ml serum medium and transferred to a T25 cell culture flask.

4.3.2 Transfections

1,5 x 106 cells/wells were seeded in a 6-well plate and incubated over-night. The next day, 5 µg pDNA and 4 µl Cellfectin II reagent (Gibco) were each separately added to 200 µl Serum-free Medium (SFM). Both mixtures were combined and incubated at RT for 45 min. Serum free S2 medium (SFM) was added up to 1 ml. Cells were washed once with SFM, after which the transfection medium was added. The cells were incubated for 4 h at 25°C, after which 1 ml of 20% serum medium was added. To avoid medium evaporation, the 6-well plates were sealed with parafilm. Cells were incubated at 25°C until confluent and then transferred to a T25 flask with the appropriate selection medium. As a control, untransfected S2 cells were grown in the same selection medium. The selection of transfected cells was considered complete, when all untransfected cells had died.

4.3.3 RNAi in S2 cells

1,5 x 106 cells/wells were seeded in a 6-well plate and incubated over-night. The next day, 20 µg dsRNA was incubated in 1 ml serum-free medium (SFM) for 15 min. Next, the cells were washed with SFM and the dsRNA was added to the well. After 1h incubation at 25°C, 1 ml of 20% serum medium was added and cells were incubated for 4 more days. To avoid medium evaporation, the 6-well plate was sealed with parafilm.

4.3.4 dsRNA synthesis

First, a DNA template with the T7 promoter sequence on either side was synthesized by PCR (see primer list). Primer sequences were derived from the (https://www.flyrnai.org/cgi-bin/DRSC_gene_lookup.pl). The product was run on a 1% agarose gel, cut out and purified with the NucleoSpin Gel and PCR Clean-up kit (Machery Nagel) according to manufacturer's protocol. The purified template was used for in vitro transcription with the MegaScript RNAi kit (Invitrogen).

4.3.5 Induction of pMT-V5-His expression

Cells containing pMT-V5-His plasmids with various protein genes were grown until confluent and incubated with various concentrations of copper sulfate (ranging from 0,05 - 1 µM) over-night.

4.3.6 Immunofluorescent staining of cells

3-5 x 105 cells were settled for 30 min on Polysine Slides (Thermo Fisher) marked with a PAPpen. Consecutively, the cells were fixed in 4% PFA in PBS for 10 min, washed 3x 5 min. with PBS and permeabilised with 0.1% Triton X-100 in PBS for 5 min, before washing again 3x 5 min. with PBS. Cells were blocked 30 min. with 4% BSA in PBS in a humid chamber, after which the primary antibody diluted in 4% BSA in PBS was applied and incubated over night at 4°C (humid chamber). Cells were washed 3x 10 min. with PBS before incubating with the fluorescent secondary antibody diluted 1:500 in 4% BSA in PBS for 1 h at RT protected from light (humid chamber). Cells were washed 3x 10 min. with PBS (protected from light). Cells were counterstained with 1 µg/ml DAPI in PBS for 5 min. and washed 3x 10 min. with PBS, before mounting with Aqua-Poly/Mount (Polysciences) and coverslips (Neolab). Finished slides were incubated over night at RT and stored at 4°C until imaging.

4.3.7 RNA FISH with immunofluorescent staining in S2 cells

Per well (25-well plate), 150.000 cells were seeded on a 12mm circular coverslip for 30 min. Cells were fixated for 10 min. in 4% PFA and rinsed with PBS. Then the cells were permeabilized with 0,1% Triton X-100 in PBS for 5 min and washed twice 5 min. with 2x SSC. Meanwhile, 50 ng of sat III RNA probe were added to the FISH hybridization buffer to a final volume of 25 µl/cover slip. The sat III RNA FISH probe was heated 5 min. at 65°C and placed on ice for 5 min. Then, the sat III RNA FISH probe was carefully pipetted on top of the coverslip and incubated over-night at 37˚C in a humid chamber protected from light. The next day, the coverslips were washed 3x 5 min with pre-heated 2x SSC and fixated again in 4% PFA for 5 min. at 37˚C. After 3x 5 min. PBS washes, the samples were blocked with 4% BSA in PBS for 30 min. Then the primary antibodies were added and incubated over-night at 4˚C in a humid chamber protected from light. Next, the cells were washed 3x 10 min. with PBS and incubated with the secondary anybody in 4% BSA in PBS for 1h at RT in a humid chamber. Samples were again washed 3x 5 min. with PBS, followed by incubation with 1 µg/ml DAPI in PBS for 5 min. After more PBS washing steps, the coverslips were mounted on drops of Aqua/Polymount medium on microscope slides, left to dry and stored at 4˚C until imaging.

Hybridization buffer

50% formamide
10% dextran sulfate salt
in 2xSSC

SatIII RNA FISH probe preparation

First, a T7 sequence-containing DNA template was synthesised by PCR, using Q5 polymerase (NEB) to amplify one sat III repeat from the pSP73 satIII sense 4xS1m (3') plasmid. The product was used in an in vitro transcription reaction with the MEGAscript T7 kit (Invitrogen) according to the protocol. In the 20 ul reaction 0,75 µl 10 mM UTP and 2,5 µl 1 mM ChromaTide UTP-Alexa488 (Life Technologies) were used to fluorescently label the RNA probe. The reaction was incubated over-

night at 37˚C and the probe was purified by standard ethanol precipitation (1 h -80 °C incubation in 100% ethanol with 1 µl GlycoBlue coprecipitant, followed by centrifugation and resuspension in RNase-free H_2O).

4.4 Drosophila techniques

4.4.1 Drosophila husbandry

Flies in use were kept in vials at 25°C or 21°C depending on their robustness, while stocks were kept at 18°C with vial exchange every 3-4 weeks. Fly food consisted of 0.72% (w/v) agar, 7.2% (w/v) maize, 2.4% molasses, 7.2% (w/v) malt, 0.88% (w/v) soya, 1.464% (w/v) yeast and acid mix (1% propionic acid + 0.064% orthophosphoric acid).

For virgin collection, dark pupae on the wall of the vial were collected and put on a glass slide with H2O. The pupae were observed under a Light microscope and females were identified by the absence of sex combes. All females were collected in a fresh vial and kept at 18°C or 25°C, depending on the timing of the experiment, until hatching.

Crosses were set up with 2/3 virgins and 1/3 males and generally kept at 25°C unless specified differently.

4.4.2 Generation of transgenic flies

The Centagon 1 sequence including its upstream and downstream regions was cloned into the pATTB vector, with the change that the region targeted by the dsRNA of the trip Centagon 1 fly line was designed with alternative codons. The plasmid was sent to the fly facility of Cambridge University for injection into vas-int;attp40 embryos and the resulting flies were crossed until a homozygous stock was obtained.

4.4.3 Survival assay

First, crosses were set up with different UAS-RNAi lines (females) and the Mat 67.15-Gal4 line (males) to obtain females with ovary-specific KDs. An equal number of newly hatched F1 flies (30 females and 20 males) per cross were placed in cages with grape juice plates and fresh yeast paste and left to acclimatize at 25°C for 2 days, with changing plates daily. Eggs layed o/n were collected the next morning and transferred to a new grape juice plate with Nipagin (Sigma) and sorted in to groups of 10. For the RNAi flies, the eggs were also sorted into groups with different phenotypes. After 24 h, the number of hatched eggs was assessed. Eggs were collected 5 consecutive nights to monitor egg laying at different ages.

Grapejuice plates

3,5 g Agar were dissolved in 150 ml H2O by heating it up in the microwave (2 min.). Subsequently, 50 ml of biological grapejuice (REWE) were added. Optional: 350 mg of NIPAGIN was diluted in 2 ml 100% ethanol and added to the slightly cooled solution (approximately 50°C). The solution was mixed by swirling and poured into 5 cm round plastic dishes up to a height of approximately 5 mm. The plates were stored at 4°C.

4.4.4 Ovary IF

After hatching, flies were maintained in vails with additional fresh yeast paste. Ovaries were dissected in 1x PBS and fixed in 4% PFA in PBS for 20 min. The ovaries were washed 3x 15min. in PBST (0,1% Tween in PBS) and permeabilised in 1% Triton-X in PBS for 30 min. After three 15 min. washes in PBST, the ovaries were blocked 2 h in antibody blocking solution, followed by incubation with the primary antibody in PBST o/n at 4°C. The next day, ovaries were washed again 3x 15min. in PBST, followed by incubation with the fluorescent secondary antibody for 2 h at RT, protected from light. The ovaries were rinsed once and washed twice for 15 min. with PBST and counterstained with DAPI (1:000) in PBS for 5 min. After two more 5 min. PBST washes, the ovaries were pipetted onto a coverslip, the excess PBST was removed and replaced by Aqua Polymount mounting medium. The ovaries were broken apart to single ovarioles with two needles under the microscope and mounted on slides. Finished slides were incubated over night at RT and stored at 4°C until imaging.

Antibody blocking solution

0,1% (v/v)	Tween-20
0,1%	BSA
10%	FBS

in PBS

4.4.5 Ovary RNA FISH

Flies were kept with fresh yeast to stimulate ovary growth and dissected in PBS. The ovaries were added to PCR tubes and fixated in 4% PFA for 30 min. After two 5 min. washes with PBS, the ovaries were kept in 70% ethanol over-night at 4°C for permeabilization. The next day, the ovaries were washed 2x 10 min. with HULU wash buffer, before adding 50 µl HULU hybridization buffer and 0,5 µl HULU probe. The PCR tubes were placed in water-filled Eppendorf tubes in a heat block set to 30°C. The samples were incubated over-night in the dark. The next day, the ovaries were washed 4x 10 min. with HULU wash buffer and incubated with 1 µg/µl DAPI in HULU wash buffer for 5 min. The ovaries were washed 2x 5 min. with HULU wash buffer and mounted with Aqua/Polymount and coverslips. Slides were dried for 24 h at RT and stored at 4°C until imaging. All used solutions were RNase-free.

HULU wash buffer

2x	SSC
2M	Urea

In DEPC-treated H_2O

HULU hybridization buffer

2x	SSC
2M	Urea
10%	extran sulfate sodium salt
5x	Denhardt's solution

In DEPC-treated H_2O

Denhardt's solution

2% (w/v)	BSA
2% (w/v)	Ficoll 400
2% (w/v)	Polyvinylpyrrolidone (PVP)

In RNase-free H_2O, filter-sterilized

4.4.6 Larval ovary IF

Larval ovaries were stained according to (Maimon and Gilboa 2011). Briefly, 3rd instar larvae were dissected in Ringer's medium and the fat body was transferred to a strainer filled with Ringer's medium placed on ice. The fat bodies were fixated with 5% formaldehyde in Ringer's medium for 20 min. under gentle agitation. Next, the fat bodies were washes 5 min., 10 min., and 45 min. with 1% Triton X-100 in PBS (PBT). After blocking 1 h with 1% BSA in 0,3% PBT, the fat bodies were transferred to a PCR tube and primary antibody was added for over-night incubation at 4°C on a nutator. The next day, the fat bodies were transferred back to the strainers and washed 3x 30 min. with 0,3% PBT, followed by a 2h incubation step with secondary antibody in 5% FBS, 1% BSA in 0,3% PBT in PCR tubes on a nutator protected from light. Afterwards, the fat bodies were washed again 3x 30 min. with 0,3% PBT and incubated 5 min. with 1 µg/µl DAPI in 0,3% PBT. After two additional washes, the fat bodies were transferred to a microscope slide with a cut pipet tip and residual PBT was removed with a 10 µl pipet. Immediately afterwards, a drop of Aqua/Polymount medium was added on the slide and the excess fat body surrounding the gonads was removed under the Light microscope. The samples were mounted with coverslips, dried for 24 h at RT and stored at 4°C until imaging.

Ringer's medium

128 mM	NaCl
2 mM	KCl
1.8 mM	$CaCl_2$
4 mM	$MgCl_2$
35.5 mM	Sucrose
5 mM	Hepes pH 6.9

In dH_2O

4.5 Microscopic techniques

4.6 Light microscope

For dissections and fly sorting, the Stereomicroscope from Zeiss with external light source was used.

4.6.1 DeltaVision microscope

S2 cells with immunofluorescence staining were imaged with the DeltaVision Core system (Applied Precision) using the Olympus UPlanSApo 100x (NA 1.4). Z-slices were 0,2 µm. Deconvolution was performed with the Applied Precisions softWoRx 3.7.1 suite with the following settings: Ratio (conservative), 10 cycles. Images used as examples in figures were

adjusted for brightness and contrast in FIJI (ImageJ).

4.6.2 Zeiss LSM 900 laser scanning microscope

For the sat III RNA FISH in S2 cells, the Zeiss LSM 900 laser scanning microscope was used on Airyscan mode with the Plan-Apochromat 63X Oil DIC M27 (NA 1.4) objective and the ZEN 3.0 software by Zeiss.
Images used as examples in figures were adjusted for brightness and contrast in FIJI (ImageJ).

4.6.3 Confocal microscopy

For the Drosophila tissues, either the Leica TCS SP5II confocal microscope with the HCX Plan APO 40x/1.30 Oil Cs objective was used or the Leica TSC SP8 confocal microscope with the PLAN APO 20x, multi immersion (NA 0.75) and PLAN APO 63x, glycerol immersion (NA 1.3) objectives.
2 µm z-slices were imaged for whole ovaries and egg chamer and 0,5 µm z-slices were used for the imaging of germaria. Images used as examples in figures were adjusted for brightness and contrast in FIJI (ImageJ).

4.6.4 Quantifications

Microscopic images were analysed in FIJI (ImageJ). In case of intensity measurements, background was removed with the rolling ball tool and a z-projection of the z-slices with the signal of interest was made. Then, the region of interest was selected and the Raw Int Den was measured.

sat III signal in egg chambers

The fragmentation of nurse cell chromatin was assessed by eye and egg chambers with comparable sizes were selected for intensity measurements.

pMad levels in MTD-Gal4-induced KD ovaries

GSCs were selected one by one for intensity measurements. The number of cystoblasts with pMad signal were counted and groups of pMad-expressing cystoblasts were selected together for one intensity measurement. The obtained value was divided by the number of cells counted in the selected area.

5. Materials

5.1 Chemicals/reagents/enzymes

Acetone	Sigma Aldrich
Agarose	Sigma Aldrich
Ampicillin	Sigma Aldrich
Aprotinin	Applichem
Bacto Agar	Difco
Bacto yeast nitrogen without amino acids	Difco
Bovine serum albumin (BSA)	Applichem
Bromphenol blue	Applichem
Calcium chloride ($CaCl_2$)	Applichem
Chloroform	Sigma Aldrich
Copper Sulfate	Th. Geyer
DAPI	Sigma Aldrich
DEPC	BioChemica
Dithiothreitol (DDT)	Sigma Aldrich
Dextran sulfate salt	Applichem
Dimethyl Sulfoxide (DMSO)	Sigma
Dimethylformamide (DMF)	Fluka
Distilled water, DNase/RNase-free	Gibco
EDTA	Applichem
EDTA disodium dihydrate (Na_2EDTA)	Roth
EGTA	Applichem
Ethanol absolute (EtOH)	Sigma Aldrich
Ethidium bromide (EtBr)	Applichem
Fetal bovine serum (FBS)	PAN
Ficoll	Sigma
Formaldehyde 37%	Sigma Aldrich
Formamide	Merck
Glucose	Applichem
Glycerol	Honeywell
GlycoBlue	Invitrogen
Glycogen	Thermo Scientific
Heparin sodium salt, RNase free	Sigma Aldrich
Hepes	Sigma Aldrich
Hygromycin	Sigma Aldrich
IPTG	Roth

Isopropanol	Sigma Aldrich
Kanamycin sulfate	Applichem
Leupeptin-Hemisulfate	Applichem
Magnesium chloride ($MgCl_2$)	Applichem
MOPS	Sigma Aldrich
Mounting medium aqua/polymount	Polysciences
NIPAGIN	Sigma Aldrich
Nonidet P-40 (NP-40)	Applichem
Penicillin/Streptomycin	Capricorn Scientific
Pepstatin	Applichem
Phenol-Choroform-Isoamyl alcohol (25:24:1)	Applichem
Phenylmethylsulfonylfluoride (PMSF)	Sigma Aldrich
Paraformaldehyde (PFA)	Applichem
Polyvinylpyrrolidone 40000 (PVP)	Sigma Aldrich
Potassium chloride (KCl)	Applichem
Puromycin	Sigma Aldrich
Restriction enzymes	NEB
RNase A	Applichem
RNaseZAP	Sigma Aldrich
RNasin Plus Ribonuclease Inhibitor	Promega
Ribonucleoside Vanadyl Complex (RVC)	NEB
Schneider's Drosophila medium	Gibco
Sodium acetate (NaOAc)	Sigma
Sodium chloride (NaCl)	Sigma
Sodium citrate	Sigma Aldrich
Sodium hydroxide (NaOH)	Applichem
Sodium phosphate, dibasic (Na_2HPO_4)	Applichem
Sodium phosphate, monobasic (NaH_2PO_4)	Sigma Aldrich
Sucrose	Sigma Aldrich
Synperonic	Sigma Aldrich
Tris	Applichem
TriSure	Bioline
Triton X-100	Merck
Trizol	Thermo Scientific
tRNA (yeast)	Ambion
Tween-20	AppliChem
Turbo DNase	Thermo Scientific
Urea	Sigma Aldrich
X-Gal	Sigma Aldrich
Yeast cube (biological)	REWE

5.2 General solutions

10x Phosphate Buffered Saline (PBS)

137 mM NaCl
2.7 mM KCl
10 mM Na2HPO
41.7 mM KH2PO4
adjusted to pH 7.5 with HCl

20x SSC

175.3 g/l NaCl
88.2 g/l sodium citrate-2H2O
adjusted to pH 7.0 with HCl

50x Tris-acetate-EDTA (TAE)

242 g/l Tris-HCl
18.6 g/l EDTA pH 7.7
adjusted with acetic acid in ddH2O

Protease inhibitor solution A

1 mg/ml Aprotinin
1 mg/ml Leupeptin-Hemisulfate

Protease inhibitor solution B

0,5 g/ml Pepstatin
in EtOH

5.3 General equipment and consumables

Agarose gel trays	Workshop ZMBH
Balance	Sartorius, Kern EG
Cell culture flasks	TPP
Coverslips	Neolab
Fly vials	Gosslein
Microscopy slides (polylysine)	Thermo Fisher Scientific
Nanodrop	A260 Nanodrop
PCR-cycler	BioRad
Petri dishes	Greiner Bio-one
pH-meter	Sartorius, Kern EG
Pipette filtertips	Stein
Power supplies	Biorad, EMBL PS143
Tabletop centrifuges	Eppendorf
Tubes 0,2 µl – 50 ml	Sarstedt

5.4 Antibodies

α-fasciclin III 7G10	1:100	mouse	DSHB
α-hts 1B1	1:30	mouse	DSHB
α-modulo	1:5000	mouse	Jaques Pradel lab
α-pMad	1:500	rabbit	Abcam 52903
α-traffic jam	1:5000	guinea pig	Dorothea Godt
α-tubulin	1:1000	mouse	Sigma T9026
α-vasa	1:30	rabbit	DSHB
α-vasa	1:250	rabbit	Santa Cruz d-260

5.5 Primers

Sat III FISH template T7 Fw	TAATACGACTCACTATAGGGTGTTTTGAGCAGCTAATTA
Sat III FISH template Rv	GTGACCATTTTTAGCCAACT
hsr omega IVT template T7 Fw	TAATACGACTCACTATAGGGAAGTGCATTCAAAGTGAAGCTGAA
hsr omega IVT template Rv	GATTCAACAGGTACACTTACATCAG
tubulin IVT template T7 Fw	TAATACGACTCACTATAGGGATGCGTGAATGTATCTCT
tubulin IVT template Rv	TTAGTACTCCTCAGCGCCCTCACCCT
Actin qPCR Fw	TGGCACCGTCGACCATGAAGATC
Actin qPCR Rv	TTAGAAGCACTTGCGGTGCAC
GAPDH qPCR Fw	GCTCCGGGAAAAGGAAAA
GAPDH qPCR Rv	TCCGTTAATTCCGATCTTCG
Sat III qPCR Fw	AATGGAAATTAAATTTTTTGGCC
Sat III qPCR Rv	GTTTTGAGCAGCTAATTACC
Centagon 1 qPCR Fw	TGCAGGCAGGCAAAAATCAC
Centagon 1 qPCR Rv	AGCAAGCGTTTCATGAAGGC
Centagon 2 qPCR Fw	GGCCTCAGAGATTGCTCGTC
Centagon 2 qPCR Rv	ATCCAAGTTGACGCCACGAT
Centagon 3 qPCR Fw	CCTTTTTGGGCAAGAACACCC
Centagon 3 qPCR Rv	CCACCGGAACGGCAATTAGA
Centagon 4 qPCR Fw	CGTCCTGGTGGTACCGTTTT
Centagon 4 qPCR Rv	CCTCGTCTATGTCCTCTTCTGC

5.6 FLY LINES

w^{1118}		Erhardt lab
trip Centagon 1	y1 sc* v1 sev21; P{TRiP.GL00421}attP2	Bloomington 35587
trip Centagon 2	y1 sc* v1 sev21; P{TRiP.HMC04440}attP40/CyO	Bloomington 56998
trip Centagon 3	y1 sc* v1 sev21; P{TRiP.HMS00206}attP2	Bloomington 33340
trip Centagon 4	y1 v1; P{TRiP.HMJ23354}attP40	Bloomington 61865
Mat67.15-Gal4	y1 w*; P{matα4-GAL-VP16}67; P{matα4-GAL-VP16}15	Bloomington 80361
MTD-Gal4	P{w[+mC]=otu-GAL4::VP16.R}1, w[*]; P{w[+mC]=GAL4-nos.NGT}40;P{w[+mC]=GAL4::VP16-nos.UTR}CG6325[MVD1]	Bloomington 31777
GR1-Gal4	Sco/CyO; GR1-Gal4, Sb/TM3, Ser	Veit Riechmann lab
Tj-Gal4	UAS-dicer; traffic-jam-Gal4	Veit Riechmann lab
zhr^{1}, balanced	zhr^{1}; +; Dr/TM3 or zhr^{1}; Sp/CyO; Dr/TM3	Erhardt lab

Publication bibliography

Allshire, Robin C.; Karpen, Gary H. (2008): Epigenetic regulation of centromeric chromatin: old dogs, new tricks? In Nature reviews. Genetics 9 (12), pp. 923–937. DOI: 10.1038/nrg2466.

Amin, Mohammed Abdullahel; Matsunaga, Sachihiro; Ma, Nan; Takata, Hideaki; Yokoyama, Masami; Uchiyama, Susumu; Fukui, Kiichi (2007): Fibrillarin, a nucleolar protein, is required for normal nuclear morphology and cellular growth in HeLa cells. In Biochemical and biophysical research communications 360 (2), pp. 320–326. DOI: 10.1016/j.bbrc.2007.06.092.

Baltz, Alexander G.; Munschauer, Mathias; Schwanhäusser, Björn; Vasile, Alexandra; Murakawa, Yasuhiro; Schueler, Markus et al. (2012): The mRNA-bound proteome and its global occupancy profile on protein-coding transcripts. In Molecular cell 46 (5), pp. 674–690. DOI: 10.1016/j.molcel.2012.05.021.

Barth, Teresa K.; Schade, Georg O.M.; Schmidt, Andreas; Vetter, Irene; Wirth, Marc; Heun, Patrick et al. (2015): Identification of Drosophila centromere associated proteins by quantitative affinity purification-mass spectrometry. In Data in brief 4, pp. 544–550. DOI: 10.1016/j.dib.2015.07.016.

Baxley, Ryan M.; Soshnev, Alexey A.; Koryakov, Dmitry E.; Zhimulev, Igor F.; Geyer, Pamela K. (2011): The role of the Suppressor of Hairy-wing insulator protein in Drosophila oogenesis. In Developmental biology 356 (2), pp. 398–410. DOI: 10.1016/j.ydbio.2011.05.666.

Bilinski, Szczepan M.; Jaglarz, Mariusz K.; Tworzydlo, Waclaw (2017): The Pole (Germ) Plasm in Insect Oocytes. In Results and problems in cell differentiation 63, pp. 103–126. DOI: 10.1007/978-3-319-60855-6_5.

Biscotti, Maria Assunta; Canapa, Adriana; Forconi, Mariko; Olmo, Ettore; Barucca, Marco (2015): Transcription of tandemly repetitive DNA: functional roles. In Chromosome Research 23 (3), pp. 463–477. DOI: 10.1007/s10577-015-9494-4.

Blattes, Roxane; Monod, Caroline; Susbielle, Guillaume; Cuvier, Olivier; Wu, Jian Hong; Hsieh, Tao Shih et al. (2006): Displacement of D1, HP1 and topoisomerase II from satellite heterochromatin by a specific polyamide. In EMBO Journal 25 (11), pp. 2397–2408. DOI: 10.1038/sj.emboj.7601125.

Blower, M. D.; Karpen, G. H. (2001): The role of Drosophila CID in kinetochore formation, cell-cycle progression and heterochromatin interactions. In Nature cell biology 3 (8), pp. 730–739. DOI: 10.1038/35087045.

Blower, Michael D. (2016): Centromeric Transcription Regulates Aurora-B Localization and Activation. In Cell reports 15 (8), pp. 1624–1633.

Bobkov, Georg O.M.; Gilbert, Nick; Heun, Patrick (2018): Centromere transcription allows CENP-A to transit from chromatin association to stable incorporation. In Journal of Cell Biology 217 (6), pp. 1957–1972. DOI: 10.1083/jcb.201611087.

Borkakoti, Nivedita (1983): Enzyme specificity: base recognition and hydrolysis of RNA by ribonuclease A. In FEBS Letters 162 (2), pp. 367–373. DOI: 10.1016/0014-5793(83)80789-3.

Bouzinba-Segard, Haniaa; Guais, Adeline; Francastel, Claire (2006): Accumulation of small murine minor satellite transcripts leads to impaired centromeric architecture and function. In Proceedings of the National Academy of Sciences 103 (23), pp. 8709–8714. DOI: 10.1073/pnas.0508006103.

Bury, Leah; Moodie, Brittania; Ly, Jimmy; McKay, Liliana S.; Miga, Karen Hh; Cheeseman, Iain M. (2020): Alpha-satellite RNA transcripts are repressed by centromere-nucleolus associations. In eLife 9. DOI: 10.7554/eLife.59770.

Buszczak, Michael; Spradling, Allan C. (2006): The Drosophila P68 RNA helicase regulates transcriptional deactivation by promoting RNA release from chromatin. In Genes & development 20 (8), pp. 977–989. DOI: 10.1101/gad.1396306.

Carroll, Christopher W.; Straight, Aaron F. (2006): Centromere formation: From epigenetics to self-assembly. In Trends in cell biology 16 (2), pp. 70–78. DOI: 10.1016/j.tcb.2005.12.008.

Cauchi, Ruben J. (2012): Conserved requirement for DEAD-box RNA helicase Gemin3 in Drosophila oogenesis. In BMC Res Notes 5 (1), p. 120. DOI: 10.1186/1756-0500-5-120.

Cecco, Marco de; Criscione, Steven W.; Peckham, Edward J.; Hillenmeyer, Sara; Hamm, Eliza A.; Manivannan, Jayameenakshi et al. (2013): Genomes of replicatively senescent cells undergo global epigenetic changes leading to gene silencing and activation of transposable elements. In Aging cell 12 (2), pp. 247–256. DOI: 10.1111/acel.12047.

Cerutti, Federico; Gamba, Riccardo; Mazzagatti, Alice; Piras, Francesca M.; Cappelletti, Eleonora; Belloni, Elisa et al. (2016): The major horse satellite DNA family is associated with centromere competence. In Molecular cytogenetics 9, p. 35. DOI: 10.1186/s13039-016-0242-z.

Chan, David Y.L.; Moralli, Daniela; Khoja, Suhail; Monaco, Zoia L. (2017): Noncoding Centromeric RNA Expression Impairs Chromosome Stability in Human and Murine Stem Cells. In Disease markers 2017. DOI: 10.1155/2017/7506976.

Chan, F. Lyn; Marshall, Owen J.; Saffery, Richard; Kim, Bo Won; Earle, Elizabeth; Choo, K. H. Andy; Wong, Lee H. (2012): Active transcription and essential role of RNA polymerase II at the centromere during mitosis. In Proceedings of the National Academy of Sciences 109 (6), pp. 1979–1984. DOI: 10.1073/pnas.1108705109.

Chang, Ching-Ho; Chavan, Ankita; Palladino, Jason; Wei, Xiaolu; Martins, Nuno M. C.; Santinello, Bryce et al. (2019): Islands of retroelements are major components of Drosophila centromeres. In PLoS biology 17 (5), e3000241. DOI: 10.1371/journal.pbio.3000241.

Chen, Chin Chi; Bowers, Sarion; Lipinszki, Zoltan; Palladino, Jason; Trusiak, Sarah; Bettini, Emily et al. (2015): Establishment of Centromeric Chromatin by the CENP-A Assembly Factor CAL1 Requires FACT-Mediated Transcription. In Developmental cell 34 (1), pp. 73–84. DOI: 10.1016/j.devcel.2015.05.012.

Cheng, Mei-Hsin; Andrejka, Laura; Vorster, Paul J.; Hinman, Albert; Lipsick, Joseph S. (2017): The Drosophila LIN54 homolog Mip120 controls two aspects of oogenesis. In Biology open 6 (7), pp. 967–978. DOI: 10.1242/bio.025825.

Cheung, Man-Hei; Amin, Aftab; Wu, Rentian; Qin, Yan; Zou, Lan; Yu, Zhiling; Liang, Chun (2019): Human NOC3 is essential for DNA replication licensing in human cells. In Cell cycle (Georgetown, Tex.) 18 (5), pp. 605–620. DOI: 10.1080/15384101.2019.1578522.

Choi, Eun Shik; Strålfors, Annelie; Castillo, Araceli G.; Durand-Dubief, Mickaël; Ekwall, Karl; Allshire, Robin C. (2011): Identification of noncoding transcripts from within CENP-A chromatin at fission yeast centromeres. In Journal of Biological Chemistry 286 (26), pp. 23600–23607. DOI: 10.1074/jbc.M111.228510.

Cramton, S. E.; Laski, F. A. (1994): string of pearls encodes Drosophila ribosomal protein S2, has Minute-like characteristics, and is required during oogenesis. In Genetics 137 (4), pp. 1039–1048.

Cuevas, M. de; Lilly, M. A.; Spradling, A. C. (1997): Germline cyst formation in Drosophila. In Annual review of genetics 31, pp. 405–428. DOI: 10.1146/annurev.genet.31.1.405.

Dansereau, David A.; Lasko, Paul (2008): The Development of Germline Stem Cells in Drosophila. In Methods in molecular biology (Clifton, N.J.) 450, pp. 3–26. DOI: 10.1007/978-1-60327-214-8.

Dapples, C. C.; King, R. C. (1970): The development of the nucleolus of the ovarian nurse cell of Drosophila melanogaster. In Zeitschrift fur Zellforschung und mikroskopische Anatomie (Vienna, Austria : 1948) 103 (1), pp. 34–47. DOI: 10.1007/BF00335399.

Dattoli, Anna Ada; Carty, Ben L.; Kochendoerfer, Antje M.; Morgan, Conall; Walshe, Annie E.; Dunleavy, Elaine M. (2020): Asymmetric assembly of centromeres epigenetically regulates stem cell fate. In Journal of Cell Biology 219 (4). DOI: 10.1083/jcb.201910084.

Decotto, Eva; Spradling, Allan C. (2005): The Drosophila ovarian and testis stem cell niches: similar somatic stem cells and signals. In Developmental cell 9 (4), pp. 501–510.

DeFalco, Tony; Camara, Nicole; Le Bras, Stéphanie; van Doren, Mark (2008): Nonautonomous sex determination controls sexually dimorphic development of the Drosophila gonad. In Developmental cell 14 (2), pp. 275–286. DOI: 10.1016/j.devcel.2007.12.005.

DeFalco, Tony J.; Verney, Geraldine; Jenkins, Allison B.; McCaffery, J.Michael; Russell, Steven; van Doren, Mark (2003): Sex-Specific Apoptosis Regulates Sexual Dimorphism in the Drosophila Embryonic Gonad. In Developmental cell 5 (2), pp. 205–216. DOI: 10.1016/S1534-5807(03)00204-1.

Dej, Kimberley J.; Spradling, Allan C. (1999): The endocycle controls nurse cell polytene chromosome structure during Drosophila oogenesis. In Development (Cambridge, England) 126 (2), pp. 293–303.

Deng, W.; Lin, H. (1997): Spectrosomes and fusomes anchor mitotic spindles during asymmetric germ cell divisions and facilitate the formation of a polarized microtubule array for oocyte specification in Drosophila. In Developmental biology 189 (1), pp. 79–94. DOI: 10.1006/dbio.1997.8669.

Donati, Giulio; Peddigari, Suresh; Mercer, Carol A.; Thomas, George (2013): 5S ribosomal RNA is an essential component of a nascent ribosomal precursor complex that regulates the Hdm2-p53 checkpoint. In Cell Reports 4 (1), pp. 87–98. DOI: 10.1016/j.celrep.2013.05.045.

Du, Yaqing; Topp, Christopher N.; Dawe, R. Kelly (2010): DNA binding of centromere protein C (CENPC) is stabilized by single-stranded RNA. In PLoS genetics 6 (2), pp. 1–10. DOI: 10.1371/journal.pgen.1000835.

Duffy, Joseph B. (2002): GAL4 system in Drosophila: a fly geneticist's Swiss army knife. In Genesis (New York, N.Y. : 2000) 34 (1-2), pp. 1–15. DOI: 10.1002/gene.10150.

Erhardt, Sylvia; Mellone, Barbara G.; Betts, Craig M.; Zhang, Weiguo; Karpen, Gary H.; Straight, Aaron F. (2008): Genome-wide analysis reveals a cell cycle-dependent mechanism controlling centromere propagation. In The Journal of cell biology 183 (5), pp. 805–818. DOI: 10.1083/jcb.200806038.

Fachinetti, Daniele; Han, Joo Seok; McMahon, Moira A.; Ly, Peter; Abdullah, Amira; Wong, Alex J.; Cleveland, Don W. (2015): DNA Sequence-Specific Binding of CENP-B Enhances the Fidelity of Human Centromere Function. In Developmental cell 33 (3), pp. 314–327. DOI: 10.1016/j.devcel.2015.03.020.

Ferree, Patrick M.; Barbash, Daniel A. (2009): Species-specific heterochromatin prevents mitotic chromosome segregation to cause hybrid lethality in Drosophila. In PLoS biology 7 (10), e1000234. DOI: 10.1371/journal.pbio.1000234.

Ferri, Federica; Bouzinba-Segard, Haniaa; Velasco, Guillaume; Hubé, Florent; Francastel, Claire (2009): Non-coding murine centromeric transcripts associate with and potentiate Aurora B kinase. In Nucleic acids research 37 (15), pp. 5071–5080. DOI: 10.1093/nar/gkp529.

Fichelson, Pierre; Moch, Clara; Ivanovitch, Kenzo; Martin, Charlotte; Sidor, Clara M.; Lepesant, Jean-Antoine et al. (2009): Live-imaging of single stem cells within their niche reveals that a U3snoRNP component segregates asymmetrically and is required for self-renewal in Drosophila. In Nature cell biology 11 (6), pp. 685–693. DOI: 10.1038/ncb1874.

Fioriniello, Salvatore; Marano, Domenico; Fiorillo, Francesca; D'Esposito, Maurizio; Della Ragione, Floriana (2020): Epigenetic Factors That Control Pericentric Heterochromatin Organization in Mammals. In Genes 11 (6). DOI: 10.3390/genes11060595.

Flora, Pooja; Schowalter, Sean; Wong-Deyrup, SiuWah; DeGennaro, Matthew; Nasrallah, Mohamad Ali; Rangan, Prashanth (2018): Transient transcriptional silencing alters the cell cycle to promote germline stem cell differentiation in Drosophila. In Developmental biology 434 (1), pp. 84–95. DOI: 10.1016/j.ydbio.2017.11.014.

Fonagy, A.; Swiderski, C.; Dunn, M.; Freeman, J. W. (1992): Antisense-mediated specific inhibition of P120 protein expression prevents G1- to S-phase transition. In Cancer research 52 (19), pp. 5250–5256.

Frescas, David; Guardavaccaro, Daniele; Bassermann, Florian; Koyama-Nasu, Ryo; Pagano, Michele (2007): JHDM1B/FBXL10 is a nucleolar protein that represses transcription of ribosomal RNA genes. In Nature 450 (7167), pp. 309–313. DOI: 10.1038/nature06255.

Gall, J. G.; Cohen, E. H.; Polan, M. L. (1971): Reptitive DNA sequences in drosophila. In Chromosoma 33 (3), pp. 319–344. DOI: 10.1007/BF00284948.

Garavís, Miguel; Escaja, Núria; Gabelica, Valérie; Villasante, Alfredo; González, Carlos (2015a): Centromeric Alpha-Satellite DNA Adopts Dimeric i-Motif Structures Capped by AT Hoogsteen Base Pairs. In Chemistry (Weinheim an der Bergstrasse, Germany) 21 (27), pp. 9816–9824. DOI: 10.1002/chem.201500448.

Garavís, Miguel; Méndez-Lago, María; Gabelica, Valérie; Whitehead, Siobhan L.; González, Carlos; Villasante, Alfredo (2015b): The structure of an endogenous Drosophila centromere reveals the prevalence of tandemly repeated sequences able to form i-motifs. In Sci Rep 5 (1), p. 13307. DOI: 10.1038/srep13307.

Gaubatz, J. W.; Cutler, R. G. (1990): Mouse satellite DNA is transcribed in senescent cardiac muscle. In The Journal of biological chemistry 265 (29), pp. 17753–17758.

Gibson, Daniel G.; Young, Lei; Chuang, Ray-Yuan; Venter, J. Craig; Hutchison, Clyde A.; Smith, Hamilton O. (2009): Enzymatic assembly of DNA molecules up to several hundred kilobases. In Nat Methods 6 (5), pp. 343–345. DOI: 10.1038/nmeth.1318.

Gilboa, Lilach (2015): Organizing stem cell units in the Drosophila ovary. In Current opinion in genetics & development 32, pp. 31–36. DOI: 10.1016/j.gde.2015.01.005.

Gilboa, Lilach; Lehmann, Ruth (2004): Repression of primordial germ cell differentiation parallels germ line stem cell maintenance. In Current biology : CB 14 (11), pp. 981–986. DOI: 10.1016/j.cub.2004.05.049.

Goentoro, Lea A.; Yakoby, Nir; Goodhouse, Joseph; Schüpbach, Trudi; Shvartsman, Stanislav Y. (2006): Quantitative analysis of the GAL4/UAS system in Drosophila oogenesis. In Genesis (New York, N.Y. : 2000) 44 (2), pp. 66–74. DOI: 10.1002/gene.20184.

Gönczy, P.; DiNardo, S. (1996): The germ line regulates somatic cyst cell proliferation and fate during Drosophila spermatogenesis. In Development (Cambridge, England) 122 (8), pp. 2437–2447.

Goodrich, Jennifer S.; Clouse, K. Nicole; Schüpbach, Trudi (2004): Hrb27C, Sqd and Otu cooperatively regulate gurken RNA localization and mediate nurse cell chromosome dispersion in Drosophila oogenesis. In Development (Cambridge, England) 131 (9), pp. 1949–1958. DOI: 10.1242/dev.01078.

Grenfell, Andrew W.; Heald, Rebecca; Strzelecka, Magdalena (2016): Mitotic noncoding RNA processing promotes kinetochore and spindle assembly in Xenopus. In Journal of Cell Biology 214 (2), pp. 133–141. DOI: 10.1083/jcb.201604029.

Guerreiro, Isabel; Kind, Jop (2019): Spatial chromatin organization and gene regulation at the nuclear lamina. In Current opinion in genetics & development 55, pp. 19–25. DOI: 10.1016/j.gde.2019.04.008.

Guse, Annika; Carroll, Christopher W.; Moree, Ben; Fuller, Colin J.; Straight, Aaron F. (2011): In vitro centromere and kinetochore assembly on defined chromatin templates. In Nature 477 (7364), pp. 354–358. DOI: 10.1038/nature10379.

Gutbrod, M. J.; Roche, B.; Steinberg, J. I.; Lakhani, A. A.; Chang, K.; Schorn, A. J.; Martienssen, R. A. (2021): Dicer promotes genome stability via the bromodomain transcriptional co-activator Brd4. In bioRxiv, 2021.01.08.425946. DOI: 10.1101/2021.01.08.425946.

Haaf, T.; Mater, A. G.; Wienberg, J.; Ward, D. C. (1995): Presence and abundance of CENP-B box sequences in great ape subsets of primate-specific alpha-satellite DNA. In Journal of molecular evolution 41 (4), pp. 487–491. DOI: 10.1007/BF00160320.

Handler, Dominik; Meixner, Katharina; Pizka, Manfred; Lauss, Kathrin; Schmied, Christopher; Gruber, Franz Sebastian; Brennecke, Julius (2013): The genetic makeup of the Drosophila piRNA pathway. In Molecular cell 50 (5), pp. 762–777. DOI: 10.1016/j.molcel.2013.04.031.

Hartl, Tom A.; Smith, Helen F.; Bosco, Giovanni (2008): Chromosome alignment and transvection are antagonized by condensin II. In Science (New York, N.Y.) 322 (5906), pp. 1384–1387. DOI: 10.1126/science.1164216.

Hay, Bruce; Jan, Lily Yeh; Jan, Yuh Nung (1988): A protein component of Drosophila polar granules is encoded by vasa and has extensive sequence similarity to ATP-dependent helicases. In Cell 55 (4), pp. 577–587. DOI: 10.1016/0092-8674(88)90216-4.

Hédouin, Sabrine; Grillo, Giacomo; Ivkovic, Ivana; Velasco, Guillaume; Francastel, Claire (2017): CENP-A chromatin disassembly in stressed and senescent murine cells. In Scientific reports 7 (January), pp. 1–14. DOI: 10.1038/srep42520.

Hernandez-Verdun, Danièle (2011): Assembly and disassembly of the nucleolus during the cell cycle. In Nucleus (Austin, Tex.) 2 (3), pp. 189–194. DOI: 10.4161/nucl.2.3.16246.

Hernandez-Verdun, Danièle; Roussel, Pascal; Thiry, Marc; Sirri, Valentina; Lafontaine, Denis L. J. (2010): The nucleolus: structure/function relationship in RNA metabolism. In Wiley interdisciplinary reviews. RNA 1 (3), pp. 415–431. DOI: 10.1002/wrna.39.

Heun, Patrick; Erhardt, Sylvia; Blower, Michael D.; Weiss, Samara; Skora, Andrew D.; Karpen, Gary H. (2006): Mislocalization of the drosophila centromere-specific histone CID promotes formation of functional ectopic kinetochores. In Developmental cell 10 (3), pp. 303–315. DOI: 10.1016/j.devcel.2006.01.014.

Hong, Juyeong; Lee, Ji Hoon; Chung, In Kwon (2016): Telomerase activates transcription of cyclin D1 gene through an interaction with NOL1. In Journal of cell science 129 (8), pp. 1566–1579. DOI: 10.1242/jcs.181040.

Huettner, Alfred F. (1923): The origin of the germ cells in Drosophila melanogaster. In J. Morphol. 37 (2), pp. 385–423. DOI: 10.1002/jmor.1050370204.

Hughes, Stacie E.; Miller, Danny E.; Miller, Angela L.; Hawley, R. Scott (2018): Female Meiosis: Synapsis, Recombination, and Segregation in Drosophila melanogaster. In Genetics 208 (3), pp. 875–908. DOI: 10.1534/genetics.117.300081.

Iarovaia, Olga V.; Minina, Elizaveta P.; Sheval, Eugene V.; Onichtchouk, D.; Dokudovskaya, Svetlana; Razin, Sergey V.; Vassetzky, Yegor S. (2019): Nucleolus: A Central Hub for Nuclear Functions. In Trends in cell biology 29 (8), pp. 647–659. DOI: 10.1016/j.tcb.2019.04.003.

Ideue, Takashi; Cho, Yukiko; Nishimura, Kanako; Tani, Tokio (2014): Involvement of satellite I noncoding RNA in regulation of chromosome segregation. In Genes to Cells 19 (6), pp. 528–538. DOI: 10.1111/gtc.12149.

Illmensee, K.; Mahowald, A. P. (1974): Transplantation of posterior polar plasm in Drosophila. Induction of germ cells at the anterior pole of the egg. In Proceedings of the National Academy of Sciences 71 (4), pp. 1016–1020. DOI: 10.1073/pnas.71.4.1016.

Inaba, Mayu; Yamashita, Yukiko M. (2012): Asymmetric stem cell division: precision for robustness. In Cell Stem Cell 11 (4), pp. 461–469. DOI: 10.1016/j.stem.2012.09.003.

Ishizuka, Akira; Siomi, Mikiko C.; Siomi, Haruhiko (2002): A Drosophila fragile X protein interacts with components of RNAi and ribosomal proteins. In Genes & development 16 (19), pp. 2497–2508. DOI: 10.1101/gad.1022002.

Jagannathan, Madhav; Cummings, Ryan; Yamashita, Yukiko M. (2018): A conserved function for pericentromeric satellite DNA. In eLife Sciences Publications, Ltd, 3/26/2018. Available online at https://elifesciences.org/articles/34122, checked on 9/6/2021.

Jazdowska-Zagrodzińska, B. (1966): Experimental studies on the role of 'polar granules' in the segregation of pole cells in Drosophila melanogaster. In Journal of embryology and experimental morphology 16 (3), pp. 391–399. Available online at https://dev.biologists.org/content/16/3/391.long.

Jia, Dongyu; Xu, Qiuping; Xie, Qian; Mio, Washington; Deng, Wu-Min (2016): Automatic stage identification of Drosophila egg chamber based on DAPI images. In Scientific reports 6, p. 18850. DOI: 10.1038/srep18850.

Johmura, Yoshikazu; Osada, Shigehiro; Nishizuka, Makoto; Imagawa, Masayoshi (2008): FAD24 acts in concert with histone acetyltransferase HBO1 to promote adipogenesis by controlling DNA replication. In The Journal of biological chemistry 283 (4), pp. 2265–2274. DOI: 10.1074/jbc.M707880200.

Jolly, Caroline; Metz, Alexandra; Govin, Jérôme; Vigneron, Marc; Turner, Bryan M.; Khochbin, Saadi; Vourc'H, Claire (2004): Stress-induced transcription of satellite III repeats. In The Journal of cell biology 164 (1), pp. 25–33. DOI: 10.1083/jcb.200306104.

Joyce, Eric F.; Apostolopoulos, Nicholas; Beliveau, Brian J.; Wu, C-ting (2013): Germline progenitors escape the widespread phenomenon of homolog pairing during Drosophila development. In PLOS Genetics 9 (12), e1004013. DOI: 10.1371/journal.pgen.1004013.

Kai, Toshie; Williams, Dianne; Spradling, Allan C. (2005): The expression profile of purified Drosophila germline stem cells. In Developmental biology 283 (2), pp. 486–502. DOI: 10.1016/j.ydbio.2005.04.018.

Kalifa, Yossi; Armenti, Stephen T.; Gavis, Elizabeth R. (2009): Glorund interactions in the regulation of gurken and oskar mRNAs. In Developmental biology 326 (1), pp. 68–74. DOI: 10.1016/j.ydbio.2008.10.032.

Kanne, Julian; Hussong, Michelle; Isensee, Jörg; Muñoz-López, Álvaro; Wolffgramm, Jan; Heß, Felix et al. (2021): Pericentromeric Satellite III transcripts induce etoposide resistance. In Cell Death and Disease 12 (6), p. 530. DOI: 10.1038/s41419-021-03810-9.

Kasinathan, Sivakanthan; Henikoff, Steven (2018): Non-B-form DNA is enriched at centromeres. In Molecular biology and evolution. DOI: 10.1093/molbev/msy010.

Kato, Hiroaki; Goto, Derek B.; Martienssen, Robert A.; Urano, Takeshi; Furukawa, Koichi; Murakami, Yota (2005): RNA polymerase II is required for RNAi-dependent heterochromatin assembly. In Science 309 (5733), pp. 467–469. DOI: 10.1126/science.1114955.

Kiger, A. A.; Jones, D. L.; Schulz, C.; Rogers, M. B.; Fuller, M. T. (2001): Stem cell self-renewal specified by JAK-STAT activation in response to a support cell cue. In Science (New York, N.Y.) 294 (5551), pp. 2542–2545. DOI: 10.1126/science.1066707.

King, R. C.; Aggarwal, S. K.; Aggarwal, U. (1968): The development of the female Drosophila reproductive system. In Journal of Morphology 124 (2), pp. 143–166. DOI: 10.1002/jmor.1051240203.

King, R. C.; Mohler, D.; Riley, S. F.; Storto, P. D.; Nicolazzo, P. S. (1986): Complementation between alleles at the ovarian tumor locus of Drosophila melanogaster. In Dev. Genet. 7 (1), pp. 1–20. DOI: 10.1002/dvg.1020070102.

Klusza, Stephen; Novak, Amanda; Figueroa, Shirelle; Palmer, William; Deng, Wu Min (2013): Prp22 and spliceosome components regulate chromatin dynamics in germ-line polyploid cells. In PloS one 8 (11), pp. 1–11. DOI: 10.1371/journal.pone.0079048.

Knop, Michael; Siegers, Katja; Pereira, Gislene; Zachariae, Wolfgang; Winsor, Barbara; Nasmyth, Kim; Schiebel, Elmar (1999): Epitope tagging of yeast genes using a PCR-based strategy: more tags and improved practical routines. In Yeast (Chichester, England) 15 (10B), pp. 963–972. DOI: 10.1002/(SICI)1097-0061(199907)15:10B<963::AID-YEA399>3.0.CO;2-W.

Leppek, Kathrin; Stoecklin, Georg (2014): An optimized streptavidin-binding RNA aptamer for purification of ribonucleoprotein complexes identifies novel ARE-binding proteins. In Nucleic acids research 42 (2), e13. DOI: 10.1093/nar/gkt956.

Li, Michelle A.; Alls, Jeffrey D.; Avancini, Rita M.; Koo, Karen; Godt, Dorothea (2003): The large Maf factor Traffic Jam controls gonad morphogenesis in Drosophila. In Nature cell biology 5 (11), pp. 994–1000. DOI: 10.1038/ncb1058.

Li, N.; Zhao, G.; Chen, T.; Xue, L.; Ma, L.; Niu, J.; Tong, T. (2012): Nucleolar protein CSIG is required for p33ING1 function in UV-induced apoptosis. In Cell Death and Disease 3 (3), pp. 1–11. DOI: 10.1038/cddis.2012.22.

Li, Yun; Minor, Nicole T.; Park, Joseph K.; McKearin, Dennis M.; Maines, Jean Z. (2009): Bam and Bgcn antagonize Nanos-dependent germ-line stem cell maintenance. In PNAS 106 (23), pp. 9304–9309. DOI: 10.1073/pnas.0901452106.

Lin, H.; Yue, L.; Spradling, A. C. (1994): The Drosophila fusome, a germline-specific organelle, contains membrane skeletal proteins and functions in cyst formation. In Development (Cambridge, England) 120 (4), pp. 947–956. DOI: 10.1242/dev.120.4.947.

Lin, Haifan (2002): The stem-cell niche theory: lessons from flies. In Nature Reviews Genetics 3 (12), pp. 931–940. DOI: 10.1038/nrg952.

Linder, Patrick; Jankowsky, Eckhard (2011): From unwinding to clamping - the DEAD box RNA helicase family. In Nature Reviews Molecular Cell Biology 12 (8), pp. 505–516. DOI: 10.1038/nrm3154.

Liu, Ji-Long; Murphy, Christine; Buszczak, Michael; Clatterbuck, Sarah; Goodman, Robyn; Gall, Joseph G. (2006): The Drosophila melanogaster Cajal body. In J Cell Biol 172 (6), pp. 875–884. DOI: 10.1083/jcb.200511038.

Lohe, A. R.; Hilliker, A. J.; Roberts, P. A. (1993): Mapping simple repeated DNA sequences in heterochromatin of Drosophila melanogaster: Genetics Society of America (134). In Genetics (4). Available online at http://www.ncbi.nlm.nih.gov/pubmed/8375654 http://www.pubmedcentral.nih.gov/articlerender.fcgi?artid=PMC1205583.

Lu, Junjie; Gilbert, David M. (2007): Proliferation-dependent and cell cycle-regulated transcription of mouse pericentric heterochromatin. In The Journal of cell biology 179 (3), pp. 411–421. DOI: 10.1083/jcb.200706176.

Lu, Kevin L.; Nelson, Jonathan O.; Watase, George J.; Warsinger-Pepe, Natalie; Yamashita, Yukiko M. (2018): Transgenerational dynamics of rDNA copy number in Drosophila male germline stem cells. In eLife 7. DOI: 10.7554/eLife.32421.

M. Demerec (Ed.) (1950): Biology of Drosophila. With assistance of Dietrich Bodenstein, Kenneth W. Cooper, G. F. Ferris, Albert Miller, D. F. Poulson, B. P. Sonnenblick, Warren P. Spencer. Facsimile Edition. New York, NY: Cold Spring Harbor Laboratory Press.

Ma, Liwei; Chang, Na; Shuzhen, Guo; Li, Qian; Zhang, Zongyu; Wang, Wengong; Tong, Tanjun (2008): CSIG Inhibits PTEN Translation in Replicative Senescence. In Molecular and cellular biology 28 (20), pp. 6290–6301. DOI: 10.1128/mcb.00142-08.

Ma, Nan; Matsunaga, Sachihiro; Takata, Hideaki; Ono-Maniwa, Rika; Uchiyama, Susumu; Fukui, Kiichi (2007): Nucleolin functions in nucleolus formation and chromosome congression. In Journal of cell science 120 (12), pp. 2091–2105. DOI: 10.1242/jcs.008771.

Mahowald, Anthony P. (2001): Assembly of the Drosophila germ plasm. In Laurence D. Etkin (Ed.): Cell lineage specification and patterning of the embryo, vol. 203. San Diego: Academic Press (International Review of Cytology), pp. 187–213.

Maimon, Iris; Gilboa, Lilach (2011): Dissection and staining of Drosophila larval ovaries. In Journal of visualized experiments : JoVE (51). DOI: 10.3791/2537.

Martin, Elliot T.; Blatt, Patrick; Ngyuen, Elaine; Lahr, Roni; Selvam, Sangeetha; Yoon, Hyun Ah M. et al. (2021): A translation control module coordinates germline stem cell differentiation with ribosome biogenesis during Drosophila oogenesis.

Masumoto, H.; Masukata, H.; Muro, Y.; Nozaki, N.; Okazaki, T. (1989): A human centromere antigen (CENP-B) interacts with a short specific sequence in alphoid DNA, a human centromeric satellite. In J Cell Biol 109 (5), pp. 1963–1973. DOI: 10.1083/jcb.109.5.1963.

Matheson, Timothy D.; Kaufman, Paul D. (2016): Grabbing the genome by the NADs. In Chromosoma 125 (3), pp. 361–371. DOI: 10.1007/s00412-015-0527-8.

May, Bruce P.; Lippman, Zachary B.; Fang, Yuda; Spector, David L.; Martienssen, Robert A. (2005): Differential regulation of strand-specific transcripts from Arabidopsis centromeric satellite repeats. In PLOS Genetics 1 (6), e79. DOI: 10.1371/journal.pgen.0010079.

McKechnie, S. W.; Halford, M. M.; McColl, G.; Hoffmann, A. A. (1998): Both allelic variation and expression of nuclear and cytoplasmic transcripts of Hsr-omega are closely associated with thermal phenotype in Drosophila. In Proceedings of the National Academy of Sciences 95 (5), pp. 2423–2428. DOI: 10.1073/pnas.95.5.2423.

McNulty, Shannon M.; Sullivan, Lori L.; Sullivan, Beth A. (2017): Human Centromeres Produce Chromosome-Specific and Array-Specific Alpha Satellite Transcripts that Are Complexed with CENP-A and CENP-C. In Developmental cell 42 (3), 226-240.e6. DOI: 10.1016/j.devcel.2017.07.001.

Mellone, Barbara G.; Grive, Kathryn J.; Shteyn, Vladimir; Bowers, Sarion R.; Oderberg, Isaac; Karpen, Gary H. (2011): Assembly of Drosophila centromeric chromatin proteins during mitosis. In PLOS Genetics 7 (5), e1002068. DOI: 10.1371/journal.pgen.1002068.

Meng, L.; Yasumoto, H.; Tsai, R. Y. L. (2006): Multiple controls regulate nucleostemin partitioning between nucleolus and nucleoplasm. In Journal of cell science 119 (24), pp. 5124–5136. DOI: 10.1242/jcs.03292.

Milek, Miha; Imami, Koshi; Mukherjee, Neelanjan; Bortoli, Francesca de; Zinnall, Ulrike; Hazapis, Orsalia et al. (2017): DDX54 regulates transcriptome dynamics during DNA damage response. In Genome research 27 (8), pp. 1344–1359. DOI: 10.1101/gr.218438.116.

Milkereit, Philipp; Gadal, Olivier; Podtelejnikov, Alexander; Trumtel, Stephanie; Gas, Nicole; Petfalski, Elisabeth et al. (2001): Maturation and intranuclear transport of pre-ribosomes requires Noc proteins. In Cell 105 (4), pp. 499–509. DOI: 10.1016/S0092-8674(01)00358-0.

Mills, Wilbur Kyle; Lee, Yuh Chwen G.; Kochendoerfer, Antje M.; Dunleavy, Elaine M.; Karpen, Gary H. (2019): RNA from a simple-tandem repeat is required for sperm maturation and male fertility in Drosophila melanogaster. In eLife 8. DOI: 10.7554/eLife.48940.

Molina, Oscar; Vargiu, Giulia; Abad, Maria Alba; Zhiteneva, Alisa; Jeyaprakash, A. Arockia; Masumoto, Hiroshi et al. (2016): Epigenetic engineering reveals a balance between histone modifications and transcription in kinetochore maintenance. In Nat Commun 7 (1), p. 13334. DOI: 10.1038/ncomms13334.

Motola, Shmulik; Neuman-Silberberg, F. Shira (2004): spoonbill, a new Drosophila female-sterile mutation, interferes with chromosome organization and dorsal-ventral patterning of the egg. In Developmental dynamics : an official publication of the American Association of Anatomists 230 (3), pp. 535–545. DOI: 10.1002/dvdy.20066.

Neumüller, Ralph A.; Betschinger, Joerg; Fischer, Anja; Bushati, Natascha; Poernbacher, Ingrid; Mechtler, Karl et al. (2008): Mei-P26 regulates microRNAs and cell growth in the Drosophila ovarian stem cell lineage. In Nature 454 (7201), pp. 241–245. DOI: 10.1038/nature07014.

Neumüller, Ralph A.; Richter, Constance; Fischer, Anja; Novatchkova, Maria; Neumüller, Klaus G.; Knoblich, Juergen A. (2011): Genome-wide analysis of self-renewal in Drosophila neural stem cells by transgenic RNAi. In Cell Stem Cell 8 (5), pp. 580–593. DOI: 10.1016/j.stem.2011.02.022.

Nishibuchi, Gohei; Déjardin, Jérôme (2017): The molecular basis of the organization of repetitive DNA-containing constitutive heterochromatin in mammals. In Chromosome Res 25 (1), pp. 77–87. DOI: 10.1007/s10577-016-9547-3.

Nishimura, Kanako; Cho, Yukiko; Tokunaga, Kazuaki; Nakao, Mitsuyoshi; Tani, Tokio; Ideue, Takashi (2019): DEAH box RNA helicase DHX38 associates with satellite I noncoding RNA involved in chromosome segregation. In Genes to Cells 24 (8), pp. 585–590. DOI: 10.1111/gtc.12707.

Nystul, Todd; Spradling, Allan (2010): Regulation of epithelial stem cell replacement and follicle formation in the Drosophila ovary. In Genetics 184 (2), pp. 503–515. DOI: 10.1534/genetics.109.109538.

Ohlstein, B.; McKearin, D. (1997): Ectopic expression of the Drosophila Bam protein eliminates oogenic germline stem cells. In Development (Cambridge, England) 124 (18), pp. 3651–3662.

Ohta, S.; Wood, L.; Toramoto, I.; Yagyu, K.-I.; Fukagawa, T.; Earnshaw, W. C. (2015): CENP-32 is required to maintain centrosomal dominance in bipolar spindle assembly. In Molecular biology of the cell 26 (7), pp. 1225–1237. DOI: 10.1091/mbc.E14-09-1366.

Ohta, Shinya; Bukowski-Wills, Jimi Carlo; Sanchez-Pulido, Luis; Alves, Flavia de Lima; Wood, Laura; Chen, Zhuo A. et al. (2010): The Protein Composition of Mitotic Chromosomes Determined Using Multiclassifier Combinatorial Proteomics. In Cell 142 (5), pp. 810–821. DOI: 10.1016/j.cell.2010.07.047.

Orr-Weaver, Terry L. (2015): When bigger is better: the role of polyploidy in organogenesis. In Trends in genetics : TIG 31 (6), pp. 307–315. DOI: 10.1016/j.tig.2015.03.011.

Padeken, Jan; Mendiburo, María José; Chlamydas, Sarantis; Schwarz, Hans Jürgen; Kremmer, Elisabeth; Heun, Patrick (2013): The Nucleoplasmin Homolog NLP Mediates Centromere Clustering and Anchoring to the Nucleolus. In Molecular cell 50 (2), pp. 236–249. DOI: 10.1016/j.molcel.2013.03.002.

Pal-Bhadra, M. (2013): Heterochromatic silencing and HP1 localization in Drosophila are dependent on the RNAi machinery (Science (2004) (669)). In Science (New York, N.Y.) 340 (6135), p. 924. DOI: 10.1126/science.340.6135.924-b.

Pathak, Rashmi U.; Mamillapalli, Anitha; Rangaraj, Nandini; Kumar, Ram P.; Vasanthi, Dasari; Mishra, Krishnaveni; Mishra, Rakesh K. (2013): AAGAG repeat RNA is an essential component of nuclear matrix in Drosophila. In RNA biology 10 (4), pp. 564–571. DOI: 10.4161/rna.24326.

Pezer, Z.; Ugarković, D. (2009): Transcription of pericentromeric heterochromatin in beetles-satellite DNAs as active regulatory elements. In Cytogenetic and genome research 124 (3-4), pp. 268–276. DOI: 10.1159/000218131.

Poulson, D. F. (1947): The Pole Cells of Diptera, Their Fate and Significance. In Proceedings of the National Academy of Sciences 33 (6), pp. 182–184. DOI: 10.1073/pnas.33.6.182.

Prasanth, K. V.; Rajendra, T. K.; Lal, A. K.; Lakhotia, S. C. (2000): Omega speckles - a novel class of nuclear speckles containing hnRNPs associated with noncoding hsr-omega RNA in Drosophila. In Journal of cell science 113 Pt 19, pp. 3485–3497. Available online at http://www.ncbi.nlm.nih.gov/pubmed/10984439.

Quan, Jiayuan; Tian, Jingdong (2009): Circular polymerase extension cloning of complex gene libraries and pathways. In PloS one 4 (7). DOI: 10.1371/journal.pone.0006441.

Rabinowitz, Morris (1941): Studies on the cytology and early embryology of the egg of Drosophila melanogaster. In Journal of Morphology 69 (1), pp. 1–49. DOI: 10.1002/jmor.1050690102.

Rajendran, Ramji R.; Nye, Anne C.; Frasor, Jonna; Balsara, Rashna D.; Martini, Paolo G.V.; Katzenellenbogen, Benita S. (2003): Regulation of nuclear receptor transcriptional activity by a novel DEAD box RNA helicase (DP97). In The Journal of biological chemistry 278 (7), pp. 4628–4638. DOI: 10.1074/jbc.M210066200.

Ramanathan, Nardev; Lim, Nicole; Stewart, Colin L. (2015): DDX5/p68 RNA helicase expression is essential for initiating adipogenesis. In Lipids in health and disease 14, p. 160. DOI: 10.1186/s12944-015-0163-6.

Ranjan, Rajesh; Snedeker, Jonathan; Chen, Xin (2019): Asymmetric Centromeres Differentially Coordinate with Mitotic Machinery to Ensure Biased Sister Chromatid Segregation in Germline Stem Cells. In Cell Stem Cell 25 (5), 666-681.e5. DOI: 10.1016/j.stem.2019.08.014.

Régnier, Vinciane; Vagnarelli, Paola; Fukagawa, Tatsuo; Zerjal, Tatiana; Burns, Elizabeth; Trouche, Didier et al. (2005): CENP-A is required for accurate chromosome segregation and sustained kinetochore association of BubR1. In Molecular and cellular biology 25 (10), pp. 3967–3981. DOI: 10.1128/MCB.25.10.3967-3981.2005.

Riechmann, V.; Ephrussi, A. (2001): Axis formation during Drosophila oogenesis. In Current Opinion in Genetics and Development 11 (4), pp. 374–383. DOI: 10.1016/S0959-437X(00)00207-0.

Rošić, Silvana; Köhler, Florian; Erhardt, Sylvia (2014): Repetitive centromeric satellite RNA is essential for kinetochore formation and cell division. In Journal of Cell Biology 207 (3), pp. 335–349. DOI: 10.1083/jcb.201404097.

Royzman, Irena; Hayashi-Hagihara, Aki; Dej, Kimberley J.; Bosco, Giovanni; Lee, Janice Y.; Orr-Weaver, Terry L. (2002): The E2F cell cycle regulator is required for Drosophila nurse cell DNA replication and apoptosis.

Rudert, F.; Bronner, S.; Garnier, J. M.; Dollé, P. (1995): Transcripts from opposite strands of gamma satellite DNA are differentially expressed during mouse development. In Mammalian genome : official journal of the International Mammalian Genome Society 6 (2), pp. 76–83. DOI: 10.1007/BF00303248.

Rudra, Dipayan; Warner, Jonathan R. (2004): What better measure than ribosome synthesis? In Genes & development 18 (20), pp. 2431–2436. DOI: 10.1101/gad.1256704.

Runge, K. W.; Wellinger, R. J.; Zakian, V. A. (1991): Effects of excess centromeres and excess telomeres on chromosome loss rates. In Molecular and cellular biology 11 (6), pp. 2919–2928. DOI: 10.1128/mcb.11.6.2919-2928.1991.

Sahai-Hernandez, Pankaj; Nystul, Todd G. (2013): A dynamic population of stromal cells contributes to the follicle stem cell niche in the Drosophila ovary. In Development 140 (22), pp. 4490–4498. DOI: 10.1242/dev.098558.

Sahut-Barnola, Isabelle; Dastugue, Bernard; Couderc, Jean-Louis (1996): Terminal filament cell organization in the larval ovary of Drosophila melanogaster: ultrastructural observations and pattern of divisions. In Roux's archives of developmental biology : the official organ of the EDBO 205 (7-8), pp. 356–363. DOI: 10.1007/BF00377215.

Salvany, Lara; Aldaz, Silvia; Corsetti, Elise; Azpiazu, Natalia (2009): A new role for hth in the early pre-blastodermic divisions in drosophila. In Cell cycle (Georgetown, Tex.) 8 (17), pp. 2748–2755. DOI: 10.4161/cc.8.17.9388.

Salzmann, Viktoria; Chen, Cuie; Chiang, C-Y Ason; Tiyaboonchai, Amita; Mayer, Michael; Yamashita, Yukiko M. (2014): Centrosome-dependent asymmetric inheritance of the midbody ring in Drosophila germline stem cell division. In Molecular biology of the cell 25 (2), pp. 267–275. DOI: 10.1091/mbc.E13-09-0541.

Sanchez, Carlos G.; Teixeira, Felipe Karam; Czech, Benjamin; Preall, Jonathan B.; Zamparini, Andrea L.; Seifert, Jessica R. K. et al. (2016): Regulation of Ribosome Biogenesis and Protein Synthesis Controls Germline Stem Cell Differentiation. In Cell stem cell 18 (2), pp. 276–290. DOI: 10.1016/j.stem.2015.11.004.

Sawamura, K.; Yamamoto, M. T.; Watanabe, T. K. (1993): Hybrid lethal systems in the Drosophila melanogaster species complex. II. The Zygotic hybrid rescue (Zhr) gene of D. melanogaster. In Genetics.

Schuh, Melina; Lehner, Christian F.; Heidmann, Stefan (2007): Incorporation of Drosophila CID/CENP-A and CENP-C into centromeres during early embryonic anaphase. In Current Biology 17 (3), pp. 237–243. DOI: 10.1016/j.cub.2006.11.051.

Scott, Kristin C.; Sullivan, Beth A. (2014): Neocentromeres: a place for everything and everything in its place. In Trends in Genetics 30, pp. 66–74. DOI: 10.1016/j.tig.2013.11.003.

Sharma, Sunny; Yang, Jun; Watzinger, Peter; Kötter, Peter; Entian, Karl-Dieter (2013): Yeast Nop2 and Rcm1 methylate C2870 and C2278 of the 25S rRNA, respectively. Nucleic Acids Research, 41(19), 9062-9076. In Nucleic acids research 41 (19), pp. 9062–9076. DOI: 10.1093/NAR/GKT679.

Shatskikh, Aleksei S.; Kotov, Alexei A.; Adashev, Vladimir E.; Bazylev, Sergei S.; Olenina, Ludmila V. (2020): Functional Significance of Satellite DNAs: Insights From Drosophila. In Frontiers in cell and developmental biology 8, p. 312. DOI: 10.3389/fcell.2020.00312.

Shrestha, Roshan L.; Rossi, Austin; Wangsa, Darawalee; Hogan, Ann K.; Zaldana, Kimberly S.; Suva, Evelyn et al. (2021): CENP-A overexpression promotes aneuploidy with karyotypic heterogeneity. In Journal of Cell Biology 220 (4). DOI: 10.1083/jcb.202007195.

Slaidina, Maija; Banisch, Torsten U.; Gupta, Selena; Lehmann, Ruth (2020): A single-cell atlas of the developing Drosophila ovary identifies follicle stem cell progenitors. In Genes and Development 34 (3-4), pp. 239–249. DOI: 10.1101/gad.330464.119.

Sloan, Katherine E.; Bohnsack, Markus T.; Watkins, Nicholas J. (2013): The 5S RNP couples p53 homeostasis to ribosome biogenesis and nucleolar stress. In Cell Reports 5 (1), pp. 237–247. DOI: 10.1016/j.celrep.2013.08.049.

Smith, A. V.; Orr-Weaver, T. L. (1991): The regulation of the cell cycle during Drosophila embryogenesis: the transition to polyteny. In Development (Cambridge, England) 112 (4), pp. 997–1008. DOI: 10.1242/dev.112.4.997.

Somma, Maria Patrizia; Ceprani, Francesca; Bucciarelli, Elisabetta; Naim, Valeria; Arcangelis, Valeria de; Piergentili, Roberto et al. (2008): Identification of Drosophila Mitotic Genes by Combining Co-Expression Analysis and RNA Interference. In PLoS genetics 4 (7). DOI: 10.1371/journal.pgen.1000126.

Song, Xiaoqing; Call, Gerald B.; Kirilly, Daniel; Xie, Ting (2007): Notch signaling controls germline stem cell niche formation in the Drosophila ovary. In Development (Cambridge, England) 134 (6), pp. 1071–1080. DOI: 10.1242/dev.003392.

Song, Xiaoqing; Wong, Marco D.; Kawase, Eihachiro; Xi, Rongwen; Ding, Bee C.; McCarthy, John J.; Xie, Ting (2004): Bmp signals from niche cells directly repress transcription of a differentiation-promoting gene, bag of marbles, in germline stem cells in the Drosophila ovary. In Development (Cambridge, England) 131 (6), pp. 1353–1364. DOI: 10.1242/dev.01026.

Song, Xiaoqing; Zhu, Chun-Hong; Doan, Chuong; Xie, Ting (2002): Germline stem cells anchored by adherens junctions in the Drosophila ovary niches. In Science 296 (5574), pp. 1855–1857. DOI: 10.1126/science.1069871.

Sonnenblick, B. P. (1941): Germ Cell Movements and Sex Differentiation of the Gonads in the Drosophila Embryo. In Proceedings of the National Academy of Sciences 27 (10), pp. 484–489. DOI: 10.1073/pnas.27.10.484.

Steinhauer, W. R.; Kalfayan, L. J. (1992): A specific ovarian tumor protein isoform is required for efficient differentiation of germ cells in Drosophila oogenesis. In Genes & development 6 (2), pp. 233–243. DOI: 10.1101/gad.6.2.233.

Stormo, Benjamin M.; Fox, Donald T. (2017): Polyteny: still a giant player in chromosome research. In Chromosome Research 25 (3-4), pp. 201–214. DOI: 10.1007/s10577-017-9562-z.

Sullivan, Beth A.; Karpen, Gary H. (2004): Centromeric chromatin exhibits a histone modification pattern that is distinct from both euchromatin and heterochromatin. In Nature structural & molecular biology 11 (11), pp. 1076–1083. DOI: 10.1038/nsmb845.

Swanson, Eric C.; Manning, Benjamin; Zhang, Hong; Lawrence, Jeanne B. (2013): Higher-order unfolding of satellite heterochromatin is a consistent and early event in cell senescence. In Journal of Cell Biology 203 (6), pp. 929–942.

Talbert, Paul B.; Henikoff, Steven (2018): Transcribing Centromeres: Noncoding RNAs and Kinetochore Assembly. In Trends in Genetics 34 (8), pp. 587–599. DOI: 10.1016/j.tig.2018.05.001.

Ting, David T.; Lipson, Doron; Paul, Suchismita; Brannigan, Brian W.; Akhavanfard, Sara; Coffman, Erik J. et al. (2011): Aberrant Overexpression of Satellite Repeats in Pancreatic and Other Epithelial Cancers. In Science (New York, N.Y.) 331 (February), pp. 593–597. DOI: 10.1126/science.1200801.

Tishchenko, Svetlana; Nikonova, Ekaterina; Kljashtorny, Vladislav; Kostareva, Olga; Nevskaya, Natalia; Piendl, Wolfgang et al. (2007): Domain I of ribosomal protein L1 is sufficient for specific RNA binding. In Nucleic Acids Res 35 (21), pp. 7389–7395. DOI: 10.1093/nar/gkm898.

Tollervey, David; Lehtonen, Hanna; Jansen, Ralf; Kern, Hildegard; Hurt, Eduard C. (1993): Temperature-sensitive mutations demonstrate roles for yeast fibrillarin in pre-rRNA processing, pre-rRNA methylation, and ribosome assembly. In Cell 72 (3), pp. 443–457. DOI: 10.1016/0092-8674(93)90120-F.

Tominaga, K.; Johmura, Y.; Nishizuka, M.; Imagawa, M. (2004): Fad24, a mammalian homolog of Noc3p, is a positive regulator in adipocyte differentiation. In Journal of cell science 117 (25), pp. 6217–6226. DOI: 10.1242/jcs.01546.

Topp, C. N.; Zhong, C. X.; Dawe, R. K. (2004): Centromere-encoded RNAs are integral components of the maize kinetochore. In Proceedings of the National Academy of Sciences 101 (45), pp. 15986–15991. DOI: 10.1073/pnas.0407154101.

Tóth, Katalin Fejes; Pezic, Dubravka; Stuwe, Evelyn; Webster, Alexandre (2016): The piRNA Pathway Guards the Germline Genome Against Transposable Elements. In Advances in experimental medicine and biology 886, pp. 51–77. DOI: 10.1007/978-94-017-7417-8_4.

Tran, Vuong; Lim, Cindy; Xie, Jing; Chen, Xin (2012): Asymmetric division of Drosophila male germline stem cell shows asymmetric histone distribution. In Science 338 (6107), pp. 679–682. DOI: 10.1126/science.1226028.

Treiber, Thomas; Treiber, Nora; Plessmann, Uwe; Harlander, Simone; Daiß, Julia-Lisa; Eichner, Norbert et al. (2017): A Compendium of RNA-Binding Proteins that Regulate MicroRNA Biogenesis. In Molecular cell 66 (2), 270-284.e13. DOI: 10.1016/j.molcel.2017.03.014.

Usakin, Lev; Abad, José; Vagin, Vasily V.; Pablos, Beatriz de; Villasante, Alfredo; Gvozdev, Vladimir A. (2007): Transcription of the 1.688 satellite DNA family is under the control of RNA interference machinery in Drosophila melanogaster ovaries. In Genetics 176 (2), pp. 1343–1349. DOI: 10.1534/genetics.107.071720.

Valgardsdottir, Rut; Chiodi, Ilaria; Giordano, Manuela; Cobianchi, Fabio; Riva, Silvano; Biamonti, Giuseppe (2005): Structural and Functional Characterization of Noncoding Repetitive RNAs Transcribed in Stressed Human Cells. In Molecular biology of the cell 16 (June), pp. 2207–2217. DOI: 10.1091/mbc.E04.

Valgardsdottir, Rut; Chiodi, Ilaria; Giordano, Manuela; Rossi, Antonio; Bazzini, Silvia; Ghigna, Claudia et al. (2008): Transcription of Satellite III non-coding RNAs is a general stress response in human cells. In Nucleic acids research 36 (2), pp. 423–434. DOI: 10.1093/nar/gkm1056.

van Buskirk, Cheryl; Schüpbach, Trudi (2002): half pint Regulates Alternative Splice Site Selection in Drosophila. In Developmental cell 2 (3), pp. 343–353. DOI: 10.1016/S1534-5807(02)00128-4.

Villasante, Alfredo; Rogers, Jane; Pablos, Beatriz de; Whitehead, Siobhan L.; Wild, Jadwiga; Szybalski, Waclaw et al. (2009): Novel sequencing strategy for repetitive DNA in a Drosophila BAC clone reveals that the centromeric region of the Y chromosome evolved from a telomere†. In Nucleic acids research 37 (7), pp. 2264–2273. DOI: 10.1093/nar/gkp085.

Volpe, Alison M.; Horowitz, Heidi; Grafer, Constance M.; Jackson, Stephen M.; Berg, Celeste A. (2001): Drosophila rhino encodes a female-specific chromo-domain protein that affects chromosome structure and egg polarity. In Genetics 159 (3), pp. 1117–1134.

Volpe, Thomas A.; Kidner, Catherine; Hall, Ira M.; Teng, Grace; Grewal, Shiv I. S.; Martienssen, Robert A. (2002): Regulation of heterochromatic silencing and histone H3 lysine-9 methylation by RNAi. In Science 297 (5588), pp. 1833–1837. DOI: 10.1126/science.1074973.

Wang, Fang; Yuan, Ji Hang; Wang, Shao Bing; Yang, Fu; Yuan, Sheng Xian; Ye, Chen et al. (2014): Oncofetal long noncoding RNA PVT1 promotes proliferation and stem cell-like property of hepatocellular carcinoma cells by stabilizing NOP2. In Hepatology (Baltimore, Md.) 60 (4), pp. 1278–1290. DOI: 10.1002/hep.27239.

Wang, Huanan; Wang, Lefeng; Wang, Zizengchen; Dang, Yanna; Shi, Yan; Zhao, Panpan; Zhang, Kun (2020): The nucleolar protein NOP2 is required for nucleolar maturation and ribosome biogenesis during preimplantation development in mammals. In FASEB journal : official publication of the Federation of American Societies for Experimental Biology 34 (2), pp. 2715–2729. DOI: 10.1096/fj.201902623R.

Wei, Xiaolu; Eickbush, Danna G.; Speece, Iain; Larracuente, Amanda M. (2020): Heterochromatin-dependent transcription of satellite DNAs in the Drosophila melanogaster female germline: BioRxiv.

Whitworth, Cale; Jimenez, Erin; van Doren, Mark (2012): Development of sexual dimorphism in the Drosophila testis. In Spermatogenesis 2 (3), pp. 129–136. DOI: 10.4161/spmg.21780.

Wong, Lee H.; Brettingham-Moore, Kate H.; Chan, Lyn; Quach, Julie M.; Anderson, Melissa A.; Northrop, Emma L. et al. (2007): Centromere RNA is a key component for the assembly of nucleoproteins at the nucleolus and centromere. In Genome research 17 (8), pp. 1146–1160. DOI: 10.1101/gr.6022807.

Wooten, Matthew; Snedeker, Jonathan; Nizami, Zehra F.; Yang, Xinxing; Ranjan, Rajesh; Urban, Elizabeth et al. (2019): Asymmetric histone inheritance via strand-specific incorporation and biased replication fork movement. In Nature structural & molecular biology 26 (8), pp. 732–743. DOI: 10.1038/s41594-019-0269-z.

Yamashita, Yukiko M.; Fuller, Margaret T.; Jones, D. Leanne (2005): Signaling in stem cell niches: lessons from the Drosophila germline. In Journal of cell science 118 (Pt 4), pp. 665–672. DOI: 10.1242/jcs.01680.

Yan, Dong; Neumüller, Ralph A.; Buckner, Michael; Ayers, Kathleen; Li, Hua; Hu, Yanhui et al. (2014): A regulatory network of Drosophila germline stem cell self-renewal. In Developmental cell 28 (4), pp. 459–473. DOI: 10.1016/j.devcel.2014.01.020.

Zhang, Qiao; Shalaby, Nevine A.; Buszczak, Michael (2014): Changes in rRNA transcription influence proliferation and cell fate within a stem cell lineage. In Science (New York, N.Y.) 343 (6168), pp. 298–301. DOI: 10.1126/science.1246384.

Zhang, Xiaopei; Wang, Wei; Zhu, Weidong; Dong, Jie; Cheng, Yingying; Yin, Zujun; Shen, Fafu (2019): Mechanisms and Functions of Long Non-Coding RNAs at Multiple Regulatory Levels. In International journal of molecular sciences 20 (22). DOI: 10.3390/ijms20225573.

Zhang, Yuexuan; Yu, Zhiling; Fu, Xinrong; Liang, Chun (2002): Noc3p, a bHLH Protein, Plays an Integral Role in the Initiation of DNA Replication in Budding Yeast. In Cell 109 (7), pp. 849–860.

Zhu, Quan; Hoong, Nien; Aslanian, Aaron; Hara, Toshiro; Benner, Christopher; Heinz, Sven et al. (2018): Heterochromatin-Encoded Satellite RNAs Induce Breast Cancer. In Molecular cell 70 (5), 842-853.e7. DOI: 10.1016/j.molcel.2018.04.023.

Supplemental data

Table 1: Sat III RNA pulldown 1 - MS data

S = peptide counts in sat III sense RNA pulldown
AS = peptide counts in sat III sense RNA pulldown
L = peptide counts in loops only RNA pulldown
log2(FC) = log2 values of the fold change of S/L

Cutoff: only proteins with a log2(FC) of 1 or higher a listed
grey fields: Centagon proteins

CG number	protein ID	S	AS	L	log2(FC)
CG9684	CG9684	30	16	0	4,9
CG13900	CG13900-PA, isoform A	25	8	1	4,6
CG5787	CG5787, isoform A	20	14	0	4,3
CG2691	RRP12-like protein	19	2	1	4,2
CG8710	Isoform of A1Z7A8, Coilin, isoform E	17	0	0	4,1
CG1828	FACT complex subunit spt16	16	3	0	4,0
CG3605	CG3605, isoform A	15	2	0	3,9
CG5931	Putative U5 small nuclear ribonucleoprotein 200 kDa helicase	15	0	1	3,9
CG5720	BcDNA.LD27873	15	8	1	3,9
CG6905	Cell division cycle 5 ortholog, isoform A	13	3	1	3,7
CG2807	CG2807, isoform A	25	6	2	3,6
CG17838	Isoform of A0A0B4KHI4, Syncrip, isoform O	12	0	0	3,6
CG12785	Nucleolar protein 6	12	0	0	3,6
CG6189	FI21448p1	12	0	1	3,6
CG8545	CG8545	11	2	0	3,5
CG12819	Protein slender lobes	11	4	0	3,5
CG12085	Poly(U)-binding-splicing factor half pint	11	3	0	3,5
CG32344	CG32344	11	1	1	3,5
CG13096	Isoform of Q9VLK2, CG13096, isoform B	10	6	0	3,3
CG8877	Pre-mRNA processing factor 8	10	1	1	3,3
CG6711	Isoform of Q24325, LD23043p	9	0	0	3,2
CG2009	CG2009-PA	9	2	0	3,2
CG6701	CG6701, isoform B	9	3	0	3,2
CG17603	Isoform of P51123, TBP-associated factor 1, isoform F	9	4	0	3,2
CG5786	Protein Peter pan	9	1	1	3,2
CG1091	Isoform of A0A0B4KGN4, CG1091, isoform B	9	1	1	3,2
CG9226	Isoform of Q6NL34, WD repeat domain 79 homolog, isoform B	8	0	0	3,0
CG4817	FACT complex subunit Ssrp1	8	0	0	3,0
CG7752	CG7752-PA	8	3	1	3,0
CG11207	CG11207-PA	8	1	1	3,0
CG7757	Precursor RNA processing 3, isoform A	8	0	1	3,0
CG8801	Isoform of Q9V411, Nucleolar GTP-binding protein 1	7	2	0	2,8
CG10269	D19A	7	0	1	2,8
CG8174	SRPK, isoform D	7	2	1	2,8
CG1234	Nucleolar complex protein 3 homolog	7	1	1	2,8

CG number	protein ID	S	AS	L	log2(FC)
CG6671	Argonaute-1, isoform A	14	0	2	2,8
CG7704	Transcription initiation factor TFIID subunit 5	7	1	1	2,8
CG10042	MBD-R2	7	5	1	2,8
CG9750	RuvB-like helicase 2	7	0	1	2,8
CG6995	Scaffold attachment factor B, isoform B	6	0	0	2,6
CG1785	Uncharacterized protein CG1785	6	2	1	2,6
CG31739	CG31739, isoform A	6	1	1	2,6
CG1685	Protein penguin	17	2	3	2,5
CG10600	CG10600, isoform B	5	1	0	2,3
CG7831	Protein claret segregational	15	11	3	2,3
CG6937	CG6937	5	1	1	2,3
CG11522	RE08669p	5	3	1	2,3
CG14938	CG14938-PA, isoform A	5	0	1	2,3
CG9916	Peptidyl-prolyl cis-trans isomerase	5	0	1	2,3
CG7977	FI01658p	5	8	1	2,3
CG1796	LD24662p	5	1	1	2,3
CG2260	CG2260	4	0	0	2,0
CG10333	CG10333	4	1	0	2,0
CG16725	Survival motor neuron protein	4	0	0	2,0
CG10712	Chromator, isoform A	4	1	0	2,0
CG4951	Uncharacterized protein CG4951	4	2	0	2,0
CG1258	Kinesin-like protein	4	0	0	2,0
CG6605	Isoform of P16568, Bicaudal D, isoform D	4	0	0	2,0
CG8611	Probable ATP-dependent RNA helicase CG8611	4	1	0	2,0
CG1832	Isoform of Q9I7K0, CG1832-PA, isoform A	4	0	0	2,0
CG10270	D19B	4	0	0	2,0
CG8332	Isoform of Q7JZW2, Ribosomal protein S15, isoform B	4	1	1	2,0
CG4863	60S ribosomal protein L3	12	7	3	2,0
CG9630	Probable ATP-dependent RNA helicase DDX55 homolog	4	0	1	2,0
CG9888	rRNA 2'-O-methyltransferase fibrillarin	8	0	2	2,0
CG1866	Moca-cyp, isoform A	4	0	1	2,0
CG17136	RNA-binding protein 1	4	0	1	2,0
CG9755	Maternal protein pumilio	7	1	2	1,8
CG3231	Something that sticks like glue, isoform A	7	2	2	1,8
CG32211	Transcription initiation factor TFIID subunit 6	10	5	3	1,7
CG6322	SD09427p	10	1	3	1,7
CG7728	CG7728-PA	3	0	0	1,6
CG8817	AF4/FMR2 family member 4	3	2	0	1,6
CG4616	FLASH ortholog, isoform A	3	0	0	1,6
CG6546	Brahma associated protein 55kD	3	0	0	1,6
CG7518	Isoform of Q9VG05, CG7518, isoform F	3	2	0	1,6
CG8233	Isoform of A0A0B4KF25, Reduction in Cnn dots 1, isoform H	3	2	0	1,6
CG6988	Isoform of P54399, Protein disulfide-isomerase	3	0	0	1,6
CG31012	Isoform of A0A0B4KI34, CIN85 and CD2AP orthologue, isoform F	3	1	0	1,6
CG32763	CG32763-PA	3	1	0	1,6
CG1542	Probable rRNA-processing protein EBP2 homolog	3	0	0	1,6
CG4699	Isoform of E2QD16, Non-specific lethal 1, isoform D	3	1	0	1,6
CG18273	CG18273	3	0	0	1,6
CG17611	Eukaryotic translation initiation factor 6	3	1	0	1,6

CG number	protein ID	S	AS	L	log2(FC)
CG17064	Guanylate kinase-associated protein mars	3	2	0	1,6
CG30149	Protein rigor mortis	3	0	0	1,6
CG13345	FI24033p1	3	0	0	1,6
CG16940	CG16940-PC, isoform C	9	5	3	1,6
CG11949	Protein 4.1 homolog	3	1	1	1,6
CG10354	5’-3’ exoribonuclease 2 homolog	3	0	1	1,6
CG33106	Isoform of Q9VCA8, Multiple ankyrin repeats single KH domain, isoform D	3	1	1	1,6
CG10922	40S ribosomal protein S10b	6	0	2	1,6
CG11271	40S ribosomal protein S12	3	0	1	1,6
CG2986	40S ribosomal protein S21	3	0	1	1,6
CG3203	60S ribosomal protein L17	6	4	2	1,6
CG7035	Nuclear cap-binding protein subunit 1	3	0	1	1,6
CG3613	Isoform of Q9W255, Quaking related 58E-1, isoform D	3	1	1	1,6
CG2998	Isoform of Q9W334, Ribosomal protein S28b, isoform B	3	0	1	1,6
CG6510	60S ribosomal protein L18a	6	3	2	1,6
CG9373	FI21236p1	20	11	7	1,5
CG16901	RNA-binding protein squid	17	5	6	1,5
CG8108	CG8108, isoform A	8	2	3	1,4
CG7434	60S ribosomal protein L22	8	17	3	1,4
CG15792	Myosin heavy chain, non-muscle	8	0	3	1,4
CG5208	Protein associated with topo II related-1, isoform A	8	1	3	1,4
CG7439	Protein argonaute-2	28	9	11	1,3
CG3751	40S ribosomal protein S24	5	0	2	1,3
CG9715	CG9715	5	2	2	1,3
CG6474	Transcription initiation factor TFIID subunit 9	5	2	2	1,3
CG3314	Isoform of P46223, Ribosomal protein L7A, isoform E	5	3	2	1,3
	Histone H4	5	0	2	1,3
CG4806	CG4806	17	5	7	1,3
CG5519	BcDNA.LD02793	19	5	8	1,2
CG18811	Caprin homolog	7	0	3	1,2
CG17521	60S ribosomal protein L10	7	7	3	1,2
CG7993	Ribosome production factor 2 homolog	7	2	3	1,2
CG12505	Activity-regulated cytoskeleton associated protein 1	7	0	3	1,2
CG4003	RuvB-like helicase 1	9	0	4	1,2
CG4464	40S ribosomal protein S19a	9	3	4	1,2
CG5920	Isoform of P31009, Ribosomal protein S2, isoform B	11	4	5	1,1
CG1691	Isoform of M9NF14, IGF-II mRNA-binding protein, isoform K	19	3	9	1,1
	Histone H3	2	0	0	1,0
CG1965	CG1965, isoform A	2	0	0	1,0
CG1559	Isoform of Q9VYS3, Upf1, isoform B	2	1	0	1,0
CG7006	60S ribosome subunit biogenesis protein NIP7 homolog	2	0	0	1,0
CG9775	CG9775, isoform A	2	0	0	1,0
CG6987	LD40489p	2	0	0	1,0
CG4918	60S acidic ribosomal protein P2	2	1	0	1,0
CG10805	HEAT repeat-containing protein 1 homolog	2	0	0	1,0
CG11563	CG11563	2	0	0	1,0
CG31938	CG31938-PA	2	0	0	1,0
	Histone H1	2	3	0	1,0
CG4364	Pescadillo homolog	2	0	0	1,0

CG number	protein ID	S	AS	L	log2(FC)
CG5589	CG5589	2	0	0	1,0
CG3163	CG3163	2	0	0	1,0
CG12499	CG12499	2	0	0	1,0
CG32435	CLIP-associating protein	2	0	0	1,0
CG13298	Splicing factor 3B subunit 6-like protein	2	0	0	1,0
CG10473	Acinus, isoform A	2	0	0	1,0
CG31368	CG31368, isoform D	2	1	0	1,0
CG8264	Isoform of P39736, Bx42, isoform B	2	1	0	1,0
CG4602	LD29830p	2	0	0	1,0
CG9246	Nucleolar complex protein 2 homolog	2	0	0	1,0
CG2670	Isoform of Q9VHY5, TBP-associated factor 7, isoform B	2	0	0	1,0
CG4211	Protein no-on-transient A	2	0	0	1,0
CG9143	CG9143	2	0	0	1,0
CG3780	RE50839p	2	0	0	1,0
CG10923	Kinesin-like protein	2	0	0	1,0
CG6751	No child left behind	2	0	0	1,0
CG6197	FI18620p1	2	0	0	1,0
CG12128	CG12128, isoform A	2	0	0	1,0
CG1101	LD24793p	2	0	0	1,0
CG10341	Isoform of Q9VJ62, CG10341, isoform C	2	0	0	1,0
CG9213	Isoform of Q9VXT5, CG9213, isoform B	2	0	0	1,0
CG4051	Egalitarian, isoform B	2	1	0	1,0
CG4913	ENL/AF9-related, isoform B	2	2	0	1,0
CG9998	Isoform of Q24562, U2 small nuclear riboprotein auxiliary factor 50, isoform B	2	0	0	1,0
CG8103	Chromodomain-helicase-DNA-binding protein Mi-2 homolog	2	0	0	1,0
CG7622	60S ribosomal protein L36	2	0	0	1,0
CG17420	Isoform of O17445, Ribosomal protein L15	2	1	1	1,0
CG7185	Cleavage and polyadenylation specificity factor subunit CG7185	2	0	1	1,0
CG9641	CG9641, isoform A	2	0	1	1,0
CG11583	Ribosome biogenesis protein BRX1 homolog	2	1	1	1,0
CG9946	Isoform of P41374, Eukaryotic translation initiation factor 2alpha, isoform B	2	1	1	1,0
CG16753	CG16753-PA	2	0	1	1,0
CG2720	CG2720-PA	2	0	1	1,0
CG4709	Zinc finger CCCH-type with G patch domain-containing protein	2	0	1	1,0
CG13425	Bancal, isoform C	2	0	1	1,0
CG18572	Isoform of P05990, Rudimentary, isoform D	2	0	1	1,0
CG5726	CG5726 O	2	0	1	1,0
CG7843	Isoform of Q9V9K7, Ars2, isoform E	2	0	1	1,0
CG11696	CG11696 O	2	1	1	1,0
CG6692	Isoform of Q95029, Cysteine proteinase-1, isoform D	2	0	1	1,0
CG1622	CG1622, isoform A	2	0	1	1,0
CG10305	Isoform of P13008, Ribosomal protein S26, isoform D	2	0	1	1,0
CG5729	Dgp-1, isoform A	2	0	1	1,0
CG33505	LD17611p	4	0	2	1,0
CG10851	Isoform of P26686, B52, isoform O	6	1	3	1,0
CG2746	60S ribosomal protein L19	6	4	3	1,0
CG4849	CG4849	10	0	5	1,0
CG3661	60S ribosomal protein L23	4	2	2	1,0

CG number	protein ID	S	AS	L	log2(FC)
CG3922	40S ribosomal protein S17	8	2	4	1,0
CG13849	FI04781p	10	0	5	1,0
CG10206	CG10206-PA	12	0	6	1,0
CG3195	RE28824p	4	6	2	1,0
CG14224	LD38919p	6	5	3	1,0
CG12598	Double-stranded RNA-specific editase Adar	6	1	3	1,0
CG3735	CG3735, isoform A	8	2	4	1,0
CG5258	Isoform of Q9V3U2, NHP2, isoform B	4	0	2	1,0

Table 2: Sat III RNA pulldown 2 - MS data

S = peptide counts in sat III sense RNA pulldown
AS = peptide counts in sat III sense RNA pulldown
L = peptide counts in loops only RNA pulldown
OM = peptide counts in hsr omega RNA pulldown
log2(FC) = log2 values of the fold change of S/L

Cutoff: only proteins with a log2(FC) of 1 or higher a listed
grey fields: Centagon proteins

CG number	protein ID	S	AS	L	OM	log2(FC)
CG5394	Bifunctional glutamate/proline--tRNA ligase	32	48	0	11	5,0
CG15100	Methionyl-tRNA synthetase	30	19	0	12	4,9
CG11471	Isoleucyl-tRNA synthetase, isoform A	22	20	0	8	4,5
CG5728	CG5728	18	11	0	17	4,2
CG3821	Aspartyl-tRNA synthetase, isoform A	14	11	0	4	3,8
CG3178	Recombination repair protein 1	28	26	2	26	3,8
CG12141	Lysine--tRNA ligase	12	9	0	3	3,6
CG9020	Probable arginine--tRNA ligase, cytoplasmic	12	9	0	4	3,6
CG10302	Bicoid mRNA stability factor	22	35	2	10	3,5
CG15792	Zipper, isoform C	10	8	1	5	3,3
CG33123	SD07726p	9	5	0	0	3,2
CG10279	LP18603p	9	3	1	2	3,2
CG7070	Pyruvate kinase	8	8	1	4	3,0
CG10206	CG10206 protein	7	2	0	1	2,8
CG8470	GH05406p	7	5	0	0	2,8
CG13900	RE01065p	7	5	1	4	2,8
CG7439	Protein argonaute-2	7	0	1	3	2,8
CG7490	60S acidic ribosomal protein P0	7	11	0	7	2,8
CG8258	CG8258	7	3	0	2	2,8
CG5599	Dihydrolipoamide acetyltransferase component of pyruvate dehydrogenase complex	6	9	0	4	2,6
CG30122	GM15464p	6	3	1	1	2,6
CG5502	60S ribosomal protein L4	6	14	0	1	2,6
CG6701	CG6701, isoform B	6	8	0	4	2,6

CG number	protein ID	S	AS	L	OM	log2(FC)
CG1691	IGF-II mRNA-binding protein, isoform D	11	2	2	9	2,5
CG12128	Uncharacterized protein, isoform A	5	2	0	2	2,3
CG6203	Fmr1, isoform G	5	3	1	1	2,3
CG17369	V-type proton ATPase subunit B	5	6	1	1	2,3
CG5519	BcDNA.LD02793	5	3	0	0	2,3
CG9373	FI21236p1	5	3	1	2	2,3
CG2050	DNA-binding protein modulo	9	15	2	9	2,2
CG11949	Protein 4.1 homolog	4	9	1	6	2,0
CG13096	Ribosomal L1 domain-containing protein CG13096	12	12	3	10	2,0
CG8231	GH13725p	4	3	0	2	2,0
CG2199	FI17108p1 (Fragment)	4	4	0	2	2,0
CG1994	RNA cytidine acetyltransferase	4	2	0	4	2,0
CG8977	T-complex protein 1 subunit gamma	4	1	0	1	2,0
CG5374	T-complex protein 1 subunit alpha	4	2	0	0	2,0
CG1345	GH12731p	4	1	0	1	2,0
CG8351	LD47396p	4	1	0	1	2,0
CG7033	CG7033	4	0	0	1	2,0
CG17521	60S ribosomal protein L10	4	6	0	3	2,0
CG7283	60S ribosomal protein L10a-2	4	10	0	4	2,0
CG9684	LD24381p1 (Fragment)	4	6	0	2	2,0
CG3333	MIP05689p (Fragment)	11	4	3	2	1,9
CG10922	La protein homolog	14	25	4	7	1,8
CG10652	FI02875p (Fragment)	3	4	0	1	1,6
CG1091	Tailor, isoform C	3	3	0	2	1,6
CG1263	60S ribosomal protein L8	3	9	0	2	1,6
CG9012	Clathrin heavy chain	3	2	0	1	1,6
CG1883	GM06992p	3	1	0	0	1,6
CG2033	40S ribosomal protein S15Aa	3	1	0	1	1,6
CG5525	T-complex protein 1 subunit delta	3	2	0	1	1,6
CG10506	Probable glutamine--tRNA ligase	3	3	0	0	1,6
CG30149	Protein rigor mortis	3	1	0	5	1,6
CG4609	Failed axon connections	3	2	0	1	1,6
CG5261	Dihydrolipoamide acetyltransferase component of pyruvate dehydrogenase complex	3	1	0	0	1,6
CG9805	Eukaryotic translation initiation factor 3 subunit A	6	7	2	4	1,6
CG4747	Putative oxidoreductase GLYR1 homolog	3	0	1	1	1,6
CG4046	40S ribosomal protein S16	3	2	0	2	1,6
CG42551	La related protein, isoform F	3	1	0	2	1,6
CG4863	LP14077p (Fragment)	3	14	0	0	1,6
CG7808	40S ribosomal protein S8	3	2	0	1	1,6
CG7831	Kinesin-like protein (Fragment)	3	1	0	2	1,6
CG7434	60S ribosomal protein L22	8	7	3	8	1,4
CG5119	Polyadenylate-binding protein	12	14	5	8	1,3
CG8280	Elongation factor 1-alpha 1	11	8	5	7	1,1
CG10686	Trailer hitch, isoform G	2	0	0	0	1,0
CG10811	Eukaryotic translation initiation factor 4G, isoform B	2	1	0	1	1,0
CG11276	40S ribosomal protein S4	2	1	0	0	1,0
CG12775	RE62581p	2	5	0	2	1,0
CG12785	Nucleolar protein 6	2	2	0	3	1,0
CG16901	Squid, isoform E	2	0	0	3	1,0

CG number	protein ID	S	AS	L	OM	log2(FC)
CG2807	RH74732p (Fragment)	2	1	0	0	1,0
CG3395	40S ribosomal protein S9	2	1	0	0	1,0
CG3751	40S ribosomal protein S24	2	1	0	1	1,0
CG4464	40S ribosomal protein S19a	2	1	1	1	1,0
CG4581	Thiolase	2	2	0	4	1,0
CG3612	ATP synthase subunit alpha, mitochondrial	2	7	0	0	1,0
CG4759	60S ribosomal protein L27	2	5	0	0	1,0
CG4878	Eukaryotic translation initiation factor 3 subunit B	2	0	0	2	1,0
CG14206	RH14172p (Fragment)	2	1	0	0	1,0
CG8415	40S ribosomal protein S23	2	1	0	1	1,0
CG11154	ATP synthase subunit beta, mitochondrial	2	3	0	0	1,0
CG5920	40S ribosomal protein S2	2	1	0	2	1,0
CG7961	Coatomer subunit alpha	2	1	0	0	1,0
CG5520	Glycoprotein 93	2	0	0	0	1,0
CG12304	Probable aminoacyl tRNA synthase complex-interacting multi-functional protein 2	2	1	0	0	1,0
CG8439	T-complex chaperonin 5, isoform B	2	1	0	0	1,0
CG5642	Eukaryotic translation initiation factor 3 subunit L	2	0	0	0	1,0
CG4389	Mitochondrial trifunctional protein alpha subunit, isoform B	12	13	6	18	1,0
	Histone H2B	4	3	2	2	1,0
	Histone H2A.v	4	3	2	2	1,0
CG6143	Protein on ecdysone puffs, isoform D	8	3	4	4	1,0
CG6253	GM06787p (Fragment)	2	6	0	0	1,0
	Histone H2A	4	3	2	3	1,0
CG9748	Belle, isoform B	6	3	3	3	1,0
CG5170	Dodeca-satellite-binding protein 1, isoform A	4	5	2	3	1,0
CG7726	60S ribosomal protein L11	2	4	1	2	1,0
CG6510	60S ribosomal protein L18a	2	5	0	0	1,0
CG6779	IP15838p (Fragment)	2	0	0	2	1,0
CG6846	GEO07453p1	2	8	1	2	1,0
CG7622	60S ribosomal protein L36	2	3	0	0	1,0
CG8900	FI09342p (Fragment)	2	0	0	0	1,0
	Histone H3	2	1	0	1	1,0

Supplemental Figures

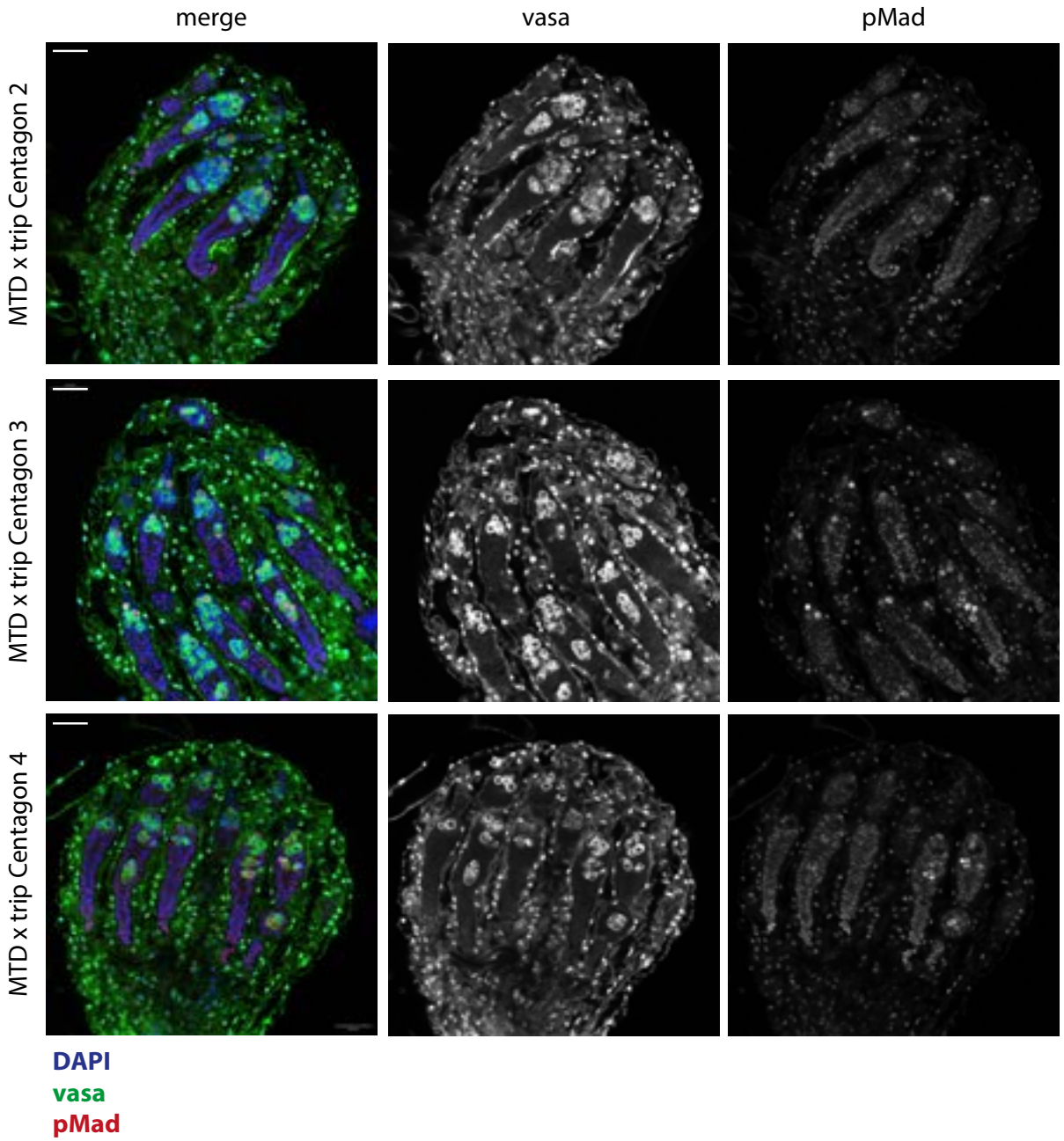

Figure S1: Ovaries of 0-1 day old MTD-GAl4 x trip Centagon flies
Ovaries are immunostained with vasa (green) and pMad (red). The scale bar indicates 20 μm.

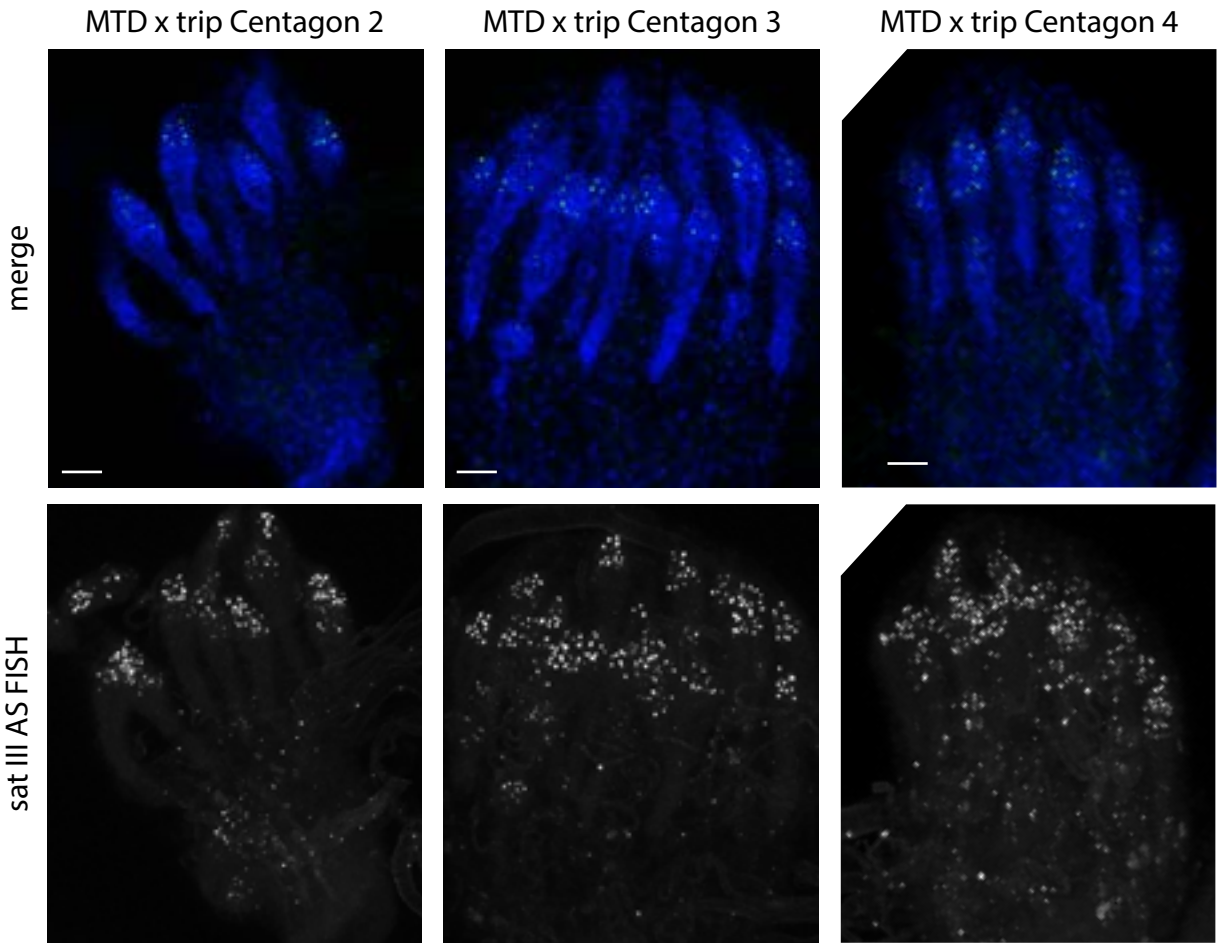

Figure S2: Sat III AS RNA FISH in MTD-GAl4 x trip Centagon flies
Ovaries of 0-1 day old flies with sat III AS RNA FISH. The lower panels are z-projections. The scale bar indicates 20 μm.

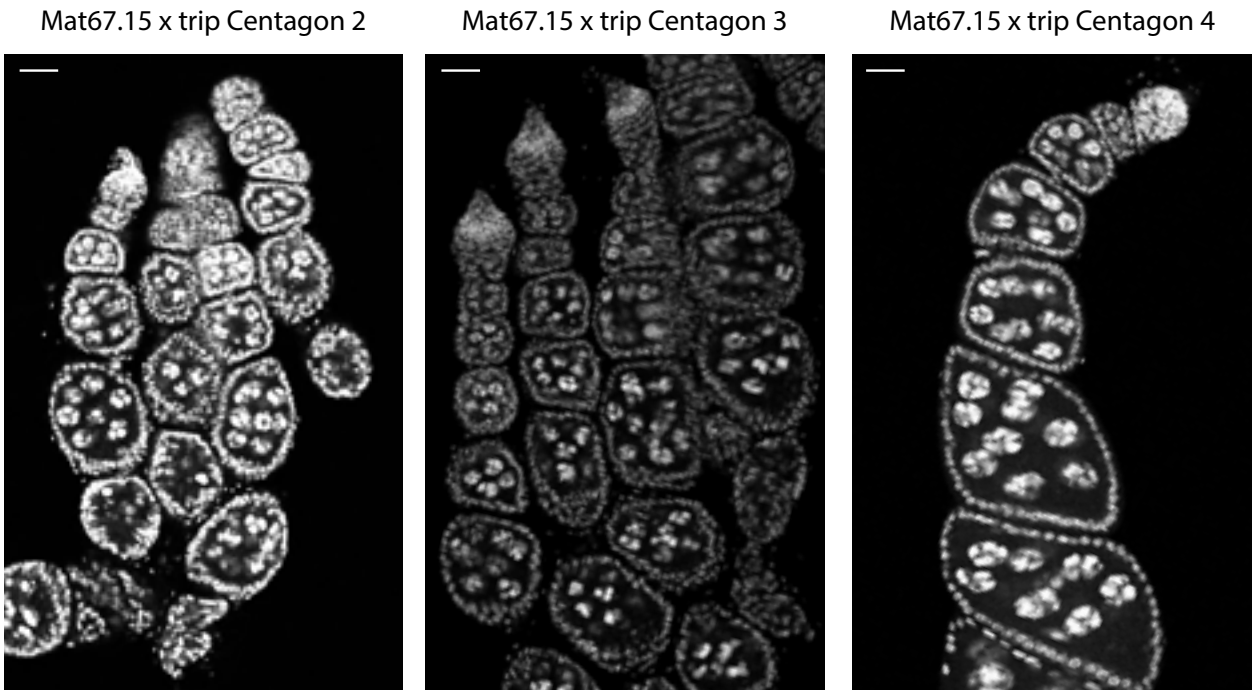

Figure S3: Fragmented nurse cells of Mat67.15-GAl4 x trip Centagon flies
Ovaries are stained with DAPI, the scale bar indicates 20 μm.

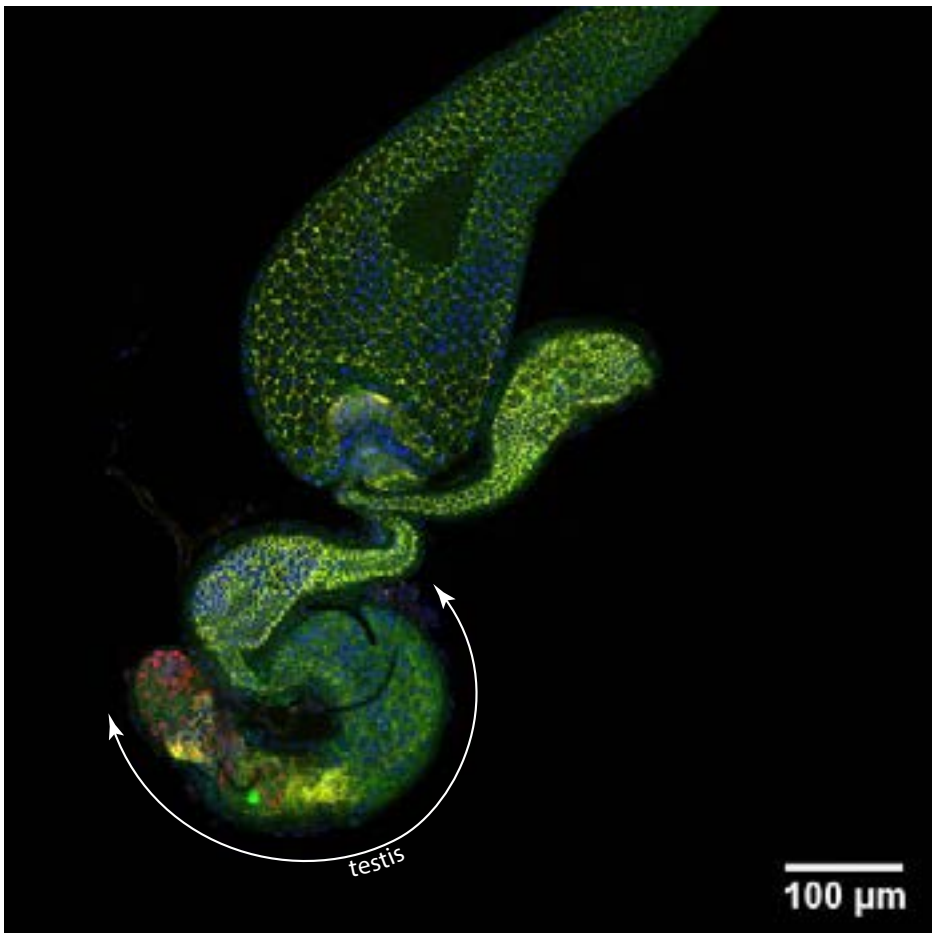

Figure S4: Testis of MTD-GAl4 x trip Centagon 1

List of figures

Acknowledgements

Dear Prof. Dr. Erhardt, dear Sylvia, thank you for giving me the opportunity to do my PhD in such an interesting field and in such a nice environment. Thank you for your time and effort, for always having an open door, for seeing potential in experiments I deemed worthless, for enrolling me in a poster contest and for your support in difficult periods.

I also want to sincerely thank my TAC and defence committee members Prof. Alexis Maizel and Prof. Georg Stöcklin for their helpful advice and making me feel supported right from the beginning.

I am very grateful to Prof. Ingrid Lohmann for being in my defence committee, but most of all for adopting me during the last stretch of my PhD. Thank you for giving me security during a time when everything seemed to be crashing down around us, for integrating me in the lab and providing me with all the facilities I needed to finish my PhD.

A big thanks also goes to the Lohmann lab members for making me feel at home so quickly. You all have been incredibly welcoming and helpful. A special thanks to Kerem for helping with the testis dissection, staining and imaging.

I also want to thank Prof. Dr. Veit Riechmann for his enthusiasm, valuable input and for sharing fly lines with me.

Dear old and new lab members! I truly enjoyed working beside you for the last 5 years. Thanks for all the encouragement and help, the nice lunches, kicker games, bouldering sessions, frisbee battles, movie and book recommendations, game nights and coffee breaks to blow off steam. Thank you Mukta for teaching me how to “fly” and thank you Iris for being such a good friend. I am very happy we could do this together.

And of course I want to thank my two students Izlem and Lili for their help and enthusiasm, it was very fun to work with you.

Last but not least, a big thanks to my family whom I always can rely on and of course Vincent, for making me laugh, having my back and convincing me to pursue a PhD in the first place.